

UNCLASSIFIED

---

AD 278 515

*Reproduced  
by the*

ARMED SERVICES TECHNICAL INFORMATION AGENCY  
ARLINGTON HALL STATION  
ARLINGTON 12, VIRGINIA



---

UNCLASSIFIED

NOTICE: When government or other drawings, specifications or other data are used for any purpose other than in connection with a definitely related government procurement operation, the U. S. Government thereby incurs no responsibility, nor any obligation whatsoever; and the fact that the Government may have formulated, furnished, or in any way supplied the said drawings, specifications, or other data is not to be regarded by implication or otherwise as in any manner licensing the holder or any other person or corporation, or conveying any rights or permission to manufacture, use or sell any patented invention that may in any way be related thereto.

62-4-4

278 515

ASD-TR-61-553

STUDY AND EXPERIMENTAL INVESTIGATION ON SAMPLING RATE  
AND ALIASING IN TIME-DIVISION TELEMETRY SYSTEMS

CATALOGED BY ASTIA  
AS AD No. \_\_\_\_\_

TECHNICAL REPORT NO. ASD-TR-61-553

June 1962

Electromagnetic Warfare & Communications Laboratory  
Aeronautical Systems Division  
Air Force Systems Command  
Wright-Patterson Air Force Base, Ohio

Project No. 4107, Task No. 410718

278 515

(Prepared under Contract No. AF 33(616)-8033  
by Aeronutronic, A Division of Ford Motor Company,  
Newport Beach, California  
Authors: J. W. Capps, W. F. Link, C. D. Eatough and D. G. Childers

## NOTICES

When Government drawings, specifications, or other data are used for any purpose other than in connection with a definitely related Government procurement operation, the United States Government thereby incurs no responsibility nor any obligation whatsoever; and the fact that the Government may have formulated, furnished, or in any way supplied the said drawings, specifications, or other data, is not to be regarded by implication or otherwise as in any manner licensing the holder or any other person or corporation, or conveying any rights or permission to manufacture, use, or sell any patented invention that may in any way be related thereto.

Qualified requesters may obtain copies of this report from the Armed Services Technical Information Agency, (ASTIA), Arlington Hall Station, Arlington 12, Virginia.

This report has been released to the Office of Technical Services, U.S. Department of Commerce, Washington 25, D.C., in stock quantities for sale to the general public.

Copies of this report should not be returned to the Aeronautical Systems Division unless return is required by security considerations, contractual obligations, or notice on a specific document.

## FOREWORD

This report was prepared by Aeronutronic, A Division of Ford Motor Company, on Air Force contract AF 33(616)-8033, under Task No. 410718 of Project No. 4107, "Study and Experimental Investigation on Sampling Rate and Aliasing in Time-Division Telemetry Systems." The work was administered under the direction of Electronic Technology Laboratory, Aeronautical Systems Division; the project engineer for the Laboratory was Mr. F. C. Karabaich.

The studies reported in this document were begun in March 1961 and were concluded in September 1961.

The key technical personnel responsible for the research activity conducted at Aeronutronic were: J. W. Capps, W. F. Link, C. D. Eatough, and D. G. Childers.

This report concludes the work on contract AF 33(616)-8033.

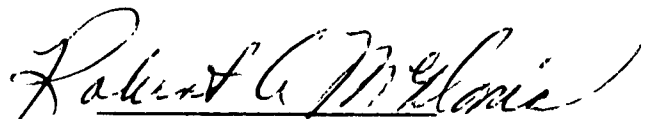
## ABSTRACT

A study to determine the effect of 1) data power spectrum and 2) system design parameters on aliasing and data interpolation error has been conducted. Results are applicable to time-division multiplexed telemetry systems. In particular, the results apply to the commonly used PAM-FM, PDM-FM and PCM-FM telemetry systems. Data was obtained on the basis of combined analysis and experiment with emphasis on the derivation of experimentally proven design parameters. The program consisted of three phases: 1) A survey was conducted to determine typical telemetry data spectra 2) Analysis was performed to predict accuracy performance of practical data and interpolation filters using selected examples. Included is a more general analysis to determine optimum filter transfer functions, both realizable and non-realizable, 3) Experimental tests using data spectral models were performed to derive proven interpolation accuracy performance on the basis of practical filters and design parameters. The experimental tests utilized a PAM-FM system to derive an accurate measurement of attainable performance and to indicate when other equipment factors begin to impose a limit on data recovery accuracy.

## PUBLICATION REVIEW

This report has been reviewed and approved.

FOR THE COMMANDER:



## CONTENTS

<u>Section</u>	<u>Page</u>
1 SUMMARY . . . . .	1
1.1 Program Objectives . . . . .	1
1.2 Data Spectra Survey . . . . .	2
1.3 Analysis . . . . .	2
1.4 Experimental Evaluation Program . . . . .	2
2 DATA SPECTRA SURVEY . . . . .	4
2.1 Basis for Data Spectra Survey . . . . .	4
2.2 Survey Data Collection . . . . .	5
2.3 Data Spectra . . . . .	7
3 ANALYSIS . . . . .	13
3.1 System Model . . . . .	15
3.2 Interpolation of Fractional Duty Cycle Pulsetrain . . . .	16
3.2.1 Power Spectrum of Sampler Output . . . . .	16
3.2.2 Power Spectrum of Interpolation Filter Output .	18
3.2.3 Normalized RMS Error . . . . .	19
3.3 Interpolation of 100% Duty Cycle PAM Pulsetrain . . . .	25
3.3.1 System Model Simplification . . . . .	25
3.3.2 Normalized RMS Error . . . . .	27
3.4 Examples and Computer Results . . . . .	28
3.4.1 Fractional Duty Cycle . . . . .	28
3.4.2 100% Duty Cycle Sampling . . . . .	35
4 EXPERIMENTAL EVALUATION PROGRAM . . . . .	39
4.1 Introduction . . . . .	39
4.2 Methods and Procedures . . . . .	39
4.3 Single Channel Sampled Data System . . . . .	41

## CONTENTS (CONTINUED)

<u>Section</u>	<u>Page</u>
4.3.1 System Description . . . . .	41
4.3.2 Test Results . . . . .	41
Sinewave . . . . .	42
Butterworth Shaped Data . . . . .	44
Butterworth Shaped EPA Data . . . . .	44
Butterworth Shaped GAP Data . . . . .	53
One Sinewave Plus Butterworth GAP Data . . . . .	67
Three Sinewaves Plus Butterworth GAP Data . . . . .	67
Step Type Butterworth GAP Data . . . . .	76
Bandpass Data . . . . .	76
4.3.3 Time Function Photographs and Spectral Measurements . . . . .	76
4.4 Multi-Channel System Tests . . . . .	87
4.4.1 System Description . . . . .	87
4.4.2 Test Results . . . . .	87
4.4.3 Time Function Photographs and Spectral Measurements . . . . .	88
5 TEST EQUIPMENT . . . . .	96
5.1 Introduction . . . . .	96
5.2 General Test Setup . . . . .	96
5.3 System Equipment . . . . .	98
5.3.1 Signal Simulators . . . . .	98
5.3.2 Data Filter . . . . .	99
5.3.3 Multiplexer . . . . .	99
5.3.4 Communication Link . . . . .	112
5.3.5 Decommunator . . . . .	112
5.3.6 Interpolation Filters . . . . .	122
5.4 Analog Error Comparator . . . . .	127
5.5 Accuracy of Measurements . . . . .	129



## CONTENTS (CONTINUED)

<u>Section</u>	<u>Page</u>
6 CONCLUSIONS AND RECOMMENDATIONS . . . . .	130
6.1 Conclusions . . . . .	130
6.1.1 Determination of Typical Data Spectra . . . . .	130
6.1.2 Analysis . . . . .	130
6.1.3 Laboratory Measurements . . . . .	131
6.1.4 Operating Parameters . . . . .	131
6.2 Recommendations . . . . .	132
A APPENDICES . . . . .	A1-1
1 PAM Multiplex System Analysis . . . . .	A1-1
2 Power Spectrum of Sampler Output . . . . .	A2-1
3 List of Reports and Conferences on Data Spectra Survey . . . . .	A3-1
4 Bibliographies Obtained for Data Spectra Survey . . . . .	A4-1
R REFERENCES . . . . .	R1-1

# ILLUSTRATIONS

Figure		Page
3-1	Simplified Single Channel Sampled Data System . . . . .	15
3-2	The Sampling Function, $s(t)$ . . . . .	16
3-3	Power Spectrum at Sampler Output . . . . .	17
3-4	Power Spectrum at Sampler Output for 100% Duty Cycle PAM . . . . .	26
3-5	Butterworth Shaped Data, $t_1 f_i = 0.02$ , $f_i/f_d = 2$ , $K=6$ . . . . .	31
3-6	Butterworth Shaped Data, $t_1 f_i = 0.02$ , $f_i/f_d = 2$ , $K=8$ . . . . .	32
3-7	Butterworth Shaped Data, 48 db/oct., $t_1 f_i = 0.02$ , $f_i/f_d = 4$ . . . . .	33
3-8	Butterworth Shaped Data, 48 db/oct., $t_1 f_i = 0.02$ , $f_i/f_d = 1$ . . . . .	34
4-1	Sinewave Tests . . . . .	43
4-2	Butterworth Shaped Data, Equi-Probable Amplitude, $t_1 f_i = 0.01$ . . . . .	45
4-3	Butterworth Shaped Data, Equi-Probable Amplitude, $t_1 f_i = 0.02$ . . . . .	46
4-4	Butterworth Shaped Data, Equi-Probable Amplitude, $t_1 f_i = 0.1$ . . . . .	47
4-5	Butterworth Shaped Data, Equi-Probable Amplitude, 100% Duty Cycle . . . . .	48
4-6	RMS Error vs. Normalized Pulsewidth . . . . .	50
4-7	Samples Per Cycle vs. Normalized Interpolation Filter Bandwidth, $t_1 f_i = 0.02$ . . . . .	51
4-8	Samples Per Cycle vs. Normalized Interpolation Filter Bandwidth, 100% Duty Cycle . . . . .	52
4-9	Butterworth Shaped Data, Gaussian Probability Distribution, $t_1 f_i = 0.01$ . . . . .	54
4-10	Butterworth Shaped Data, Gaussian Probability Distribution, $t_1 f_i = 0.02$ . . . . .	55
4-11	Butterworth Shaped Data, Gaussian Probability Distribution, $t_1 f_i = 0.1$ . . . . .	56
4-12	Butterworth Shaped Data, Gaussian Probability Distribution, 100% Duty Cycle . . . . .	57
4-13	Butterworth Shaped Data, $f_i/f_d = 1$ , $J=7$ . . . . .	58
4-14	Butterworth Shaped Data, $f_i/f_d = 2$ . . . . .	59
4-15	Butterworth Shaped Data, $f_i/f_d = 4$ , $J=7$ . . . . .	60
4-16	Butterworth Shaped Data Curves Averaged with Respect to Sample Pulsewidth . . . . .	61
4-17	Butterworth Shaped Data, Gaussian Probability Distribution, $J=5$ . . . . .	63
4-18	Butterworth Shaped Data, Gaussian Probability Distribution, $f_i/f_d = 2$ ; $K=4$ . . . . .	64
4-19	Butterworth Shaped Data, Gaussian and Equi-Probable Amplitude Probability Distribution, $f_i/f_d = 2$ ; $K=6$ . . . . .	65
4-20	Butterworth Shaped Data, Gaussian Probability Distribution, 100% Duty Cycle . . . . .	66
4-21	Butterworth Plus Sinewave Data, 100% Duty Cycle, $A_S/A_N = 12$ db . . . . .	68
4-22	Butterworth Plus Sinewave Data, 100% Duty Cycle, $A_S/A_N = 0$ db . . . . .	69
4-23	Butterworth Plus Sinewave Data, $t_1 f_i = 0.02$ , $A_S/A_N = 12$ db . . . . .	70
4-24	Butterworth Plus Sinewave Data, $t_1 f_i = 0.02$ , $A_S/A_N = 0$ db . . . . .	71
4-25	Butterworth Plus Three Sinewaves Data, $A_1/A_N = A_2/A_N = A_3/A_N = 0$ db . . . . .	72
4-26	Butterworth Plus Three Sinewaves Data, $A_1/A_N = 6$ db, $A_2/A_N = 0$ db, $A_3/A_N = 12$ db . . . . .	73

# ILLUSTRATIONS (CONTINUED)

<u>Figure</u>		<u>Page</u>
4-27	Butterworth Plus Three Sinewaves Data, $A_1/A_N=A_2/A_N=A_3/A_N=12$ db .	74
4-28	Butterworth Plus Three Sinewaves Data, $A_1/A_N=A_2/A_N=A_3/A_N=12$ db; $f_1/f_d=2$ . . . . .	75
4-29	Continuous with Step Butterworth Shaped Gaussian Data, 100% Duty Cycle . . . . .	77
4-30	Bandpass Gaussian Data with 24 db/oct. Slopes . . . . .	78
4-31	Photographs of Data, BWT Interpolation Filter Output, and Sampler Output. - Equi-Probable Amplitude Distribution, 100% Duty Cycle .	79
4-32	Photographs of Data and BWT Interpolation Filter Output. Gaussian Probability Distribution, $t_1 f_1=0.02$ . . . . .	80
4-33	Spectra of Noise Sources . . . . .	83
4-34	Single Channel System Spectra, Data: Gaussian Amplitude Probability Distribution . . . . .	84
4-35	Single Channel System Spectra, Data: Equi-Probable Amplitude Distribution . . . . .	85
4-36	Spectra of Butterworth Shaped Data, Gaussian Amplitude Probability Distribution . . . . .	86
4-37	RMS Error vs. $S/k_1 F_s^{1/2}$ . Interpolation Filter: Butterworth, 24 db/oct. Data: Butterworth, J=4 and 5 . . . . .	89
4-38	RMS Error vs. $S/k_1 F_s^{1/2}$ . Interpolation Filter: Butterworth, 24 db/oct. Data: Butterworth, J=7 and 8 . . . . .	90
4-39	RMS Error vs. $S/k_1 F_s^{1/2}$ . Interpolation Filter: Butterworth, 36 db/oct. Data: Butterworth, J=4 and 5 . . . . .	91
4-40	RMS Error vs. $S/k_1 F_s^{1/2}$ . Interpolation Filter: Butterworth, 36 db/oct. Data: Butterworth, J=7 and 8 . . . . .	92
4-41	PAM-FM, RMS Error vs. $S/k_1 F_s^{1/2}$ , RMS Deviation $f_D/\frac{1}{2}B=0.4$ . . . .	93
4-42	Photographs of Multiplexer Output Waveform . . . . .	94
4-43	Photographs of Decommutator Input and Output Waveforms . . . . .	95
5-1	Block Diagram - General Test Setup . . . . .	97
5-2	Filter Response - SKL Model 308, 24 db/oct . . . . .	100
5-3	Filter Response - SKL Model 308, 42 db/oct . . . . .	101
5-4	Multiplex Block Diagram, AL-1 . . . . .	102
5-5	Amplifier, AL-3 . . . . .	104
5-6	Commutator Switch, AL-4 . . . . .	105
5-7	Gate and Holding Circuit, AL-5 . . . . .	106
5-8	Trigger Generator, AL-6 . . . . .	107
5-9	Flip-Flop, AL-7 . . . . .	108
5-10	Multiplexer Gate Generator, AL-8 . . . . .	109
5-11	Sample Gate Generator, AL-9 . . . . .	110
5-12	Decommutator Block Diagram, AL-2 . . . . .	113
5-13	Delay Network, AL-10 . . . . .	115
5-14	Decommutator Gate, AL-11 . . . . .	116
5-15	Decommutator Gate and Holding Circuit . . . . .	117
5-16	Trigger Generator, AL-13 . . . . .	118
5-17	Gate Generator or Delay, AL-14 . . . . .	119
5-18	Frequency Divider, AL-15 . . . . .	120

# ILLUSTRATIONS (CONTINUED)

<u>Figure</u>		<u>Page</u>
5-19	Filter Response - BWT, 60 db/oct . . . . .	123
5-20	Filter Response - EMR 95D, Gaussian Characteristic, 24 db/oct . .	124
5-21	Filter Response - 4-pole Butterworth Filter, 24 db/oct . . . . .	125
5-22	Filter Response - 6-pole Butterworth Filter, 36 db/oct . . . . .	126
5-23	Block Diagram - Analog Error Comparator . . . . .	128
Al-1	Block Diagram of N Channel PAM System . . . . .	Al-2
Al-2	Simplified Block Diagram for a Single Channel . . . . .	Al-4
Al-3	Simplified Block Diagram for Signal Only . . . . .	Al-5
Al-4	Multiplier which is Equivalent to Sampling . . . . .	Al-7
Al-5	Block Diagram for Crosstalk Analysis . . . . .	Al-8
Al-6	Block Diagram for Noise Analysis . . . . .	Al-9
Al-7	Video Attenuation Factors . . . . .	Al-17

## PURPOSE

### OBJECTIVE

The objective is to provide telemetry users with a quantitative set of experimentally proven operating parameters which can be utilized to avoid a significant source of telemetry data error (aliasing error) in time-division telemetry systems.

### TASKS

Specific efforts undertaken in the conduct of this program were:

#### 1. Determination of Typical Data Spectra

A study was conducted of actual data signals to determine typical spectral characteristics.

#### 2. Extension of Past Analyses

An extension of past analyses was performed to better predict aliasing errors in actual time-division telemetry systems.

#### 3. Laboratory Measurements

Laboratory measurements were conducted on actual systems to verify and extend theoretical understanding of the error mechanisms in time-division telemetering.

Consideration was given to a number of practical design parameters in addition to the specific areas of effort described above. Examples of parameters considered include: 1) data sampling rate, 2) sampling aperture duty cycles, 3) data spectral cutoff rate, 4) interpolation filter cutoff rate, and 5) the interpolation filter bandwidth normalized with respect to the data bandwidth. Of particular interest are the test results from a 100% duty cycle PAM sampled data system. This system employed essentially instantaneous data samples which were converted to 100% duty cycle pulses. The original data was reconstructed from a multi-channel system by use of a 60% aperture sampler followed by an interpolation filter.

## SECTION 1

### SUMMARY

#### 1.1 PROGRAM OBJECTIVES

A study program was conducted to 1) evaluate the effect of errors arising from "aliasing" of data signal spectra by a sampling process 2) investigate the relationship between the aliasing error and distortion error produced by an interpolation filter, and 3) derive a practical understanding of and a proven basis for predicting the error mechanisms involved in the acquisition, transmission and reconstruction of data signals by means of a sampled-data telemetry system.

In the course of a telemetry system study recently concluded (see Reference 1) it was found that little information of a practical design nature existed which took into account the aliasing and interpolation distortion error on overall system accuracy. The complexity of present day telemetry instrumentation with the inevitable requirement for handling tens or hundreds of channels of information makes the use of time-division multiplexing almost universal, sometimes in conjunction with frequency multiplexing.

When the proper operating parameters are not certain it is common practice to assign sampling rates and other design parameters thought to be conservative from the standpoint of minimizing data recovery errors. However, conservatism carries with it performance penalties involving excessive RF spectrum bandwidth and power requirements. The net result of inadequate knowledge regarding proper selection of equipment design parameters is to impose inequitable assignment of error tolerances throughout instrumentation systems. This results in excessively stringent specifications on equipment in some areas and lack of adequate performance in others. This, in turn, leads to system designs which are excessively sensitive to small changes in equipment performance.

---

Manuscript released by the authors 30 September 1961 for publication as an ASD Technical Report.

Telemetry systems are currently designed by assuming the data source has a known bandwidth. The spectral shape of the data source is rarely taken into account. This has led to excessively conservative designs in addition to the simple fact that accuracy cannot be adequately predicted even on the basis of knowing that conservative design practice has been followed.

Detail consideration of the source of design difficulty discussed above led to the program described by phase in the following paragraphs.

## 1.2 DATA SPECTRA SURVEY

Considerable qualitative information was found as discussed in Section 2. These data were classified into five spectral types which served as models for the analytical and experimental work. A compilation was made of available data on telemetry data spectra from information gained by means of a literature search, telephone inquiries, letter inquiries, and personal contacts.

## 1.3 ANALYSIS

Two new analytical tasks were carried out. One consisted of a general PAM system analysis including such practical effects as finite sampling width, crosstalk, and noise. It specifies, in general form, the optimum sampling rate, and the optimum transfer functions, both realizable and non-realizable, for the data and interpolation filters. The other analytical work was an extension of past analyses to include the effects of practical filter transfer functions, and the effects of interpolating 100% duty cycle pulsetrains as well as impulse or short duty cycle pulsetrains. This work was programmed and a limited amount of computation performed with an IBM-709 computer. The analytical work is described in Section 3.

## 1.4 EXPERIMENTAL EVALUATION PROGRAM

Laboratory tests were performed on two systems which give information useful in design of a time-division multiplexed telemeter to handle the expected data types. The majority of tests were carried out with a single channel PAM system using no carrier since this simplified model includes the parameters of importance to interpolation error which can be considered to be composed of aliasing and distortion errors. At the same time the simplified model removes error sources which would

otherwise obscure the relationships of interest.

Selected tests were also performed on an 8 channel PAM-FM system with noise added so that all basic system error mechanisms were present. The overall system error was determined as a function of the signal-to-noise ratio. It was verified that overall performance of such a system can be accurately estimated by combining the interpolation error from single channel tests with the pulse sampling error resulting from all the other error sources in the system. Pulse sampling error may be determined for the three common time-division systems from information obtained in Reference 1 or a similar source of data. The experimental program is described in Section 4. The experimental test setup and equipment used are described in Section 5.



## SECTION 2

### DATA SPECTRA SURVEY

A survey was undertaken to determine typical spectral characteristics of actual data signals originating from information sources. Knowledge of the power spectral density of the information channels is important since the interpolation error is strongly dependent on the spectra of the data being sampled. A literature search, inquiries by telephone and letter, and personal contacts were made to gather the data which were then categorized into five basic spectral types. A broad range of general data was uncovered; however, specific details of data characteristics were usually missing. This led to recovery of a large amount of information not amenable to reduction to specific characteristics in the form of tabulated results. Therefore, a summary of the most useful references and sources is included in Appendix 3.

#### 2.1 BASIS FOR DATA SPECTRA SURVEY

A data channel, as an information source, is completely specified when the a priori symbol probability distribution and the average rate of symbol generation is defined. Interpretation of the term "symbol" is determined by the physical representation of symbols by the channel in question. These symbols may be discrete, continuously variable, or a composite of discrete and continuous states of a physical parameter. The corresponding probability distributions associated with the possible states of an information channel may be discrete, continuous or correspond to a mixed process. Selection of the method of representing a symbol, and the mechanism of changing from one symbol to another coupled with the probability distribution of the symbols permits calculation of the power spectral density of the information source. Since the power spectral density of an arbitrary waveform can be calculated from the first and second moments of the "symbol" probability distribution it is evident that the power spectral density of an information channel is specified by  $\bar{a}$ ,  $\bar{a}^2$ ,  $S(t, a)$  where  $\bar{a}$ ,  $\bar{a}^2$  are the first and second moments of the physical parameter representing the state of the information source,  $S(t, a)$  the function of time acting as a vehicle for carrying the symbol states through the communication link.

In practice, it is a matter of definition of what constitutes the point in a telemetry link where information is generated. For practical instrumentation this corresponds to the output of a transducer of a specified type. Hence the function,  $S(t,a)$  is well-defined in each individual application.

Conduct of the data survey was based on the fact that transducer characteristics are strongly established and therefore should generate spectra typical of the instrumentation application.

The effect on power spectral density by the information source is reflected by the distribution of energy over the passband of the transducer. In those cases where the transducer and telemetry link do not constitute important limits on spectral distribution of the observed source it is reasonable to use observed instrumentation data to determine the spectra generated by the data source.

## 2.2 SURVEY DATA COLLECTION

It was originally thought that much of the information on data spectra could be obtained through ASTIA in report form. The plan was to classify the data source as to transducer, missile type and transducer application, thereby obtaining a small number of representative spectra which could be simulated in the laboratory as typical data spectra. This would lead to realistic system operating parameters for reconstructing the transducer outputs to within a specified accuracy. This, in turn, permits recovery of the data symbol "a" to within a specified accuracy.

Early in the program the ASTIA bibliographies listed in Appendix 4 were ordered, obtained and examined. From several thousand bibliography cards examined about 20 reports were estimated to have the type of information on data spectra desired. The classified reports were not ordered because of security restrictions on the present contract. It is interesting to note that the majority of useful reports which have been examined were not listed in the ASTIA bibliographies. Several reasons for lack of information available through ASTIA are: 1) it is difficult to determine the proper ASTIA descriptors; and 2) the reports which appear in ASTIA files are intended to be of general usefulness and often do not include detail information on data spectra.

Additional sources of information concerning data spectra were needed and found. Important data was derived from instrumentation established by Aeronutronic on the Shillelagh and Blue Scout missile programs. It was surmised that much of the needed information existed in the form of internal memoranda and reports at various companies and military test ranges. A survey letter was prepared and mailed directly to personnel in 22 companies and 4 military test ranges requesting information on data spectra. A very limited number of replies have been obtained to date.

Several problems arise in evaluating the data spectra available in the reports obtained. These are: 1) determining the extent to which the data spectra has been modified by the transmission system used to telemeter the data when little or no mention is made of the transmission system used, 2) establishing a means of comparison of data spectra measured by different techniques which are not usually discussed and 3) most of the data spectra available is for vibration data and acoustic noise. Information about other flight test data spectra such as: Acceleration, Temperature, Pressure, Stress and Strain, Velocity, Scientific Measurements, etc. is not generally available. The same problems were encountered in another study discovered during this survey carried out by Fairchild Engine and Aircraft Corporation. Their work was summarized in a report entitled "Study and Evaluation of In-Flight Guided Missile Environmental Data", Final Report, 15 December 1958, Fairchild Engine and Aircraft Corporation, ASTIA No. AD 306 231.

In spite of the limitations in much of the data collected, it is believed this is a representative sample of that available and it is sufficiently varied to permit classification into typical spectral types permitting the simulation of data spectra for the laboratory tests.

One problem noted above, that of modification of the data spectrum by the transmission system, can be largely removed by wire line transmission in tie-down tests. One test report referenced in Appendix 3 describes a tie-down test with measurements of vibration and electrical circuit noise. The data shown indicates a significant percentage of energy exists up to and beyond 6,000 cps for both data types. Therefore, in many tests it must be assumed that the high frequency content of data signals such as vibration, and electrical and acoustical noise are limited by the telemetry system.

Survey results have been reduced in usefulness from lack of information regarding the spectral distribution of data channels requiring moderate to low frequency response. This is perhaps natural but prevents deducing the correctness of spectral models derived from consideration of the nature of the data sources and the good survey results involving mechanical vibration, acoustic vibration and other noise-like wideband data. In general, a good survey sampling was obtained for wideband data signals which currently account for most of the system bandwidth in telemetering systems.

Future extension of knowledge concerning the underlying mechanisms generating the low frequency data channels would permit better telemetering system performance and at the same time gain the benefit of significant RF bandwidth reduction.

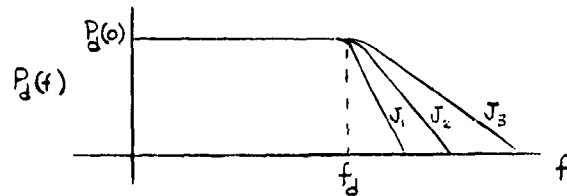
### 2.3 DATA SPECTRA

It was found that regardless of source, spectral characteristics of data reported or predicted can be categorized into five types of spectra defined by a set of parameters with variation of individual parameters permitted within each type. The classifications do not exhaust all possibilities; however, few spectra will be encountered which cannot be realistically represented by the types defined. Thought was given to categorizing the data type according to the data source, e.g. structures data (vibration, stress, strain), aerodynamic (velocity, acceleration, position), environment, subsystem performance, and so on. However, this method of classifying did not appear useful to the study or control of interpolation errors in system design and applications. The spectral shape of the data is of prime importance to the interpolation error and a given data source may not always exhibit the same spectrum. For instance, it was found that vibration and some acoustic noise data spectra can be represented by band-limited white noise with various cutoff ratios (db/oct.) for most liquid fuel rockets or missiles, while solid and some liquid fuel rockets have vibration and acoustic noise spectra exhibiting a comb spectral structure.

Practical reasons limit consideration to and definition of five general spectral types discussed below. These types were simulated in the laboratory for conducting the experimental test program.

The spectral types are considered to be models of the spectra generated by the various data sources. Only positive frequencies are shown. Classification of a data source by the telemetry design and/or instrumentation engineer permits entry and use of the parametric error curves presented in Section 4.

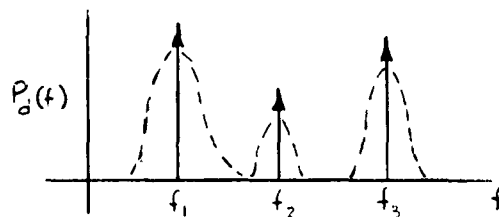
#### TYPE I - Continuous Spectrum



This is a continuous spectrum flat over the passband defined. The cutoff characteristic is parameterized and permitted to attenuate at  $6J$  db/octave where  $J$  is a positive integer.

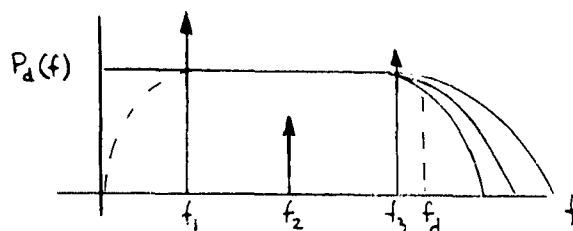
Actual data sources usually have a low frequency cutoff. This has little effect on the accuracy of interpolation or reconstruction of the source signal. The skirt characteristic beyond the cutoff frequency largely controls the seriousness of interpolation. This is considered the most important data type for general consideration since it is a common one encompassing the wideband noise-like data sources. This type represents much of the vibration and acoustic noise data observed in liquid fuel missiles, and gust turbulence which is independent of the vehicle considered. The skirt cutoff rate should be estimated by the instrumentation engineer from information supplied to him by the applicable technical groups, since data filtering is invariably used to attenuate transducer resonances and to prevent overmodulation. The chosen parameter  $J$  then defines the cutoff rate of the source spectrum determined by the application. Thus, two parameters ( $f_d, J$ ) define the spectral shape. Commonly encountered ranges for these parameters are  $0 \leq f_d \leq 10,000$ ;  $1 \leq J \leq 8$ .

## Type II - Discrete Spectra



This spectrum is made up of a sum of discrete spectral lines. Data with narrow passband (comb) characteristics may be represented by such a discrete spectrum. Data sources of this type typically have less than 12 spectral components of importance with 1 to 3 components usually being very dominant. This type is typical of vibration and noise data where strong resonances are excited. In the majority of cases some energy is observed between discrete spectral lines where structural or acoustical cavity resonances have been excited. This results in addition of spectral Type I with Type II which produces a mixture of a continuous and a comb spectrum. This results in a Type III spectrum. It was predicted and confirmed experimentally that when the energy in the continuous spectrum of data Type III drops well below the energy in the comb spectrum and the continuous spectrum cutoff frequency is not above the highest spectral line frequency the interpolation error and the system parameters are essentially determined by the comb portion of the spectrum. In this case data Type III can be simplified to Type II.

## Type III - Continuous Plus Discrete Spectrum



A Type III spectrum is the sum of a continuous and a discrete spectrum. The spectral model is defined by the frequencies of the discrete spectral lines, the relative power in each line, the cutoff frequency of the continuous spectrum and the cutoff characteristic. In addition, one more parameter is required, the ratio of power in the discrete to the power in the continuous spectrum. This defines the relative levels of the energy. Restricting attention to the most

important cases where the dominant spectral lines are 3 or less in number permits use of five or less parameters as  $(f_d, J, \alpha_1, \alpha_2, \alpha_3)$  to specify the model where  $\alpha_1, \alpha_2, \alpha_3$  are defined as:

$$\alpha_1 = \frac{P_1}{P_c}$$

$$\alpha_2 = \frac{P_2}{P_c}$$

$$\alpha_3 = \frac{P_3}{P_c}$$

$P_c$  = power in continuous spectrum

$P_i$  = power in  $i$ th spectral line

The set of five parameters define the model completely except the total power  $P_T$  of the spectrum which is expressed by the equation:

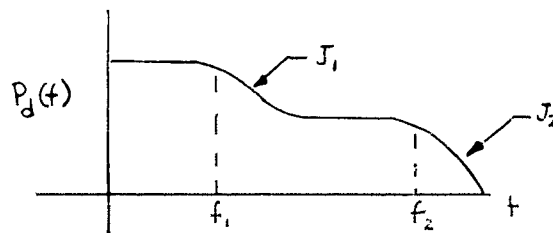
$$P_T = P_c + \sum_{i=1}^3 P_i = P_c (1 + \alpha_1 + \alpha_2 + \alpha_3)$$

This is an arbitrary parameter which does not effect the internal structure of the model.

Type III spectra often occur where a broadband noise-like energy source excites system resonances. It has been found that some engines and boosters, and gust turbulence are essentially white noise energy sources. When these sources excite structural resonances Type III spectra are seen in vibration and acceleration measurements.

A Type IV spectrum has a continuous power spectral density with a shape determined by two critical frequencies as illustrated in the diagram below.

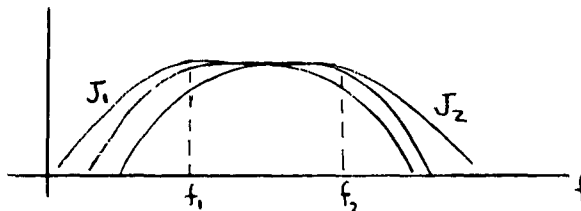
Type IV - Continuous - With Step



It does not appear worthwhile to consider and define spectral types having more than one transition from one constant level of spectral power density to another. This spectral type is defined by specifying the two critical frequencies, the transition attenuation slope  $J_1$ , the final rate of attenuation  $J_2$ , and the ratio of power residing in the two frequency bands (  $0 - f_1$  ) and (  $f_2 - \infty$  ). Thus, five parameters define the structure of the spectrum.

Type IV describes actual data sources having much of their energy in the lower frequency region where it is essentially flat. The other portion of the data spectrum of lower energy but still having significant energy relative to that in the low frequency region may extend up 1 or more octaves beyond the first critical frequency. This is thought to be a good model for many data types which are essentially low frequency functions but which have significant higher frequency perturbations. Examples are accelerations with vibration effects superimposed, and fuel and exhaust pressures with added engine and pump pulsations, or remote signal strength measurements with fading and multipath effects. This can also be considered a useful model for continuous spectra with high frequency de-emphasis. Some acoustic data looks like this, peaking near the low end and rolling off above.

#### Type V - Bandpass Spectrum



Type V are continuous bandpass spectra illustrated in the accompanying figure. This type may be considered a close relative of Type IV since transition from the first spectral region (  $0 - f_1$  ) to the second (  $f_1 - f_2$  ) is characterized by a rise in spectral power density.

Four parameters define the spectrum. These are the two critical frequencies (  $f_1$  and  $f_2$  ) the rising slope  $J_1$  up to  $f_1$  and the falling slope  $J_2$  starting at  $f_2$  and continuing beyond. Symmetric bandpass characteristics may usually be assumed which makes  $|J_1| = |J_2|$  and the parameters are reduced to three.



In this data type the energy is concentrated in a bandpass region of sometimes only one octave or even less. This data type is not too frequently instrumented so that less emphasis was given it. However, some experimental measurements were made since it is an easily distinguished data type. Data of this nature was found in the measurement of electrical and microphonic noise in electronic circuits. Some of the data found were actually the outputs of bandpass filters in the electronics. The others were wider band but still of a bandpass nature.

### SECTION 3

#### ANALYSIS

The prime objective of the present study has been to provide a quantitative set of experimentally proven operating parameters which can be utilized to avoid a significant source of telemetry data error due to imperfect interpolation in sampled data systems.

The number of methods for implementing each major element of a sampled data system are usually restricted by practical equipment design considerations. Moreover, it is evident from a review of the possible combinations of techniques capable of being used in a single system that a few specific configurations must be assumed for analysis. These configurations can then be optimized in performance experimentally as well as by analysis. Experimental departure from theoretical results, upon evaluation, displays clearly 1) the limitations of equipment and 2) limitations of the assumptions on which the analysis is based. Consequently, analysis conducted in this program served to supplement and guide the experimental program as well as to point out new possibilities worth further investigation.

A general PAM system analysis was first performed to serve as the basis for an optimum system design. The following summarizes the results of the PAM analysis which appears in Appendix 1:

- a) A simplified system model which includes the effects of finite bandwidth, finite sampling width, aliasing, cross-talk, and noise is developed for an N-channel system.
- b) A general expression for the total mean square error due to all the above effects is obtained.

- c) The error minimization is carried out for the special case in which all channels are identical and a signal power constraint is imposed.
- d) The optimum transfer functions, both realizable and non-realizable, are obtained for the data filter and the interpolation filter. In general, these transfer functions are bandlimited and can only be approximated in the practical case.
- e) The optimum sampling rate is specified in terms of the filter transfer functions.
- f) The optimum sampling delay is specified in terms of the video filters and the design of these filters to reduce crosstalk is mentioned.

From this analysis, it was found that the many parameters and error mechanisms of a multichannel radio transmission system obscures the fundamental aspects of interpolation which are of primary interest in this study. For this reason the general PAM analysis appears in Appendix 1 for reference and certain of the results are applied to the analysis of a simplified model which follows in this section.

Since the errors due to interpolation are independent of the video and carrier modulation methods, the simplified model analyzed in this section considers a single channel system and omits the carrier portion of the system. The results obtained here for interpolation errors can be applied to any sampled data system (e.g. PAM, PDM, PCM) and combined with the other error sources for a particular system (which can be obtained from the results of the Telemetry System Study, Reference 1) to obtain overall system performance.

The simplified system model is described in Section 3.1. Section 3.2 discusses the analysis of fractional duty cycle sampling; while Section 3.3 presents the analysis for 100% duty cycle sampling. The computer program utilized to evaluate some of the integrals obtained in the analysis is discussed in Section 3.4 with the computer results.

"Alias-Free" sampling is discussed in Reference 16. However, the method of implementing the sampling technique and interpolation for practical instrumentation is not known at this time. Further investigation in this direction appears worthwhile.

### 3.1 SYSTEM MODEL

The general system shown in Figure A-1-1 can be simplified as shown in Figure 3-1. This also represents the experimental single channel sampled data system.

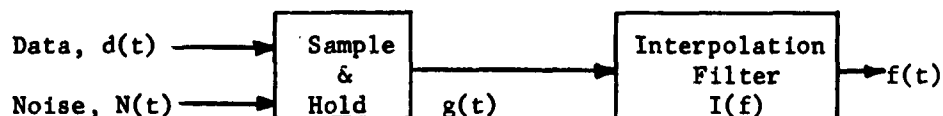


Figure 3-1 Simplified Single Channel Sampled Data System

The input data is considered to be the input to the sample and hold unit. The effects of data filtering are included in the analysis, but are not evaluated separately. The model also allows noise to be introduced with the data.

The sampling unit gates out a time sample  $t_1$ , fixed relative to the sampling period  $T_s$  of the incoming signal for fractional duty cycle sampling; the hold unit permits up to 100% duty cycle, i.e. a short time sample is obtained using the sampler; this sample is held by the hold unit until the next sample is made. Thus a 100% duty cycle PAM wavetrain can be obtained.

The interpolation filter provides an output which approximates the data input delayed a time  $t_0$ .

The data being sampled is assumed to be a stationary, random amplitude function of time, and uncorrelated with the noise.

The data characteristics considered most important are 1) the first order probability distribution and 2) the data spectrum. No constraint is applied to the data spectrum, i.e., it may have any shape desired.

The symbols introduced above and throughout this Section are defined in a glossary of symbols at the end of the section.

### 3.2 INTERPOLATION OF FRACTIONAL DUTY CYCLE PULSETRAIN

The following determines the normalized rms error between the interpolation filter output and the data input with added noise interference. The rms error is determined and the analysis is performed in the frequency domain with power spectra. Analysis is based on the data sampling process being performed by a multiplicative aperture although many other types of apertures may be considered.

#### 3.2.1 Power Spectrum of Sampler Output

The multiplicative sampling aperture is defined to be equivalent to taking the product of  $[d(t) + N(t)] \cdot s(t) = g(t)$ , where  $s(t)$  is the sampling function generating the apertures shown in Figure 2-3.

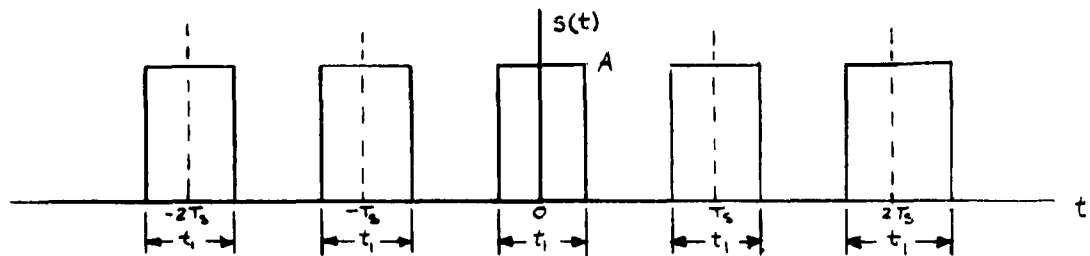


Figure 3-2 The Sampling Function,  $s(t)$

The power spectrum of  $s(t)$  is determined in Appendix 2 and is given by the expression:

$$P_s(f) = A^2 \left(\frac{t_1}{T_s}\right)^2 \sum_{n=-\infty}^{\infty} \left[ \frac{\sin(\pi n \frac{t_1}{T_s})}{\pi n \frac{t_1}{T_s}} \right]^2 \delta(f - \frac{n}{T_s}) \quad 3-1$$

note that if  $A = \frac{1}{t_1}$  and  $t_1 \rightarrow 0$ , then  $s(t)$  becomes an ideal sampling function, i.e., a train of delta functions. The power spectrum for this case becomes

$$P_s(f) = \frac{1}{T_s^2} \sum_{n=-\infty}^{\infty} \delta(f - \frac{n}{T_s}) \quad 3-2$$

The power spectrum of the sampler output with  $h(t) = d(t) + N(t)$  as the input and  $s(t)$  as the sampling function with  $A = 1$  is derived in Appendix 2. The result is:

$$\begin{aligned}
 P_g(f) &= \left(\frac{t_1}{T_s}\right)^2 \sum_{n=-\infty}^{\infty} C_n^2 P_h\left(f - \frac{n}{T_s}\right) \\
 &= \left(\frac{t_1}{T_s}\right)^2 \sum_{n=-\infty}^{\infty} C_n^2 \left[ P_d\left(f - \frac{n}{T_s}\right) + P_N\left(f - \frac{n}{T_s}\right) \right]
 \end{aligned}
 \tag{3-3}$$

where

$$C_n = \frac{\sin(\pi n \frac{t_1}{T_s})}{\pi n \frac{t_1}{T_s}}$$

Figure 3-3 illustrates the spectrum at the sampler output.

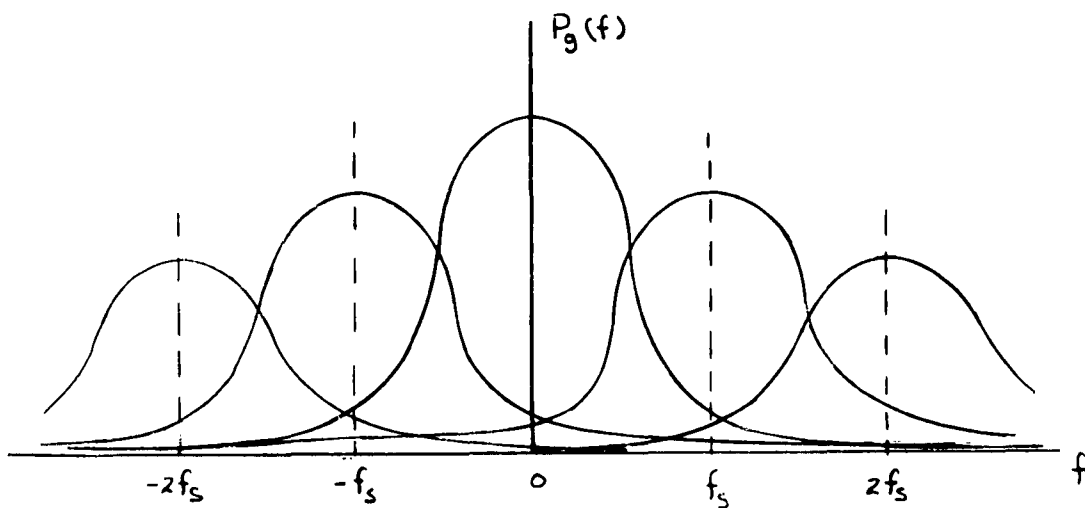


Figure 3-3 Power Spectrum at Sampler Output

The effect of the sampling function is exaggerated in the figure for illustration. Note that two effects may be noted: 1) replicas of the original data and noise spectra are repeated at all multiples of  $f_s$  2) the replicas of the noise spectra retain their additivity with the data spectra. Data aliasing errors occur due to interference with the desired data spectrum by these data and noise sideband spectra extending downward and upward in frequency from the data and noise spectral replicas centered about  $\pm f_s, \pm 2 f_s, \dots$  which lie within the passband of the data interpolation filter centered about  $f=0$ . The aliasing spectrum is given by:

$$P_A = \left(\frac{t_i}{T_s}\right)^2 \sum_{n=-\infty}^{\infty} C_n^2 \left[ P_d\left(f - \frac{n}{T_s}\right) + P_N\left(f - \frac{n}{T_s}\right) \right], \quad n \neq 0 \quad 3-4$$

The effects of linear data filtering can be considered if  $P_d(f)$  is replaced with

$$P_d(f) |D(f)|^2 \quad 3-5$$

where

$P_d(f)$  is the data input power spectrum.

$|D(f)|^2$  is the square of the magnitude of the data filter transfer function.

Derivations of optimum data filters are given in Appendix 1 and by Spilker, reference 18.

### 3.2.2 Power Spectrum of Interpolation Filter Output

The power spectrum of the interpolation filter input can be written as

$$P_g(f) = P_d'(f) + P_N'(f) \quad 3-6$$

where

$$P_d' = \left(\frac{1}{T_s}\right)^2 \sum_{n=-\infty}^{\infty} C_n^2 P_d\left(f - \frac{n}{T_s}\right)$$

$$P_N' = \left(\frac{1}{T_s}\right)^2 \sum_{n=-\infty}^{\infty} C_n^2 P_N\left(f - \frac{n}{T_s}\right)$$

The power spectrum of the interpolation filter output is

$$P_f(f) = P_g(f) |I(f)|^2$$

$$= P_d' |I(f)|^2 + P_N' |I(f)|^2$$
3-7

where

$|I(f)|^2$  is the square of the magnitude of the interpolation filter transfer function.

### 3.2.3 Normalized RMS Error

The normalized rms interpolation error is defined as

$$E = \frac{\sigma_e}{\sigma_d}$$
3-8

where

$$e(t) = f(t) - d(t - t_0)$$
3-9

with  $f(t)$  and  $d(t)$  subject to the constraint

$$\overline{f^2(t)} = \overline{d^2(t - t_0)}$$
3-10

The constraint normalizes the error simultaneously with respect to the data input and interpolated output in terms of a reference power level. This constraint is imposed automatically on an experimental basis to prevent normalization errors and to minimize the interpolation error reading.  $\sigma_e$  is defined by:

$$\sigma_e^2 = \overline{e^2(t)} = \int_{-\infty}^{\infty} P_e(f) df$$
3-11



In addition, the following relations are assumed:

$$\overline{d(t)} = \overline{f(t)} = \overline{\epsilon(t)} = 0 \quad 3-12$$

The mean values are assumed to be zero to simplify the analysis; however, this does not limit the generality of results obtained, since the assumption that  $\overline{d(t)}=0$  and  $\overline{f(t)}=0$  amounts to a d.c. shift in data signal reference level.

The power spectrum of the error is determined by means of the Fourier transform of  $\epsilon(t)$  which can be written as:

$$\begin{aligned} F_{\epsilon}(f) &= \int_{-\infty}^{\infty} \epsilon(t) e^{-j\omega t} dt \\ &= F_f(f) - F_d(f) e^{-j\omega t_0} \\ &= \left(\frac{t_1}{T_s}\right) \left\{ \sum_{n=-\infty}^{\infty} c_n \left[ F_d\left(f - \frac{n}{T_s}\right) + N\left(f - \frac{n}{T_s}\right) \right] \right\} K I(f) - F_d(f) e^{-j\omega t_0} \end{aligned} \quad 3-13$$

where

$F_d(f)$  is the Fourier transform of the data input and  
 $N(f)$  is the Fourier transform of a member of the ensemble of possible input noise functions.

The above can be re-written in the following form:

$$\begin{aligned} F_{\epsilon}(f) &= \left(\frac{t_1}{T_s}\right) F_d(f) \left\{ K I(f) - e^{-j\omega t_0} \left(\frac{T_s}{t_1}\right) \right\} \\ &\quad + K I(f) \left\{ \left(\frac{t_1}{T_s}\right) N(f) + \left(\frac{t_1}{T_s}\right) \sum_{n \neq 0} c_n \left[ F_d\left(f - \frac{n}{T_s}\right) + N\left(f - \frac{n}{T_s}\right) \right] \right\} \end{aligned}$$

This equation may be rewritten in terms of the absolute value and phase angle of the data, noise and interpolation filter. These are denoted by  $\theta_d(f)$ ,  $\theta_N(f)$ , and  $\theta_I(f)$  respectively.

The resulting expression is:

$$F_e(f) = \left(\frac{t_1}{T_s}\right) |F_d(f)| e^{-j\theta_d(f)} \left\{ K |I(f)| e^{-j\theta_i(f)} - e^{-j2\pi f t_0} \left(\frac{T_s}{t_1}\right) \right\} \quad 3-14$$

$$+ K |I(f)| e^{-j\theta_i(f)} \left\{ |N(f)| e^{-j\theta_n(f)} + \left(\frac{t_1}{T_s}\right) \sum_{n \neq 0} C_n \left[ |F_d(f - \frac{n}{T_s})| e^{-j\theta_d(f - \frac{n}{T_s})} + |N(f)| e^{-j\theta_n(f - \frac{n}{T_s})} \right] \right\}$$

The error power spectral density is obtained by means of the relation:

$$P_e(f) = \lim_{T \rightarrow 0} \frac{1}{T} \overline{|F_e(f)|^2} \quad 3-15$$

where the bar denotes an ensemble average.

Thus,

$$P_e(f) = \left(\frac{t_1}{T_s}\right)^2 P_d(f) \left\{ K^2 |I(f)|^2 - 2 \left(\frac{t_1}{T_s}\right) K |I(f)| \cos(\theta_i(f) - 2\pi f t_0) + \left(\frac{T_s}{t_1}\right)^2 \right\} \quad 3-16$$

$$+ K^2 |I(f)|^2 \left\{ \left(\frac{t_1}{T_s}\right)^2 \sum_{n \neq 0} C_n^2 \left[ P_d(f - \frac{n}{T_s}) + P_n(f - \frac{n}{T_s}) \right] + \left(\frac{t_1}{T_s}\right)^2 P_n(f) \right\}$$

where K is a gain constant associated with the interpolation filter to satisfy the constraint that

$$\sigma_f^2 = \sigma_d^2$$

The cross correlation between data, noise and sampling functions are all assumed to be zero.

The optimum linear interpolation filter transfer function minimizing  $\sigma_e^2$  can be determined by the calculus of variations.

The result is:

$$K |I(f)| = \frac{\left(\frac{t_1}{T_s}\right) P_d(f)}{\left(\frac{t_1}{T_s}\right)^2 [P_d(f) + P_N(f)] + \left(\frac{t_1}{T_s}\right)^2 \sum_{n \neq 0} \left[ P_d\left(f - \frac{n}{T_s}\right) + P_N\left(f - \frac{n}{T_s}\right) \right]} \quad 3-17$$

where

$$\theta_I(f) = 2\pi f t_0$$

A derivation of this result is performed in reference 18 and is not repeated here. It should be noted that the noise is not sampled in the referenced material whereas Equation (3-17) assumes sampling of the noise by the sample and hold unit. When the noise is added following the sampling process it is accounted for by deleting the summation of noise terms in Equation (3-17) and replacing the sum with the unsampled noise power spectrum.

The effects of non-optimum interpolation filters are of interest since the interpolation filter is difficult and frequently not possible to synthesize for non-trivial data spectra. Therefore, the optimum solution for  $|I(f)|$  will not be used. However,  $\sigma_e^2$  is minimized when  $\theta_I(f) = 2\pi f t_0$ . The phase characteristic of a well designed interpolation filter is approximately linear over the passband accounting for the average system time delay.

The mean square error is:

$$\sigma_e^2 = \int_{-\infty}^{\infty} P_e(f) df \quad 3-18$$

subject to the constraint that  $\sigma_f^2 = \sigma_d^2$

where

$$\sigma_f^2 = \int_{-\infty}^{\infty} P_f(f) df \quad 3-19$$

$$\sigma_d^2 = \int_{-\infty}^{\infty} P_d(f) df \quad 3-20$$

Let

$$\sigma_{NI}^2 = \int_{-\infty}^{\infty} \left[ \sum_{n=-\infty}^{\infty} C_n^2 P_n(t - \frac{n}{T_s}) \right] |I(t)|^2 dt \quad 3-21$$

$$\sigma_A^2 = \int_{-\infty}^{\infty} \left[ \sum_{n \neq 0} C_n^2 P_d(t - \frac{n}{T_s}) \right] |I(t)|^2 dt \quad 3-22$$

$$\sigma_{dI}^2 = \int_{-\infty}^{\infty} P_d(t) |I(t)|^2 dt \quad 3-23$$

Then

$$K^2 \left( \frac{t_1}{T_s} \right)^2 \left[ \sigma_{NI}^2 + \sigma_A^2 + \sigma_{dI}^2 \right] = \sigma_d^2 \quad 3-24$$

or

$$K^2 = \frac{\sigma_d^2}{\left( \frac{t_1}{T_s} \right)^2 \left[ \sigma_{NI}^2 + \sigma_A^2 + \sigma_{dI}^2 \right]} \quad 3-25$$

Substitution of (3-21), (3-22) and (3-23) into (3-16) gives:

$$\sigma_e^2 = K^2 \left( \frac{t_1}{T_s} \right)^2 \left[ \sigma_{NI}^2 + \sigma_A^2 + \sigma_{dI}^2 \right] + \sigma_d^2 - 2 \left( \frac{t_1}{T_s} \right) K \int_{-\infty}^{\infty} P_d(t) |I(t)| dt \quad 3-26$$

$$E^2 = K^2 \left( \frac{t_1}{T_s} \right)^2 \left[ \frac{\sigma_{NI}^2 + \sigma_A^2 + \sigma_{dI}^2}{\sigma_d^2} \right] + 1 - 2 \left( \frac{t_1}{T_s} \right) \frac{K}{\sigma_d^2} \int_{-\infty}^{\infty} P_d(t) |I(t)| dt \quad 3-27$$

$$= E_N^2 + E_A^2 + E_D^2$$

where

$$E_N^2 = \text{normalized mean square noise error} = K^2 \frac{\sigma_{NI}^2}{\sigma_d^2} \left( \frac{t_1}{T_s} \right)^2$$

$$E_A^2 = \text{normalized mean square aliasing error} = K^2 \left( \frac{t_1}{T_s} \right)^2 \frac{\sigma_A^2}{\sigma_d^2}$$

$$E_D^2 = \text{normalized mean square distortion error}$$

$$= 1 + K^2 \left( \frac{t_1}{T_s} \right)^2 \frac{\sigma_{dI}^2}{\sigma_d^2} - 2 \left( \frac{t_1}{T_s} \right) \frac{K}{\sigma_d^2} \int_{-\infty}^{\infty} P_d(f) |I(f)| df$$

The error terms can be written as follows:

$$E_N^2 = \frac{\sigma_{NI}^2}{\left[ \sigma_{NI}^2 + \sigma_A^2 + \sigma_{dI}^2 \right]} \quad 3-28$$

$$E_A^2 = \frac{\sigma_A^2}{\left[ \sigma_{NI}^2 + \sigma_A^2 + \sigma_{dI}^2 \right]} \quad 3-29$$

$$E_D^2 = 1 + \frac{\sigma_{dI}^2}{\left[ \sigma_{NI}^2 + \sigma_A^2 + \sigma_{dI}^2 \right]} - \frac{\frac{2}{\sigma_d^2} \int_{-\infty}^{\infty} P_d(f) |I(f)| df}{\sqrt{\sigma_{NI}^2 + \sigma_A^2 + \sigma_{dI}^2}} \quad 3-30$$

Using Equation (3-24) the total normalized mean square error can be written as:

$$E^2 = 2 \left\{ 1 - \frac{1}{\sigma_d \sqrt{\sigma_{NI}^2 + \sigma_A^2 + \sigma_{dI}^2}} \int_{-\infty}^{\infty} P_d(f) |I(f)| df \right\} \quad 3-31$$

Specific examples using the above equations are considered in Section 3.4. The results obtained by using numerical integration are also presented there.

### 3.3 INTERPOLATION OF 100% DUTY CYCLE PAM PULSETRAIN

#### 3.3.1 System Model Simplification

The analysis to follow is similar to that given for fractional duty cycle. Therefore, Figure 3-1 applies and some steps can be eliminated.

#### Power Spectrum of Sample & Hold Output

The sampler gates a small time sample which in the experiments is restricted to 4% or less of the sampling period. This sample is held until the next sample is taken. Thus the output waveform of the sample and hold closely approximates a 100% duty cycle FAM signal.

The power spectrum of a 100% duty cycle PAM waveform is known to be (reference 2).

$$P_g(f) = \frac{1}{T_s} |B(f)|^2 \left\{ (\overline{a^2} - \bar{a}^2) + \frac{\bar{a}^2}{T_s} \sum_{n=-\infty}^{\infty} \delta(f - \frac{n}{T_s}) \right\} \quad 3-32$$

where

$$|B(f)|^2 = T_s^2 \left[ \frac{\sin(\pi f T_s)}{\pi f T_s} \right]^2$$

$T_s$  = sampling period (seconds) =  $1/f_s$

$f_s$  = sampling frequency

$a$  = random variable, the pulse amplitude

$\overline{a^2}$  = mean square value of  $a$

$\bar{a}^2$  = square of the mean value of  $a$

$$\int_{-\epsilon}^{\epsilon} \delta(x-x_0) dx = 1, \quad -\epsilon < x_0 < \epsilon$$

= 0 otherwise

Note that functionally the sample and hold output spectrum is invariant with respect to the data spectrum; the important parameters are the mean square and mean values of the data which vary with the data amplitude probability distribution and the sampling period.

The mean is assumed zero to simplify the power spectrum expression and the mean square value can be replaced with the more familiar symbol,  $\sigma_N^2 + \sigma_d^2 = \overline{a^2} - \bar{a}^2 = \overline{a^2}$  where  $\sigma_d$  is the rms value of the input data and  $\sigma_N$  is the rms value of the noise.

Thus

$$P_g(f) = (\sigma_N^2 + \sigma_d^2) T_s \left[ \frac{\sin(\pi f T_s)}{\pi f T_s} \right]^2 \quad 3-33$$

Figure 3-4 illustrates the spectrum at the sampler output.

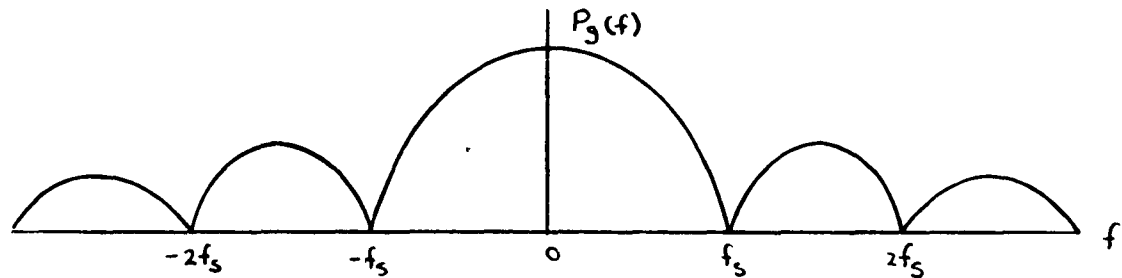


FIGURE 3-4 POWER SPECTRUM AT SAMPLER OUTPUT FOR 100% DUTY CYCLE PAM

Note that the spectrum no longer consists of spectral replicas of the noise and data spectra centered at  $0, \pm f_s, \pm 2 f_s - - -$ . Instead, the shape of the power spectral density is continuous and independent of the input noise and data spectra. The power in the continuous spectrum is distributed between the data and noise in the ratio  $\sigma_d^2 / \sigma_N^2$ .

The power spectrum of the interpolation filter output is:

$$P_f(f) = P_g(f) |I(f)|^2 = (\sigma_N^2 + \sigma_d^2) T_s \left[ \frac{\sin(\pi f T_s)}{\pi f T_s} \right]^2 |I(f)|^2 \quad 3-34$$

where

$|I(f)|^2$  = the square of the magnitude of the interpolation filter transfer function.

### 3.3.2 Normalized RMS Error

The normalized rms error is defined in Equations 3-8 through 3-12. The power spectrum of the error is:

$$\begin{aligned}
 P_e(f) &= \lim_{T \rightarrow \infty} \frac{1}{T} \overline{|E_e(f)|^2} \\
 &= (\sigma_N^2 + \sigma_d^2) K^2 T \left[ \frac{\sin(\pi f T_s)}{\pi f T_s} \right]^2 |I(f)|^2 + P_d(f) \quad 3-35 \\
 &\quad - 2 \sigma_d K \sqrt{T_s} \left[ \frac{\sin(\pi f T_s)}{\pi f T_s} \right] |I(f)| |E_d(f)| \cos(\theta_I(f) - 2\pi f t_0)
 \end{aligned}$$

where K is a gain constant associated with the interpolation filter to satisfy the constraint that

$$\sigma_d^2 = \sigma_f^2$$

Using the calculus of variations results in an expression for the optimum interpolation filter as before.

The rms error is minimized when  $\theta_I(f) = 2\pi f t_0$

$$\begin{aligned}
 K |I(f)| &= \frac{\sigma_d T_s^{-\frac{1}{2}} \left[ \frac{\sin(\pi f T_s)}{\pi f T_s} \right] |E_d(f)|}{(\sigma_N^2 + \sigma_d^2) \left[ \frac{\sin(\pi f T_s)}{\pi f T_s} \right]^2} \quad 3-36 \\
 &= \frac{\sigma_d}{\sigma_N^2 + \sigma_d^2} \frac{1}{K \sqrt{T_s}} \frac{|E_d(f)|}{\left[ \frac{\sin(\pi f T_s)}{\pi f T_s} \right]}
 \end{aligned}$$

where the above solution for  $|I(f)|$  is the optimum interpolation filter.

In order to determine the mean square error, Equations 3-18 through 3-20 will be used along with the following:

$$K^2 = \frac{\sigma_d^2}{\sigma_N^2 + \sigma_d^2} \frac{1}{T_s \int_{-\infty}^{\infty} \left[ \frac{\sin(\pi f T_s)}{\pi f T_s} \right]^2 |I(f)|^2 df} \quad 3-37$$



The mean square error is:

$$\begin{aligned}\sigma_e^2 &= \int_{-\infty}^{\infty} P_e(f) df \\ &= 2\sigma_d^2 - 2\sigma_d K \sqrt{T_s} \int_{-\infty}^{\infty} \left[ \frac{\sin(\pi f T_s)}{\pi f T_s} \right] |I(f)| |E_d(f)| df\end{aligned}\quad 3-38$$

The mean square normalized error is:

$$\begin{aligned}E^2 = \frac{\sigma_e^2}{\sigma_d^2} &= 2 \left[ 1 - \frac{K}{\sigma_d} \sqrt{T_s} \int_{-\infty}^{\infty} \left[ \frac{\sin(\pi f T_s)}{\pi f T_s} \right] |I(f)| |E_d(f)| df \right] \\ &= 2 \left[ 1 - \frac{1}{\sqrt{\sigma_A^2 + \sigma_d^2}} \frac{\int_{-\infty}^{\infty} \left[ \frac{\sin(\pi f T_s)}{\pi f T_s} \right] |I(f)| |E_d(f)| df}{\left[ \int_{-\infty}^{\infty} \left[ \frac{\sin(\pi f T_s)}{\pi f T_s} \right]^2 |I(f)|^2 df \right]^{1/2}} \right]\end{aligned}\quad 3-39$$

Specific examples using the results above are considered in the following section. The results obtained by numerical integration are also presented.

### 3.4 EXAMPLES AND COMPUTER RESULTS

#### 3.4.1 Fractional Duty Cycle

When aliasing and distortion are the only error mechanisms present the total normalized mean square error becomes:

$$E^2 = E_A^2 + E_D^2 \quad 3-40$$

by the use of equation 3-27. Using the value of K determined in 3-25 and the definitions following 3-27 results in:

$$E_A^2 = \frac{\sigma_A^2}{\sigma_A^2 + \sigma_{dI}^2} \quad 3-41$$

$$E_D^2 = 1 + \frac{\sigma_{dI}^2}{\sigma_A^2 + \sigma_{dI}^2} - 2 \frac{1}{\sigma_d \sqrt{\sigma_A^2 + \sigma_{dI}^2}} \int_{-\infty}^{\infty} P_d(f) |I(f)| df \quad 3-42$$

where

$$\sigma_d^2 = \int_{-\infty}^{\infty} P_d(f) df$$

$$\sigma_A^2 = \int_{-\infty}^{\infty} \left[ \sum_{n \neq 0} c_n^2 P_d(f - \frac{n}{T_s}) \right] |I(f)|^2 df$$

$$\sigma_{dI}^2 = \int_{-\infty}^{\infty} P_d(f) |I(f)|^2 df$$

The following example is considered:

Example

<u>Data Spectrum</u> Butterworth	<u>Interpolation Filter</u> Butterworth
$P_d(f) = \frac{1}{1 + (\frac{f}{f_d})^{2J}}$	$ I(f) ^2 = \frac{1}{1 + (\frac{f}{f_i})^{2K}}$ $ I(f)  = \frac{1}{\sqrt{1 + (\frac{f}{f_i})^{2K}}}$

The following parameters are defined:

$$Q = f_s / f_d$$

$$T = f / f_d$$

$$N = f_i / f_d$$

$$R = t_i f_i$$

The parameters defining  $E_A^2$ ,  $E_D^2$  and  $E^2$  then assume the following form:

$$\sigma_d^2 = f_d \int_{-\infty}^{\infty} \frac{1}{1 + (T)^{2J}} dT$$

$$\sigma_A^2 = f_d \sum_{n \neq 0} \int_{-\infty}^{\infty} C_n^2 \frac{1}{1 + (T - nQ)^{2J}} \cdot \frac{1}{1 + (\frac{T}{N})^{2K}} dT$$

$$\sigma_{dI}^2 = f_d \int_{-\infty}^{\infty} \frac{1}{1 + (T)^{2J}} \cdot \frac{1}{1 + (\frac{T}{N})^{2K}} dT$$

$$C_n = \frac{\sin(\pi n \frac{RQ}{N})}{\pi n \frac{RQ}{N}}$$

The evaluation of the total mean square error,  $E^2$  in terms of the component errors  $E_A^2$  and  $E_D^2$  is performed by use of a programmed IBM-709 Computer. The normalized errors in RMS percent of full scale are: 100  $E$ , 100  $E_A$  and 100  $E_D$  respectively.

Results of computer calculations presenting the theoretical aliasing and total rms error vs. samples per cycle of the data cutoff frequency is shown in Figures 3-5 through 3-8. The numerical limit of integration was  $T = f/f_d = 10$ . This results in an overall computation error of less than 5% for the case of  $J = K = 1$  with  $n$  ranging from -2 to +2;  $N = 1$ , and  $R = 0.02$ . This error is considerably reduced as  $J$  and  $K$  are increased since less energy is present beyond  $T = 10$  for the faster cutoff rates. The parameter  $R = t_1 f_1$  was fixed at 0.02 since the experimental program test results show that the fractional duty cycle is not a sensitive parameter.

Figure 3-5 shows the rms error vs. samples per cycle for a Butterworth interpolation filter with  $K = 6$  and  $f_1/f_d = 2$ . The parameter  $J$  defining the data spectral cutoff rate is variable. The solid curves correspond to the aliasing component of error, and the dashed curves correspond to the total error. The distortion error becomes constant at low samples per cycle and is the limiting error source. The reduction in distortion error is quite pronounced, being approximately a factor of 5,

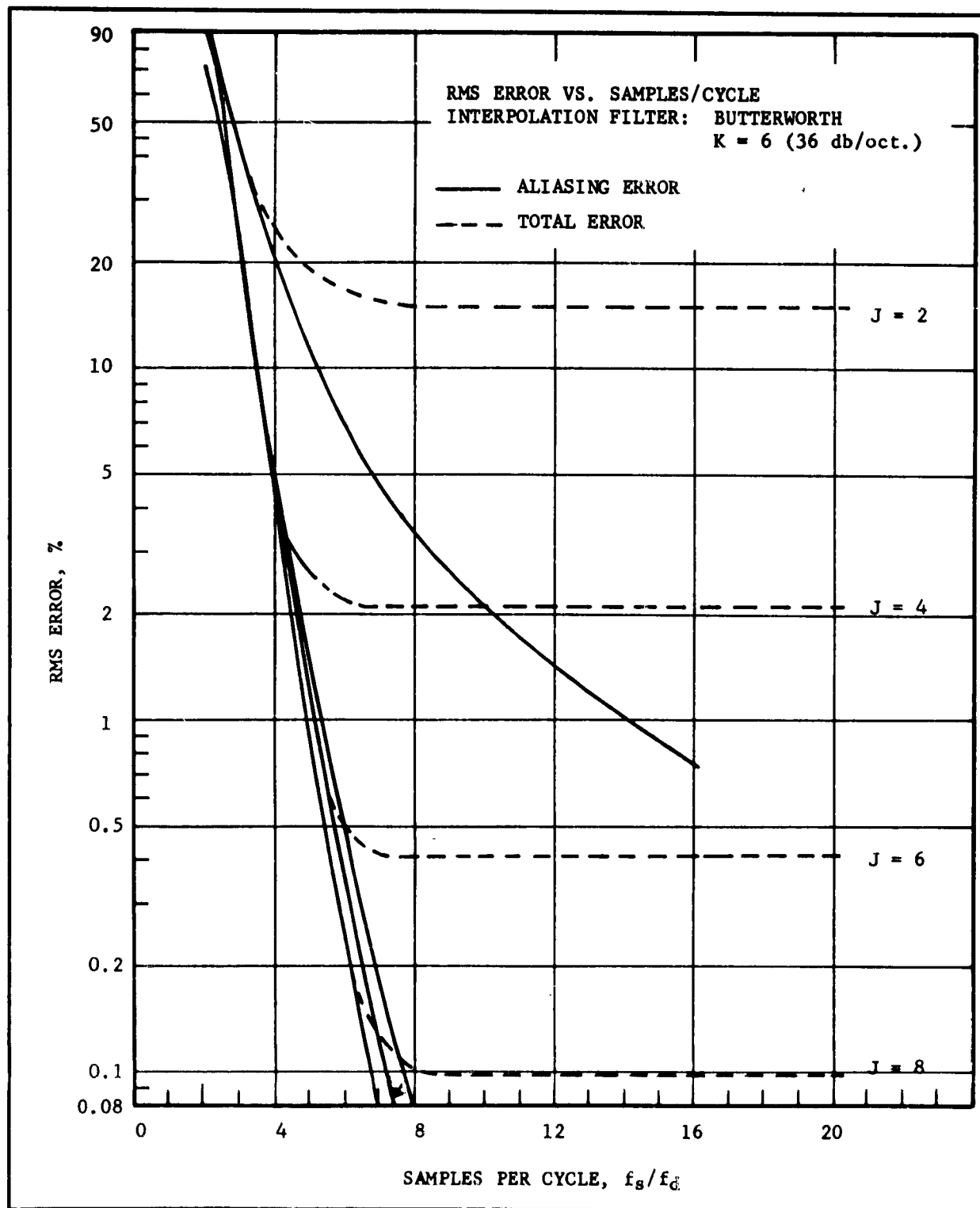


FIG. 3-5 BUTTERWORTH SHAPED DATA,  $t_1 f_1 = 0.02$ ,  $f_1/f_d = 2$ ,  $K = 6$

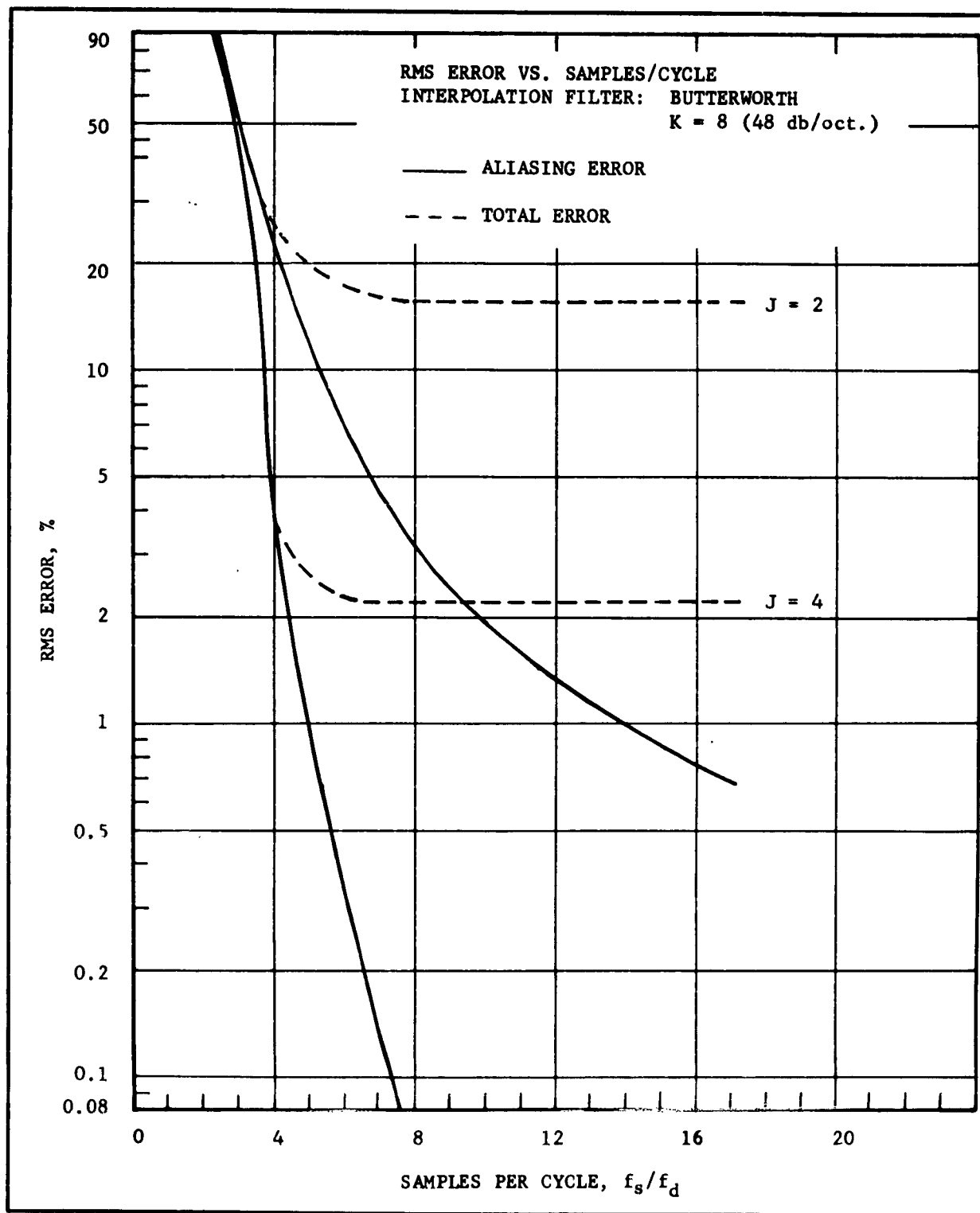


FIG. 3-6 BUTTERWORTH SHAPED DATA,  $t_1 f_i = 0.02$ ,  $f_i/f_d = 2$ ,  $K = 8$

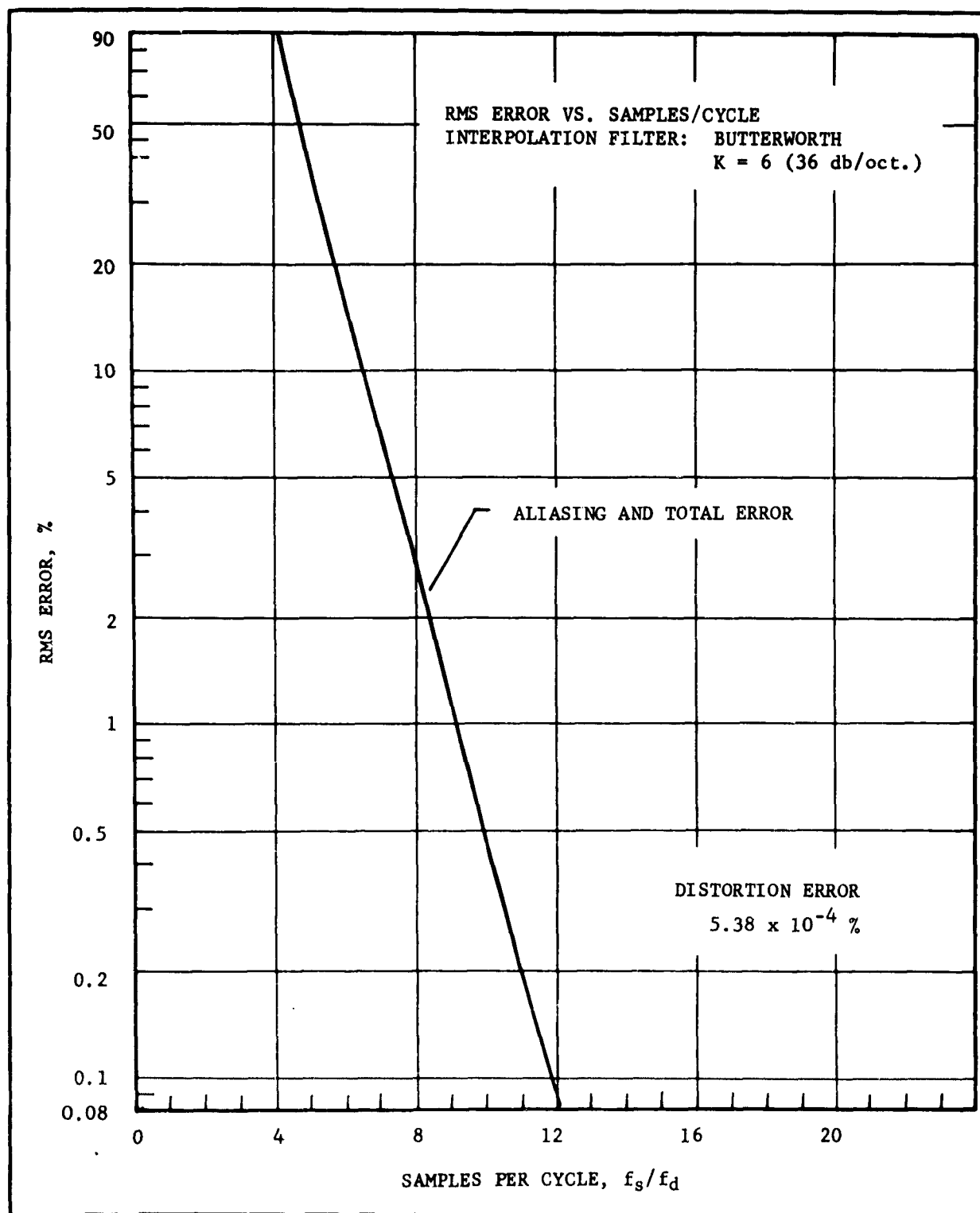


FIG. 3-7 BUTTERWORTH SHAPED DATA, 48 DB/OCT.,  $t_1 f_i = 0.02$ ,  $f_i/f_d = 4$ .

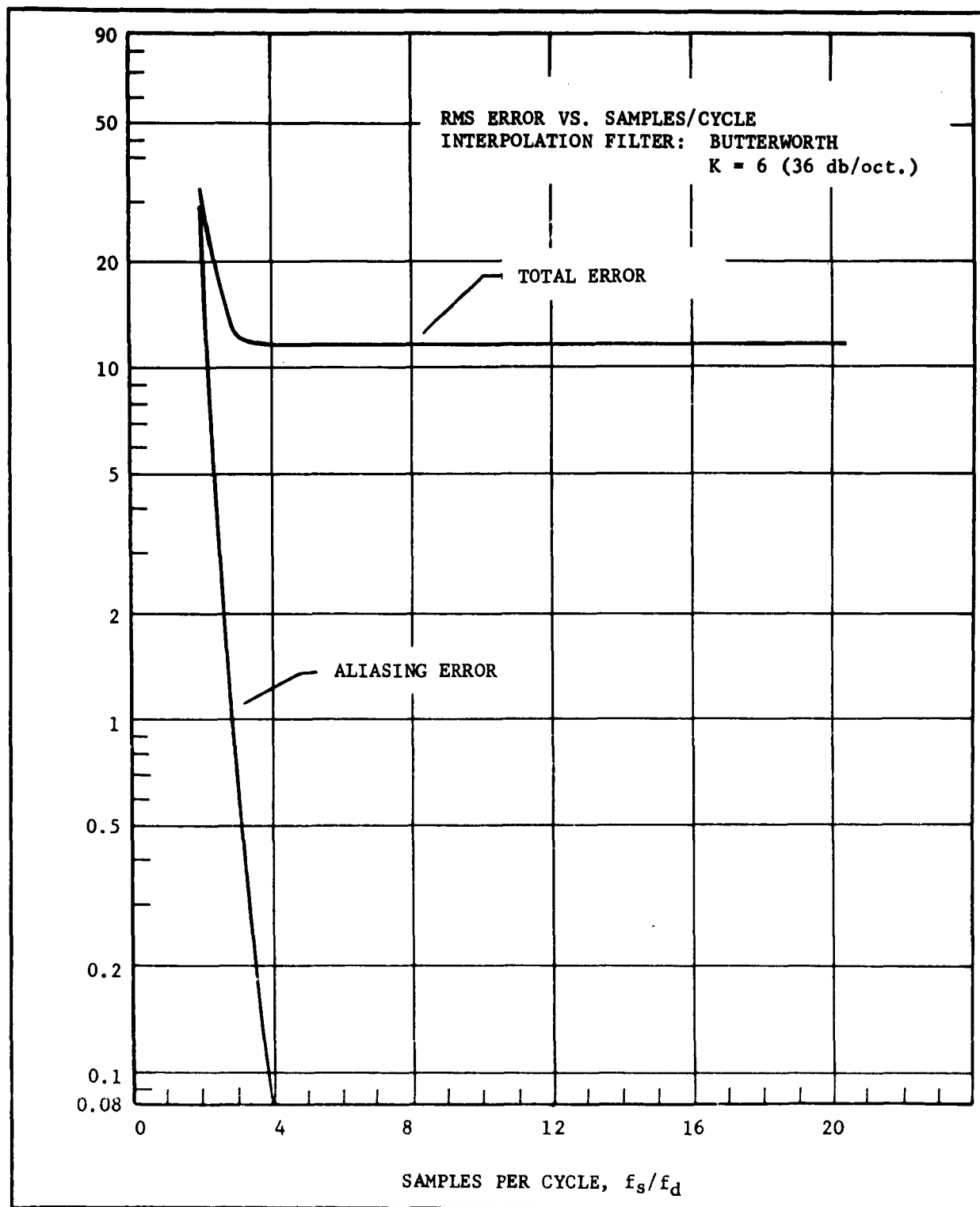


FIG. 3-8 BUTTERWORTH SHAPED DATA, 48 DB/OCT.,  $t_1 f_i = 0.02$ ,  $f_i/f_d = 1$

as the data cutoff rate is increased in increments of 12 db/oct.

In Figure 3-6 the cutoff rate on the interpolation filter has been increased by 12 db/oct. The aliasing and total error curves agree closely with curves which are approximately comparable in Figure 3-5. The rms error is slightly greater in Figure 3-6 because of increased distortion error.

Figure 3-7 is similar to Figure 3-5 for  $J = 8$  except that in Figure 3-7  $f_i/f_d = 4$ . The aliasing error has increased and the distortion error has been reduced significantly. The increase in aliasing error is due to the wide interpolation filter passing the sideband (aliasing) spectra at low samples per cycle. The curves approach each other as  $f_s/f_d$  is increased. The lower distortion error is accounted for by observing that the interpolation filter eliminates less data energy since the interpolation filter cutoff is four times the data cutoff.

Figure 3-8 can be compared with Figures 3-5 for  $J = 8$ . In Figure 3-8  $f_i/f_d = 1$  as compared to  $f_i/f_d = 2$  in Figure 3-5. In Figure 3-8 the aliasing error has been reduced and the distortion error has increased. The reduction in aliasing error is attributed to the fact that the interpolation filter rejects more of the energy in the aliasing spectra for  $f_i/f_d = 1$  than for  $f_i/f_d = 2$ . The increased distortion is due to the interpolation filter rejecting more of the data energy. These calculations have shown good agreement with the experimental results reported in Section 4.

#### 3.4.2 100% Duty Cycle Sampling

By use of Equation 3-39, the expression for total mean square error simplifies to:

$$E^2 = 2 \left[ 1 - \frac{1}{\sigma_d} \frac{\int_{-\infty}^{\infty} \left[ \frac{\sin(\pi f T_s)}{\pi f T_s} \right] |I(f)| |F_d(f)| df}{\left[ \int_{-\infty}^{\infty} \left[ \frac{\sin(\pi f T_s)}{\pi f T_s} \right]^2 |I(f)|^2 df \right]^2} \right] \quad 3-43$$

when noise interference is reduced to zero.

Below is given the expressions comparable to the fractional duty



cycle example presented in Paragraph 3.4.1 when a Butterworth data and Butterworth interpolation filter spectral characteristic is assumed.

Example

<u>Data Spectrum</u> Butterworth	<u>Interpolation Filter</u> Butterworth
$P_d(f) = \frac{1}{1 + \left(\frac{f}{f_d}\right)^{2J}}$	$ I(f) ^2 = \frac{1}{1 + \left(\frac{f}{f_i}\right)^{2K}}$
$F_d(f) = \frac{1}{\sqrt{1 + \left(\frac{f}{f_d}\right)^{2K}}}$	$ I(f)  = \frac{1}{\sqrt{1 + \left(\frac{f}{f_i}\right)^{2K}}}$

The following parameters are defined:

$$Q = f_s/f_d$$

$$T = f/f_d$$

$$N = f_i/f_d$$

$$\sigma_d^2 = f_d \int_{-\infty}^{\infty} \frac{1}{1 + (T)^{2J}} dT$$

$$\sigma_x^2 = f_d \int_{-\infty}^{\infty} \left[ \frac{\sin(\pi \frac{T}{Q})}{\pi \frac{T}{Q}} \right] \frac{1}{\sqrt{1 + (\frac{T}{N})^{2K}}} \frac{1}{\sqrt{1 + (T)^{2J}}} dT$$

$$\sigma_y^2 = f_d \int_{-\infty}^{\infty} \left[ \frac{\sin(\pi \frac{T}{Q})}{\pi \frac{T}{Q}} \right]^2 \frac{1}{1 + (\frac{T}{N})^{2K}} dT$$

$$E^2 = 2 \left[ 1 - \frac{\sigma_x^2}{\sigma_d \sigma_y} \right]$$

These parameters are used in programming of the IBM-709 computer.

The normalized rms error in percent is 100 E.

Several calculations were made using an upper limit of  $T = 10$  for integration. The parameter values selected were  $N = 2$ ,  $J = 4$ , and  $K = 6$ . The calculated results differed from those obtained experimentally. The discrepancy has not been completely resolved but is believed to be due to an error in programming. Since the calculations performed for the fractional duty cycle case agree well with the experimental results, the experimental results for 100% duty cycle have been verified.

#### GLOSSARY OF SYMBOLS

<u>Symbol</u>	<u>Definition</u>
$d(t)$	Data time function
$E = \frac{\sigma_e}{\sigma_d}$	Normalized rms error
$E_A^2$	Normalized mean square aliasing error
$E_D^2$	Normalized mean square distortion error
$E_N^2$	Normalized mean square noise error
$f(t)$	Interpolation filter output time function
$f_d$	Data cutoff frequency (3 db point)
$f_i$	Interpolation filter cutoff frequency (3 db point)
$f_s = \frac{1}{T_s}$	Sampling frequency
$F_{( )}(f)$	Fourier transform of ( ) time function
$g(t)$	Sampler output time function
$I(f)$	Interpolation filter transfer function
$J$	Data cutoff rate ( $J \times 6$ db/oct.)
$K$	Interpolation filter cutoff rate ( $K \times 6$ db/oct.)
$N(t)$	Noise time function

# GLOSSARY OF SYMBOLS (Continued)

<u>Symbol</u>	<u>Definition</u>
$P_{\zeta}(f)$	Power spectrum of ( ) time function
$s(t)$	Sampling time function
$t_o$	System time delay
$t_i$	Sample pulsewidth (fractional duty cycle)
$T_s$	Sample pulse period
$e(t)$	Error time function
$\sigma_e$	RMS error
$\sigma_d$	RMS data
$\sigma_f$	RMS interpolation filter output

## SECTION 4

### EXPERIMENTAL EVALUATION PROGRAM

#### 4.1 INTRODUCTION

This section reports the results of the experimental evaluation program to provide a quantitative set of experimentally proven interpolation design parameters. These parameters can be utilized to avoid a significant source of data recovery error in existing telemetry systems. The data reported was obtained by setting up and operating the equipment described in Section 5.

Two sampled data systems, single and multi-channel, were investigated. This permitted verifying and supplementing theoretical understanding of aliasing errors and its relationship to the other components of error in time-division multiplexed telemetry. These two systems were set up and tested under actual operating conditions with simulated data signals and noise interference introduced.

The laboratory results for the two systems are presented in Sections 4.3 and 4.4 following the methods and procedures used in the experimental program discussed in Section 4.2.

#### 4.2 METHODS AND PROCEDURES

The test program consisted of setting up the single and multi-channel sampled data systems, supply random input signals typifying actual data spectra, and to measure the system's performance with and without interference introduced. System performance was measured by means of an accurate error comparator which repetitively sampled the input and output of the system at corresponding points and compared the samples for error. The adjustments of the error comparator enable the operator to remove the effects of time delay, as well as amplitude and bias changes within the system.

The system design parameters of prime importance are: 1) the ratio of samples per second to the data bandwidth,  $f_s/f_d$ , samples per cycle, 2) interpolation filter and data cutoff rates,  $K$  and  $J$  in units of 6 db/oct., 3) the ratio of interpolation filter bandwidth to data bandwidth,  $f_i/f_d$  and 4) normalized sample pulsewidth,  $t_1 f_i$ . These symbols were used in Section 3. Particular emphasis was placed on investigating the effects of these parameters using practical interpolation filters under actual operating conditions.

The single channel tests were performed without a carrier system or added noise interference to permit thorough understanding of the effects the various parameters have on interpolation errors.

A carrier system was used for the multi-channel tests with added noise interference. The "carrier" system utilized an FM-FM 40 KC sub-carrier oscillator and discriminator equipment followed by a Gaussian video filter. This is the same equipment utilized for PAM measurements in the telemetry study program (Reference 1). It was adapted to the PAM pulse rate used (4 KC) in the current study.

Nearly all of the data described in the following sections have been normalized to dimensionless ratios. The normalized data permit the results shown to be scaled to predict performance for a system of different data rate and bandwidth. In this connection it should be observed that results may be scaled without regard to carrier frequency. Use of most of the normalized parameters are obvious except perhaps the normalized signal-to-noise parameter,  $S/k_1 F_s^{1/2}$ , used for the multi-channel system. The relations between  $S/k_1 F_s^{1/2}$  and the more commonly used  $S/k_1$  and  $S/N$  are given by:

$$\begin{aligned} \left[ \frac{S}{k_1 F_s^{1/2}} \right]_{db} &= \left[ \frac{S}{N} \right]_{db} + 10 \log \frac{B}{F_s} \\ &= \left[ \frac{S}{k_1} \right]_{db} - 10 \log F_s \end{aligned}$$

where

- S = rms carrier voltage
- $k_1$  = rms noise voltage per unit root bandwidth
- $F_s$  = system sampling frequency, equivalent to the pulse rate
- B = system design bandwidth
- N = rms noise voltage in bandwidth B

#### 4.3 SINGLE CHANNEL SAMPLED DATA SYSTEM

##### 4.3.1 System Description

The general system block diagram is given in Section 5, Figure 5-1 along with a general system and detailed equipment description. Briefly the system consists of a data source followed by a filter denoted as a data filter to provide spectral shaping in conformance with the desired spectral data model. The data filter output is sampled and the samples are supplied to an interpolation filter. The rms error is obtained by comparing the interpolation filter output with the spectral shaping filter output. It must be emphasized that for most tests the data filter was used for spectral shaping of broadband white noise with a specified amplitude probability distribution; its output was considered as the data source. This is equivalent to data filtering of an actual data signal only when the signal has a spectral characteristic which is flat over the passband of the filter and several octaves beyond.

The system parameters: 1) samples per cycle 2) sampling duty cycle 3) interpolation filter data cutoff rate and 4) the ratio of interpolation filter bandwidth to data bandwidth - were investigated for selected data spectral models and selected interpolation filter types.

##### 4.3.2 Test Results

At least one simulation of each of the five data types described in Section 2 was made and performance measured for various system parameters during the test program. The test results are discussed in the order in which they were performed as listed on the following page.

<u>Data Spectrum</u>	<u>Basic Type</u>
1) Single sinewave	II
2) Butterworth shaped data	I
a) Various cutoff rates, 24,30,42,48	
b) 2-amplitude probabilities, Gaussian and Equi-probable	
3) One Sinewave plus Butterworth shaped data	III
4) Three Sinewaves plus Butterworth shaped data	II & III
5) Continuous with step	IV
6) Bandpass data	V

Spectral measurements and waveform photographs taken at various points in the system are presented in Section 4.3.3.

#### Sinewave Test Results

The percentage rms error versus samples per cycle of a fixed sinewave frequency is shown in Figure 4-1. These tests served also to check proper system operation and to determine the dynamic residual error.

The curve for  $f_i/f_d = 1$  results from using a 100 cps sinewave and a data sample pulsewidth into the interpolation filter of 20  $\mu$  sec. A 100 cps, 36 db/octave Butterworth filter was used for interpolation.

The curve for  $f_i/f_d = 4$  results from using a 50 cps sinewave, a data sample pulsewidth of 20  $\mu$ sec. converted to a 100% duty cycle pulsetrain to the interpolation filter. The filter is a modified 200 cps Butterworth filter with a 400 cps trap and a slope of 60 db/octave around 300 cps. This filter will be denoted as BWT.

For the parameter  $f_s/f_d$  greater than 8, the two curves are nearly coincident and the minimum residual system error, achieved for 20 samples per cycle, is the same, 0.14%. However, for samples per cycle less than 8, the rms error for  $f_i/f_d = 4$  is higher than that for  $f_i/f_d = 1$ . The major reason for this difference is that  $f_s = f_i$  for the poorer curve. Consequently, the interpolation filter passes undesired spectral components.

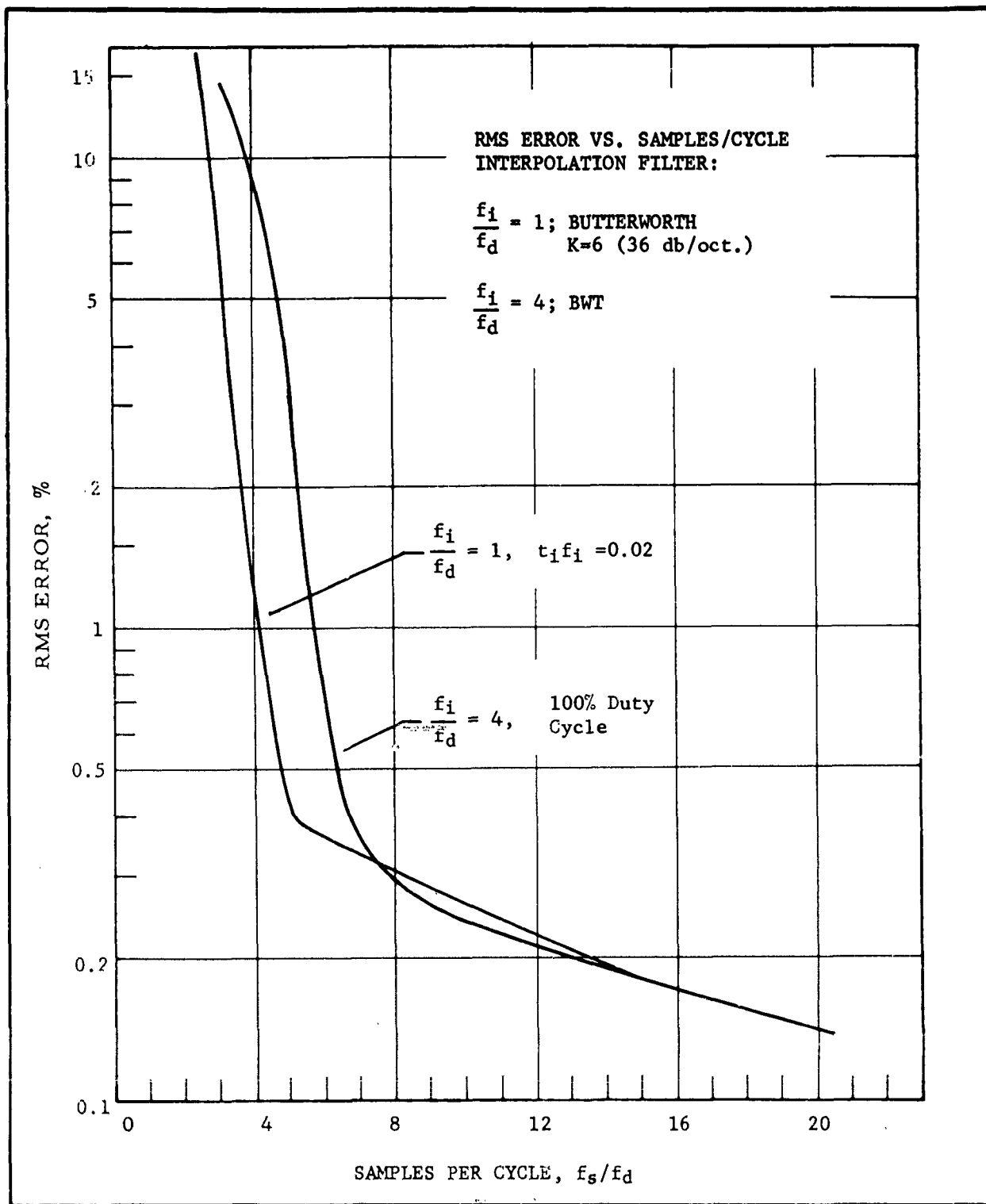


FIG. 4-1 SINEWAVE TESTS



This indicates that for practical filters  $f_s$  should be greater than  $f_i$ , and later results show that  $f_s \geq 2 f_i$  to be good practice.

Sampling frequency feed through was observed at low values of  $f_s/f_d$  for the fractional duty cycle test. Therefore, the BWT filter was designed to trap the sampling frequency at frequencies equal to or greater than 400 cps. The phase and amplitude characteristics of this filter are considerably different from the Butterworth filter. The amplitude characteristic approximates a rectangular cutoff more closely than the Butterworth filter. However, the phase characteristic is quite non-linear close to the corner frequency. The amplitude response is shown in Section 5 for all filters used.

Most of the following tests were run with the BWT filter. However, distortion errors were found to be the limiting factor in achieving low rms error with this filter due to its poorer phase response. Therefore, Gaussian and Butterworth filters were also investigated and found to give lower rms errors above values of 4 to 6 for  $f_s/f_d$  where interpolation filter distortion has a more pronounced effect than aliasing on the interpolation errors.

#### Butterworth Shaped Data Test Results

The analysis indicates that the aliasing error depends only on the first and second moments of the amplitude source and not the particular amplitude probability distribution of the data. Two noise sources were used to verify this experimentally, equi-probable and a Gaussian amplitude probability distribution. These are denoted by EPA and GAP respectively. Identical tests were conducted with both noise sources being spectrally shaped by a Butterworth filter. The results for these tests are discussed below.

#### Butterworth Shaped EPA Data

Figures 4-2 through 4-5 present the rms error versus samples per cycle of the data cutoff frequency for data sources with equi-probable amplitude distributions (EPA Data Sources). The parameters on each curve are 1) the ratio of interpolation filter bandwidth to data cutoff frequency,  $f_i/f_d$ ; and 2) the ratio of sampling frequency to interpolation filter bandwidth,  $f_s/f_i$ . The parameter which varies between figures is the sample pulsewidth.

The tests were performed using the BWT interpolation filter, holding the data cutoff frequency fixed, and varying the sampling frequency.

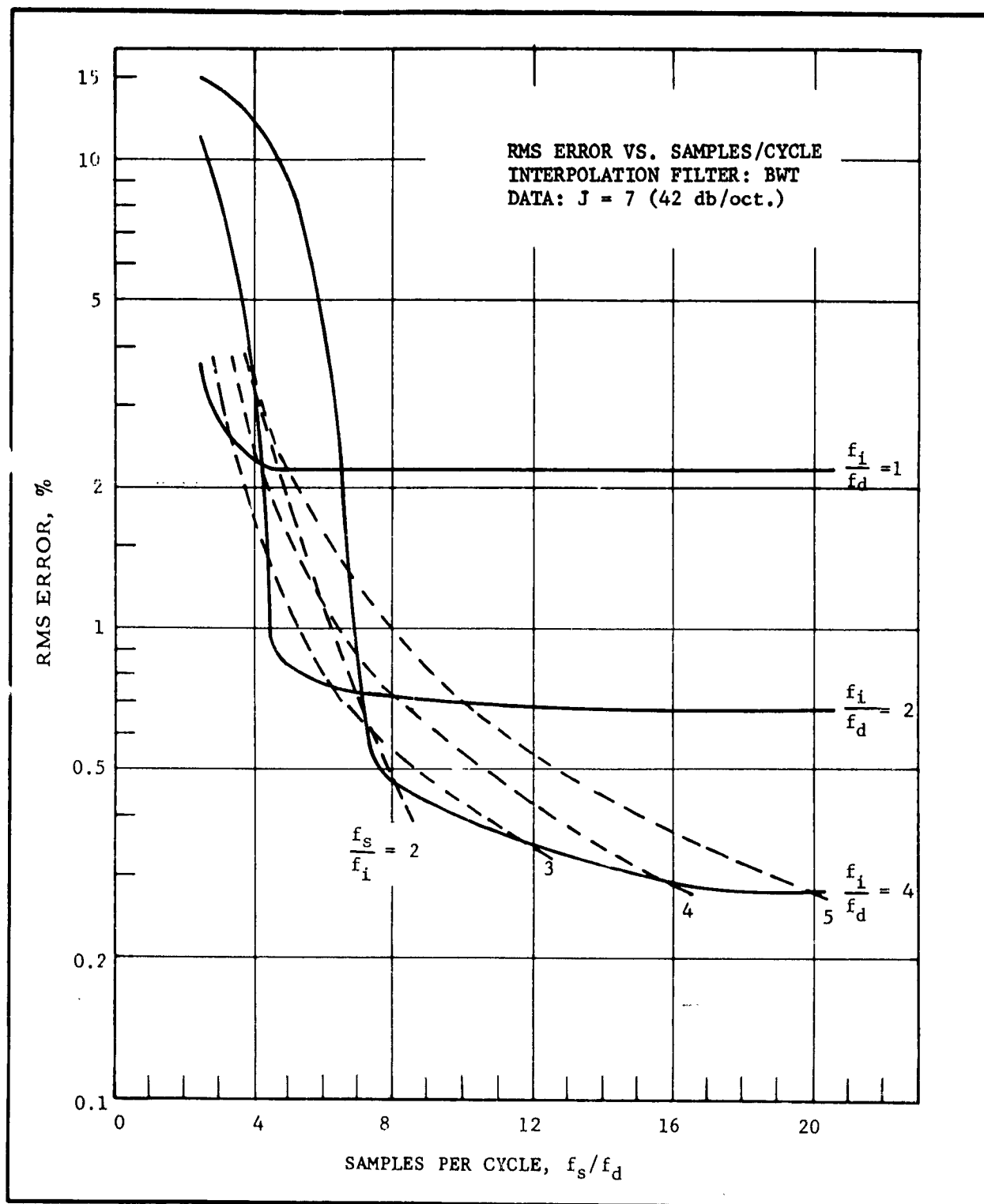


FIG. 4-2 BUTTERWORTH SHAPED DATA, EQUI-PROBABLE AMPLITUDE,  $t_1 f_i = 0.01$

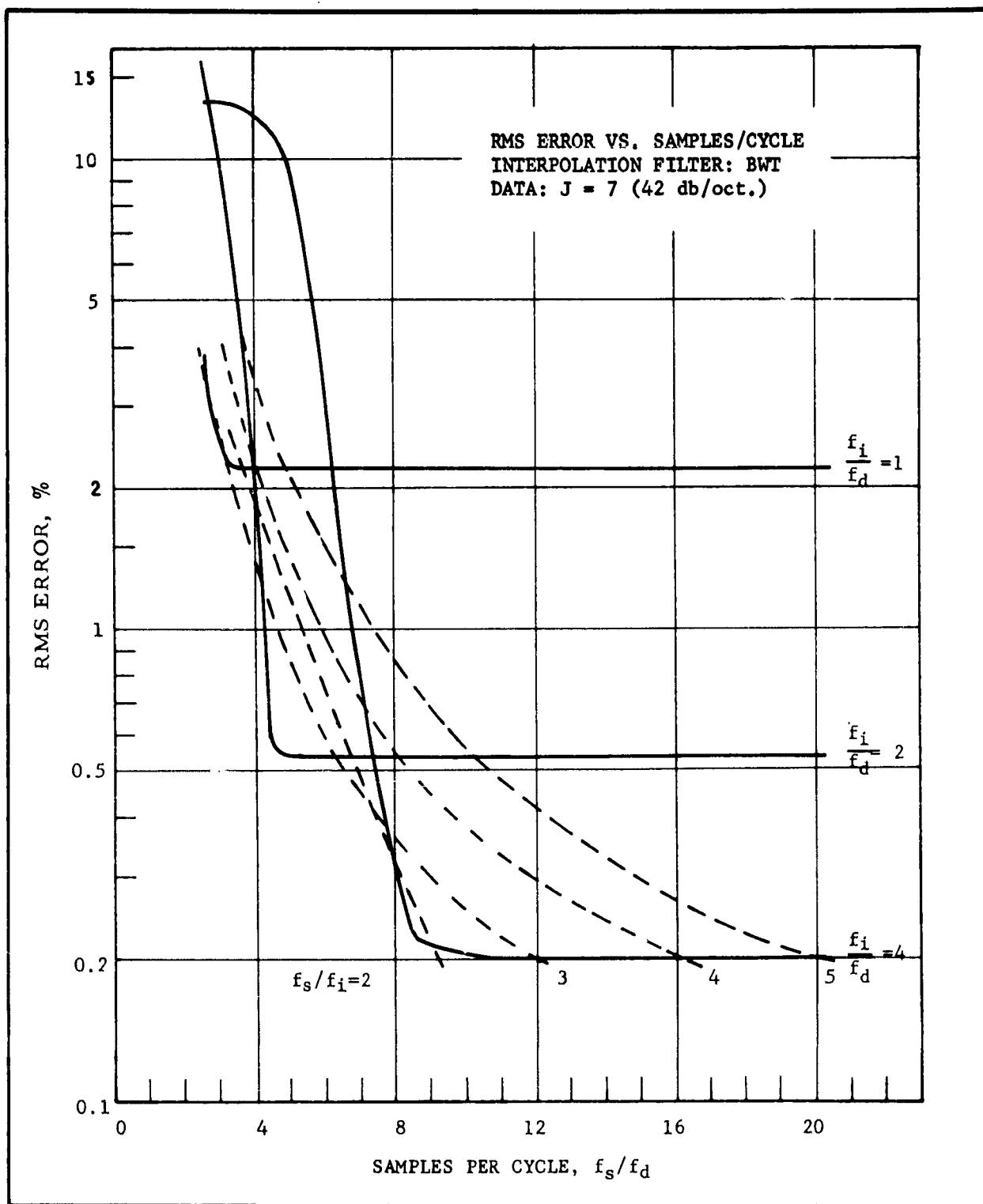


FIG. 4-3 BUTTERWORTH SHAPED DATA, EQUI-PROBABLE AMPLITUDE,  $t_1 f_i = 0.02$

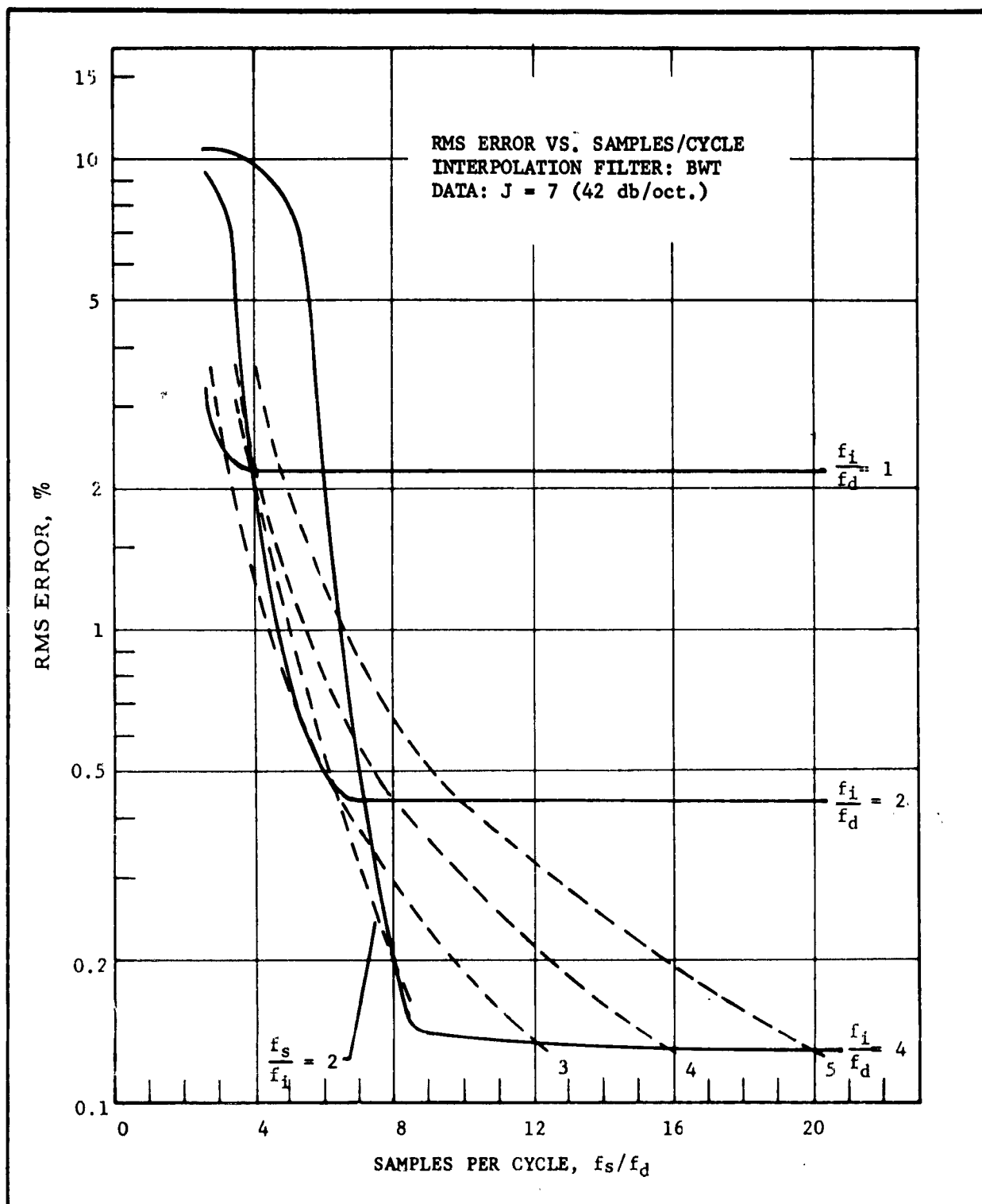


FIG. 4-4 BUTTERWORTH SHAPED DATA, EQUI-PROBABLE AMPLITUDE,  $t_1 f_i = 0.1$

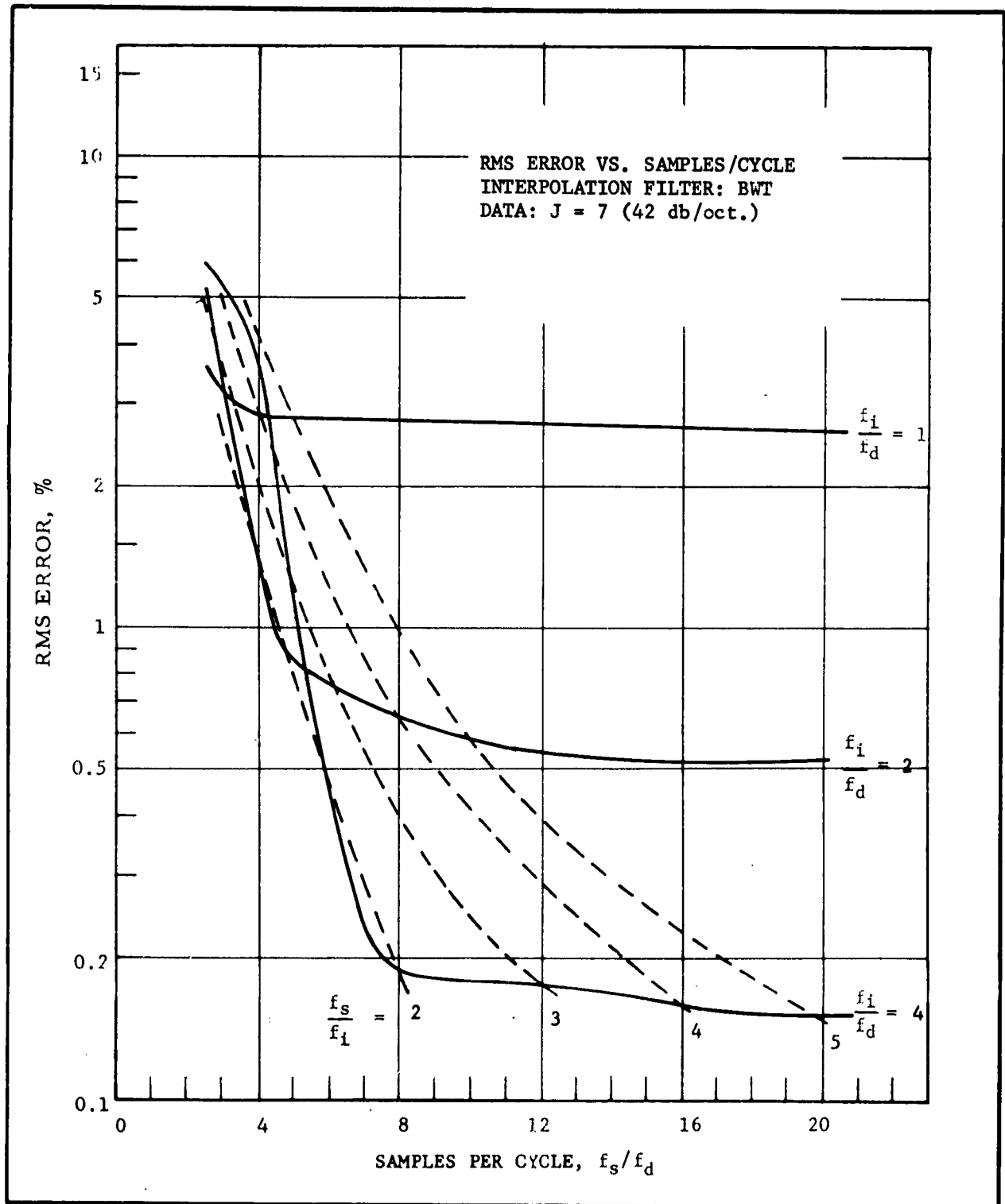


FIG. 4-5 BUTTERWORTH SHAPED DATA, EQUI-PROBABLE AMPLITUDE, 100% DUTY CYCLE

It is apparent from these curves that the sample pulsewidth has relatively little effect on the rms error. This is illustrated in Figure 4-6 where the rms error versus pulsewidth is shown for fixed  $f_s/f_d$  and  $f_s/f_i$ . If the pulsewidth times the interpolation filter bandwidth,  $t_1 f_i$ , is less than 0.5, the interpolation filter output is quite small relative to the data input and considerable amplification of the interpolation filter output is needed. This amplification increases the system residual error because of increased circuit non-linearities and noise. Amplification of the interpolation filter output can be eliminated if 100% duty cycle is used since this waveform supplies adequate power to the interpolation filter.

As the ratio of  $f_i/f_d$  is increased, the rms error curve shifts to the right and down. This is because the knee of each curve corresponds to the point at which the sampling frequency equals the tuned frequency of the trap in the BWT interpolation filter. The aliasing spectrum is less attenuated by the filter increasing the rms error at reduced samples per cycle. For  $f_s/f_d$  samples per cycle above that at the knee the aliasing spectrum is greatly attenuated and the curve is asymptotic to the distortion error plus system residual errors. The distortion error results from the non-linearities in the amplitude and phase characteristics of the interpolation filter. Lower distortion error results as the ratio of  $f_i/f_d$  is increased.

Figures 4-7 and 4-8 permit selection of the minimum sampling frequency and corresponding interpolation bandwidth to be chosen for a specified rms interpolation error and data bandwidth. Since the data is insensitive to pulsewidth only one curve is shown for fractional duty cycle.

For fixed rms error the minimum point on the curve corresponds to the proper sampling frequency and corresponding interpolation filter bandwidth for the given interpolation filter design. To the left of the minimum a sharp increase in samples per cycle is required to maintain a constant rms error; since the narrower interpolation filter bandwidth greatly increases the distortion error. To the right of the minimum the samples per cycle must increase with the wider interpolation filter bandwidth to reduce aliasing error.

The minimum samples per cycle is slightly less for 100% duty cycle than for fractional duty cycle interpolation for the same rms error.

The curves shift down and to the left as the rms increases, decreasing the samples per cycle and interpolation filter bandwidth.

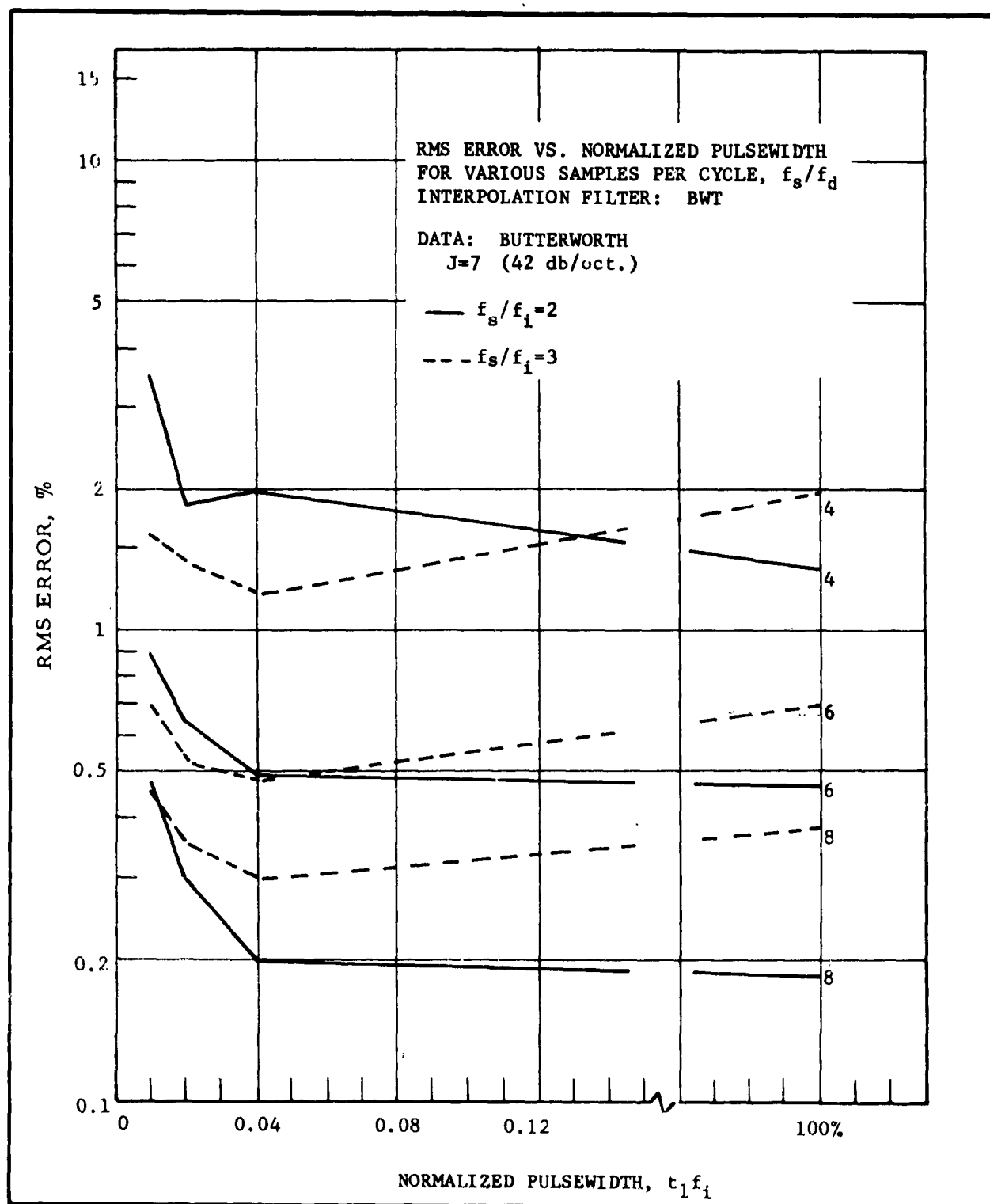


FIG. 4-6 RMS ERROR VS. NORMALIZED PULSEWIDTH

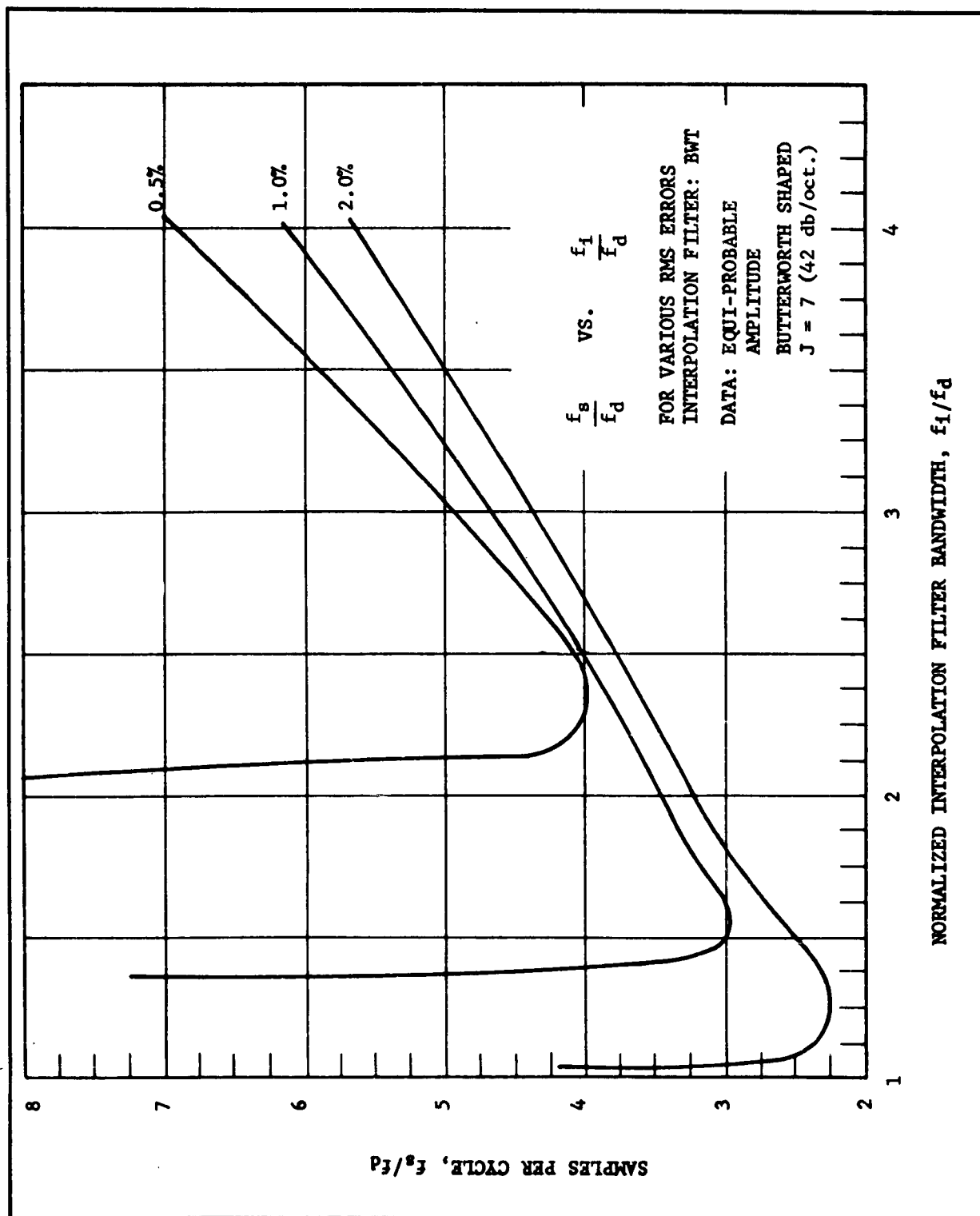


FIG. 4-7 SAMPLES PER CYCLE VS. NORMALIZED INTERPOLATION FILTER BANDWIDTH,  $t_1 f_1 = 0.02$



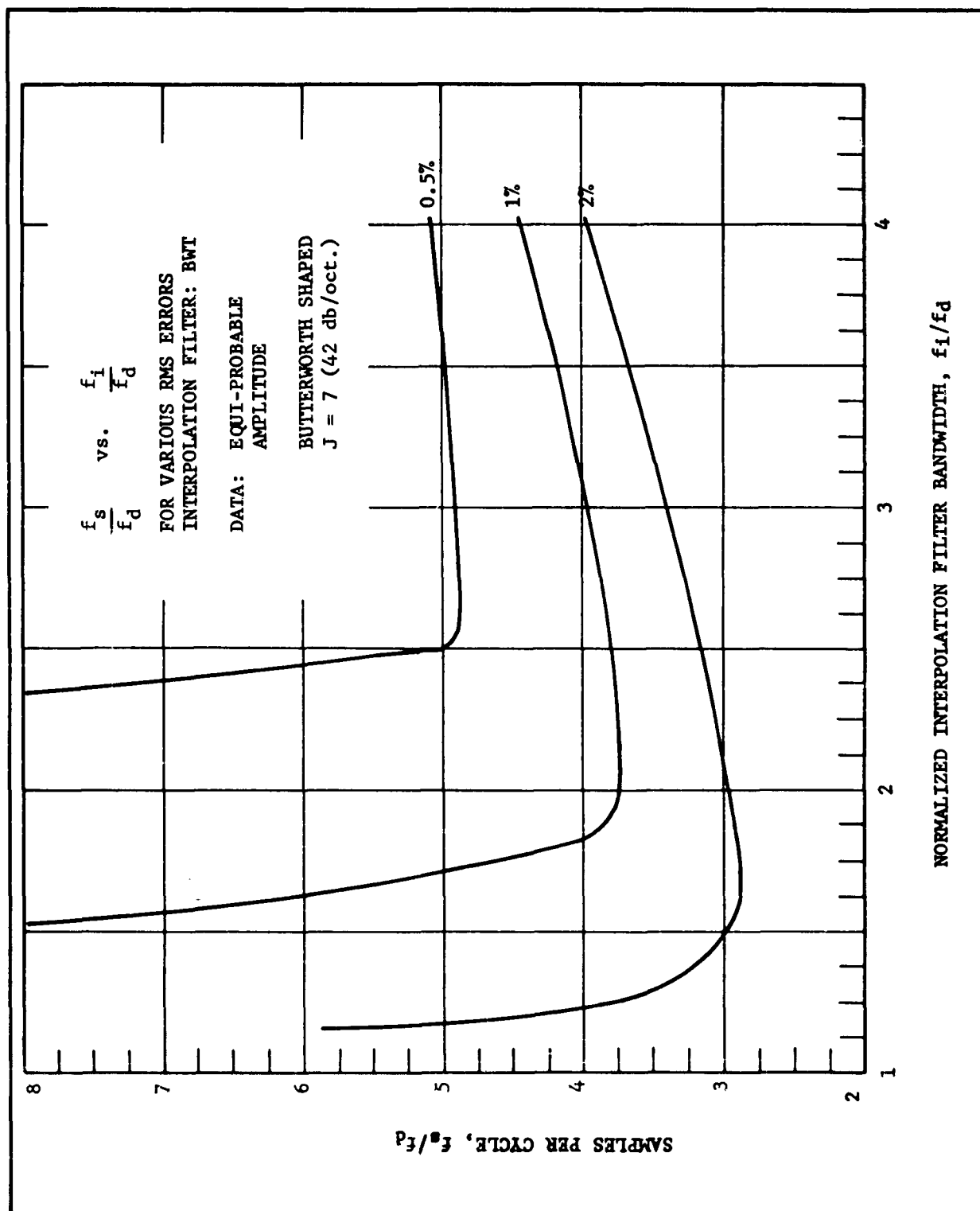


FIG. 4-8 SAMPLES PER CYCLE VS. NORMALIZED INTERPOLATION FILTER BANDWIDTH, 100% DUTY CYCLE

### Butterworth Shape GAP Data

Figures 4-9 through 4-12 present the rms error versus samples per cycle for data sources with Butterworth spectral characteristics and a Gaussian amplitude probability (GAP) distribution. The same BWT interpolation filter is used as for Figures 4-2 through 4-5. A data cutoff rate of 42 db/oct. was used to obtain the experimental results for the parametric curves given by  $f_i/f_d = 1$  and 4. The data cutoff rate was 48 db/oct. for the  $f_i/f_d = 2$  parametric curves. The different data cutoff rates resulted from the cutoff characteristics of the noise source described in Section 4.3.3.

The results agree closely with those for equi-probable amplitude distribution in spite of the significant difference between these two distributions. An apparent exception occurs for the curves with  $f_i/f_d = 2$ ; however, the cutoff rates differ and therefore are not comparable.

Comparison of data for the two distributions is presented in Figures 4-13 through 4-15. These figures are replots of Figures 4-2 through 4-5 and 4-9 through 4-12 for the various ratios of interpolation bandwidth to data bandwidth. This combines the two distributions on one set of scales for comparison. These replots show the close agreement between the equal amplitude probability distribution and the Gaussian probability distribution noise for  $f_i/f_d = 1$  and 4. Therefore, it is concluded that the test results are not significantly affected by the amplitude distribution. It should be noted that distortion error resulting from amplitude non-linearity in the system would be affected by the amplitude probability distribution.

For  $f_i/f_d = 2$  the test results using Gaussian data achieved a lower minimum rms error than for equal amplitude data due to the sharper cutoff rate of data signal. For the Gaussian data source as for equi-probable amplitude data, the sample pulsewidth is not a sensitive parameter. The close grouping of the curves for constant  $f_i/f_d$  indicates this insensitivity.

Figure 4-16 serves to show: 1) sample pulsewidth did not significantly affect interpolation accuracy over a large range of parameter values, 2) the probability distribution of the data does not affect interpolation accuracy.

Figure 4-16 was derived from Figures 4-13 through 4-15 by averaging with respect to pulsewidth for constant  $f_i/f_d$ . The averaging included both equi-probable and Gaussian probability distribution data with  $f_i/f_d = 1$  and 4.

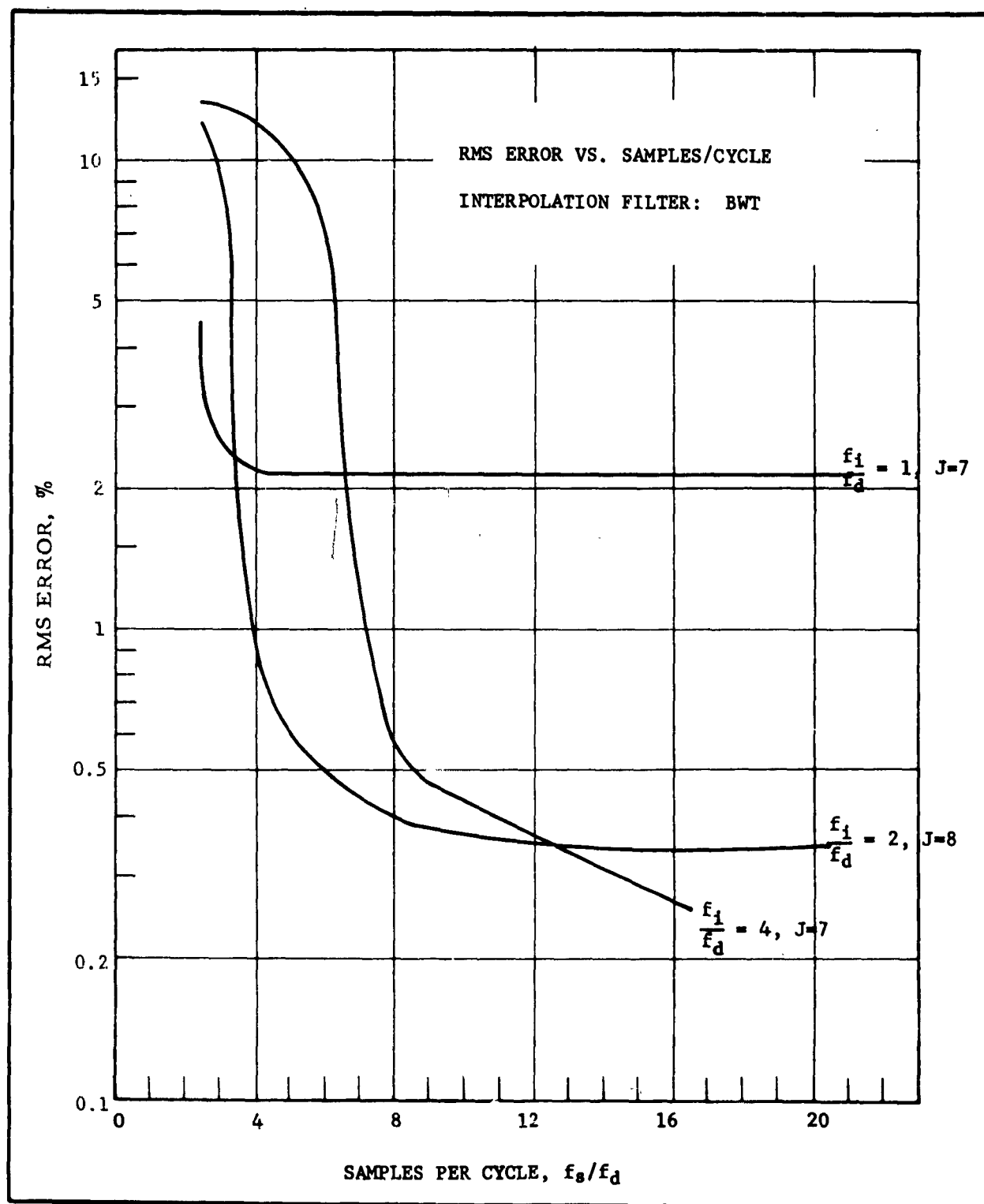


FIG. 4-9 BUTTERWORTH SHAPED DATA, GAUSSIAN PROBABILITY DISTRIBUTION,  $t_1 f_1 = 0.01$

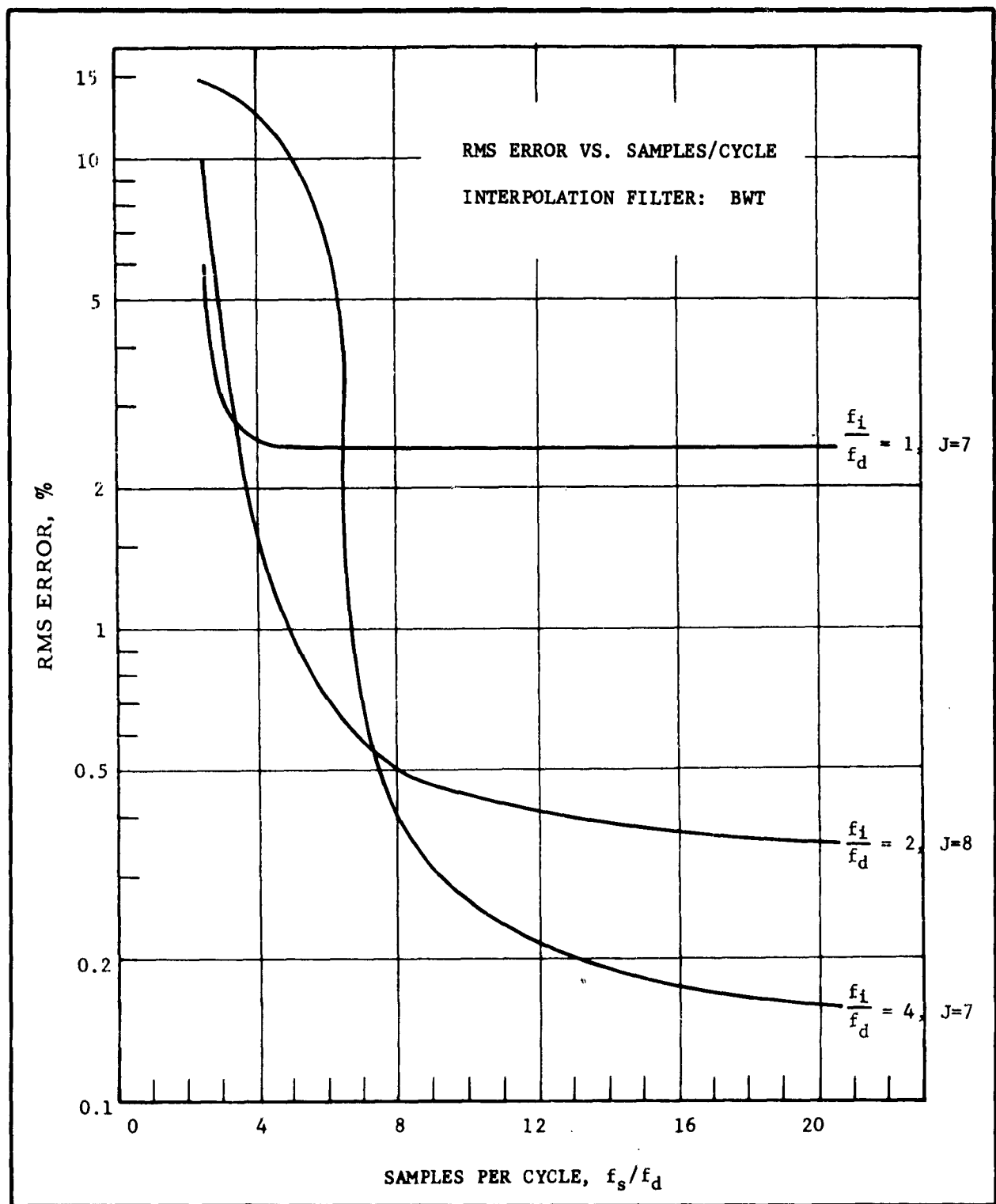


FIG. 4-10 BUTTERWORTH SHAPED DATA, GAUSSIAN PROBABILITY DISTRIBUTION,  $t_1 f_1 = 0.02$

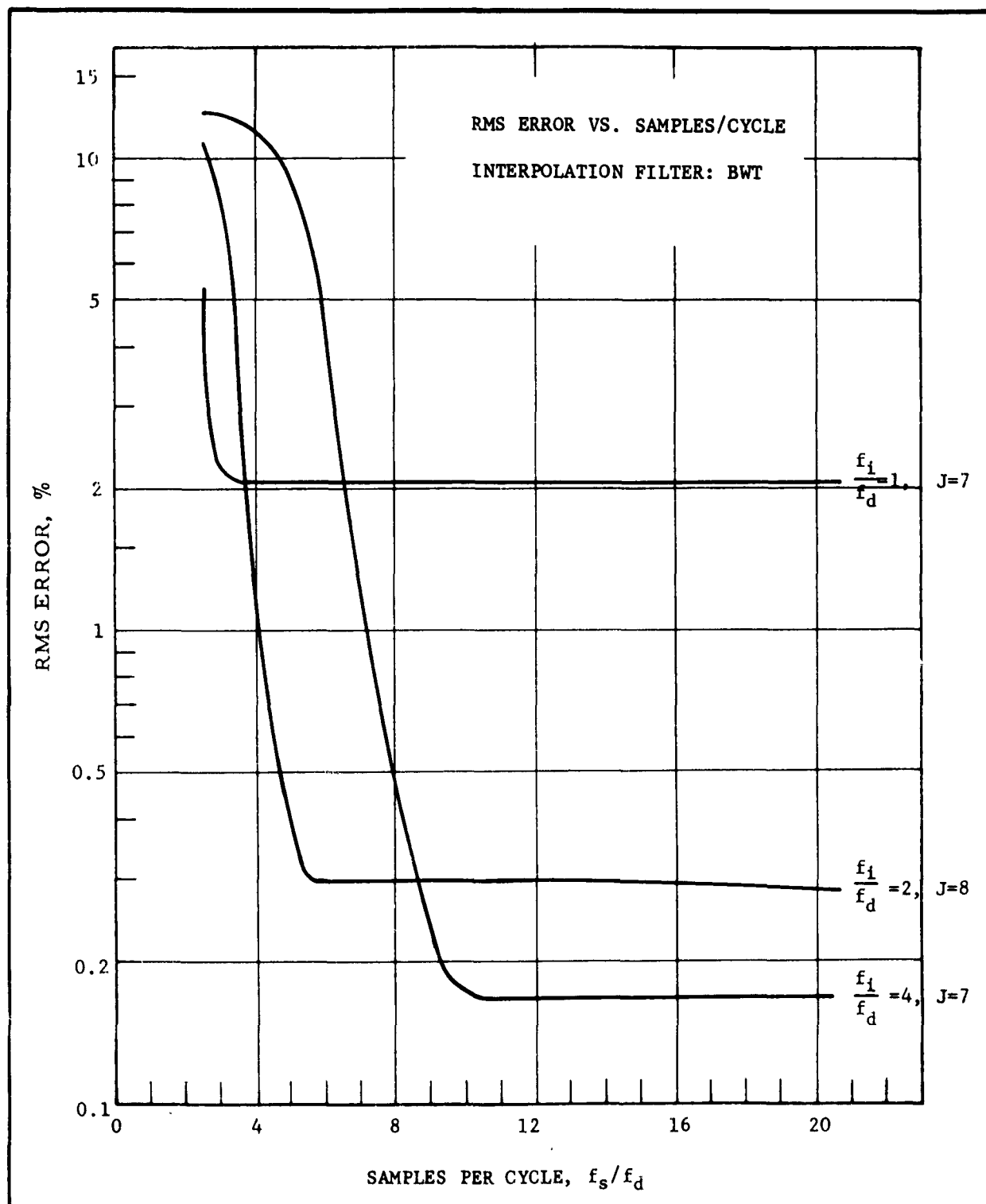


FIG. 4-11 BUTTERWORTH SHAPED DATA, GAUSSIAN PROBABILITY DISTRIBUTION,  $t_1 f_1 = 0.1$

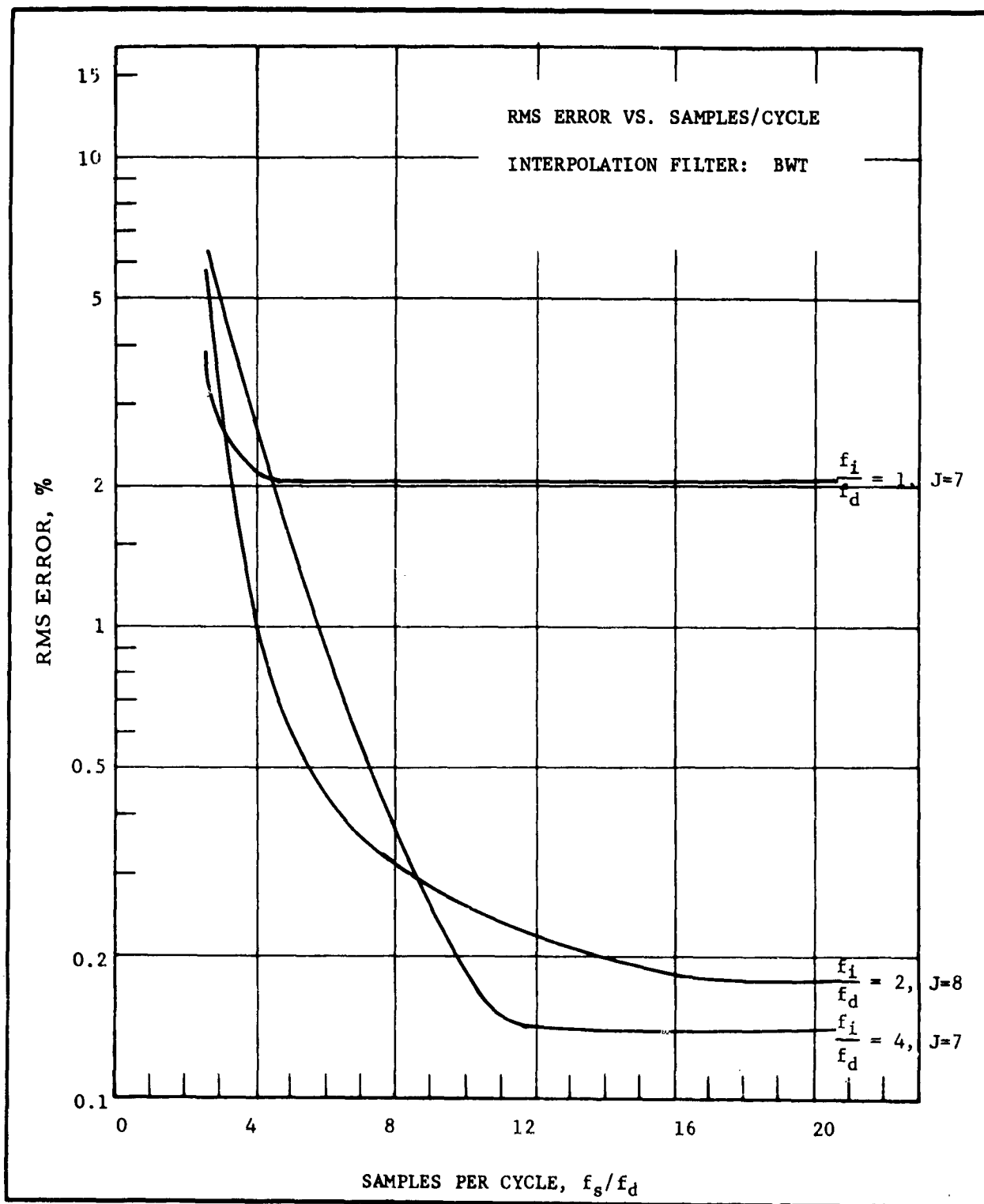


FIG. 4-12 BUTTERWORTH SHAPED DATA, GAUSSIAN PROBABILITY DISTRIBUTION, 100% DUTY CYCLE

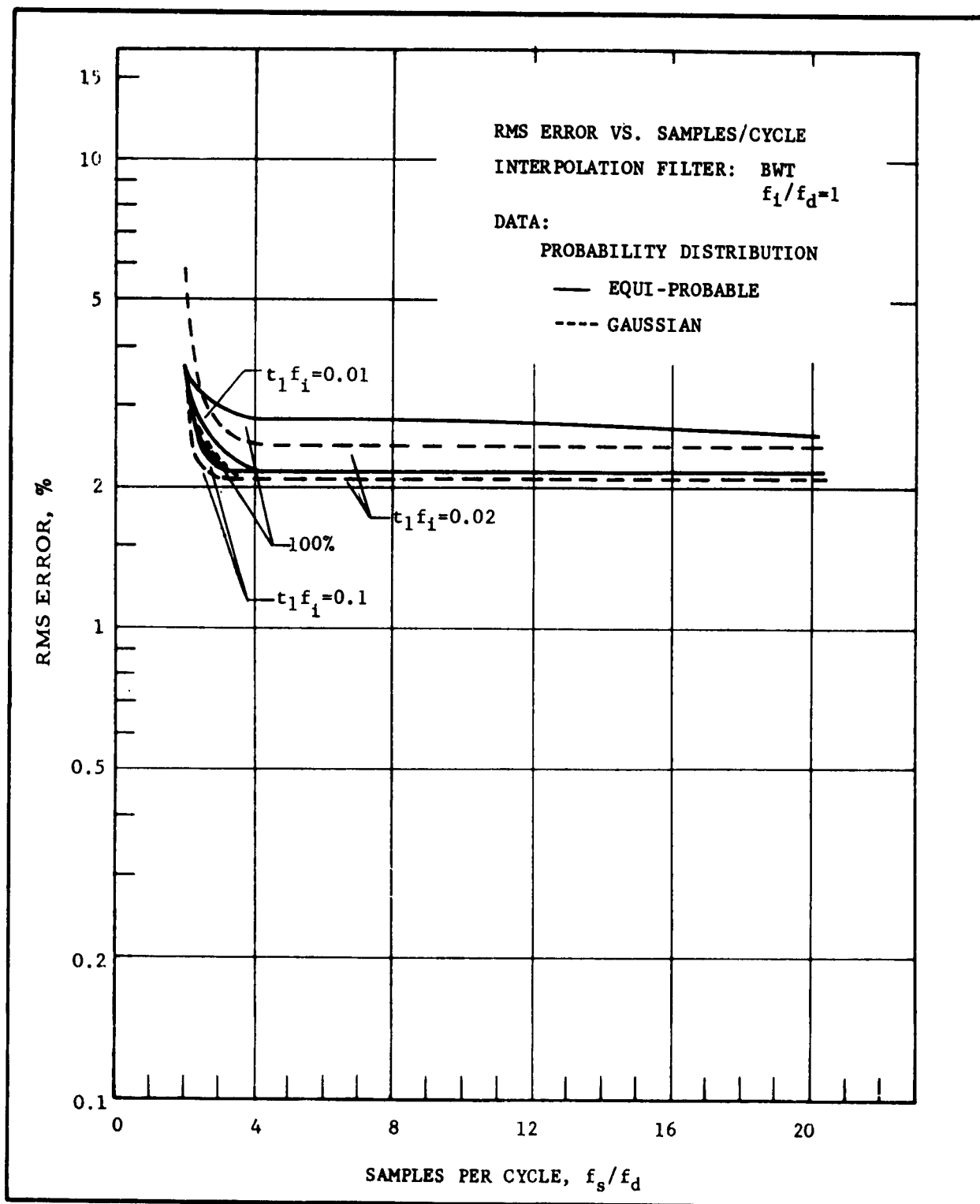


FIG. 4-13 BUTTERWORTH SHAPED DATA,  $f_1/f_d=1$ ,  $J=7$

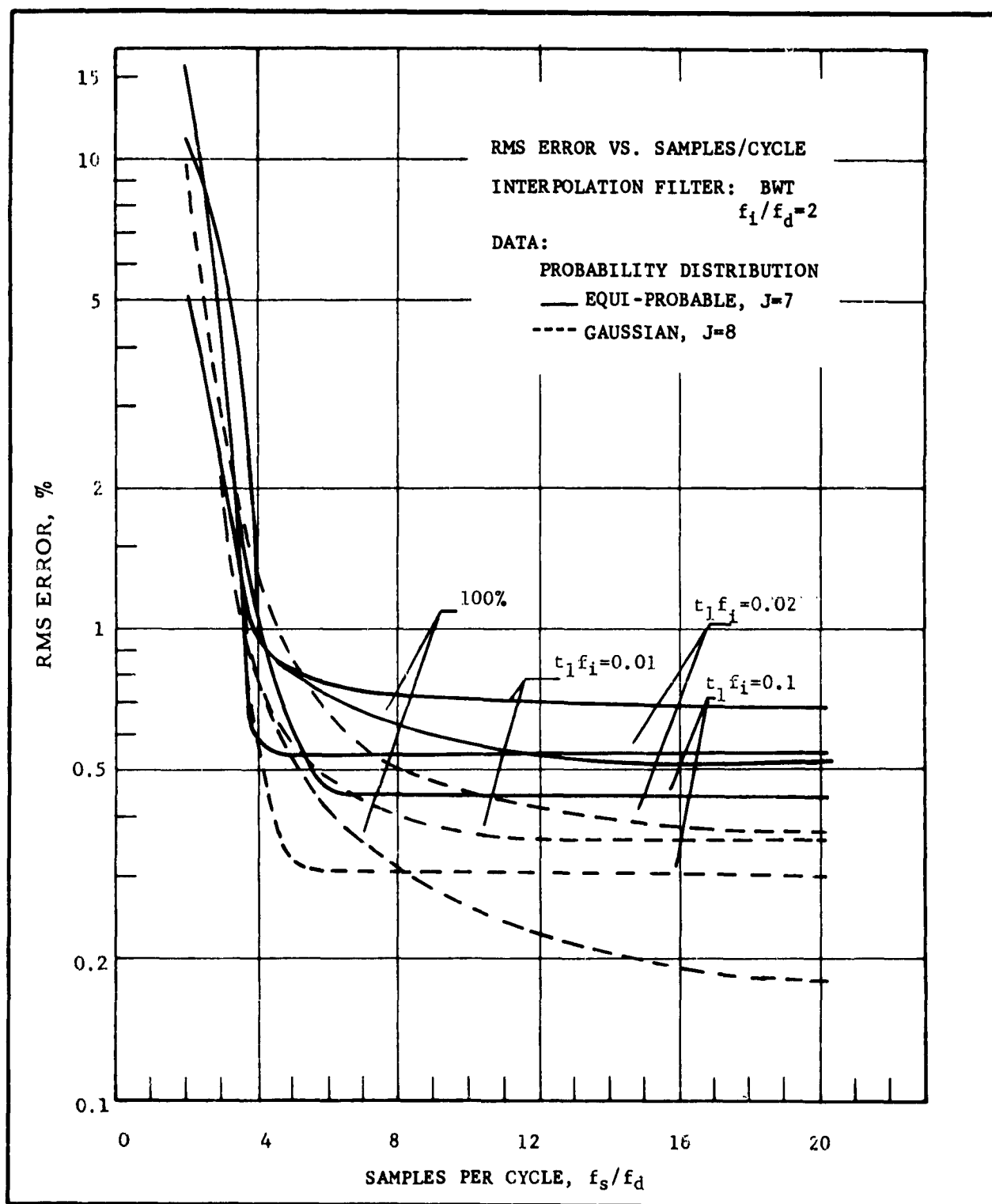


FIG. 4-14 BUTTERWORTH SHAPED DATA,  $f_i/f_d = 2$



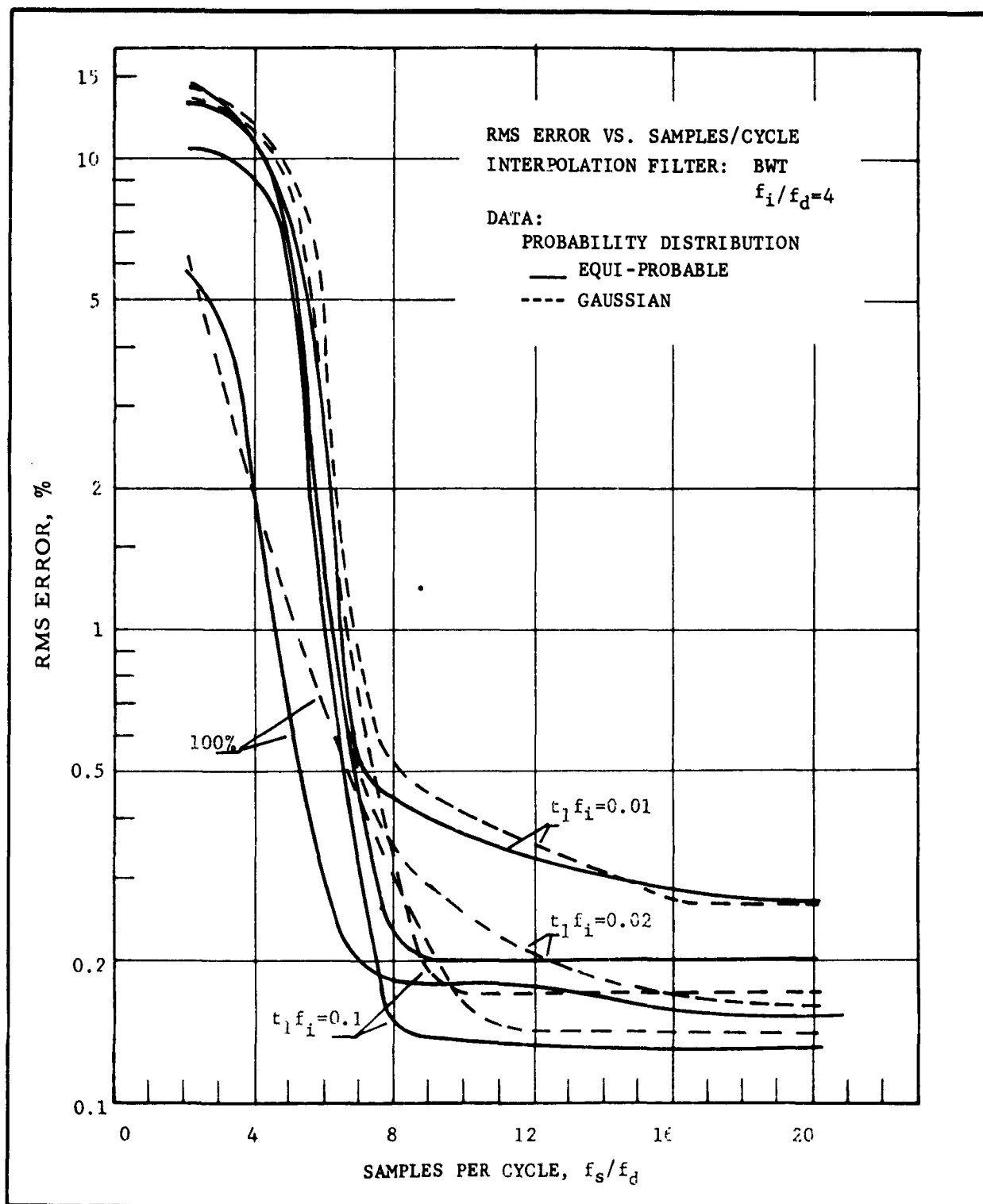


FIG. 4-15 BUTTERWORTH SHAPED DATA,  $f_i/f_d=4$ ,  $J=1$

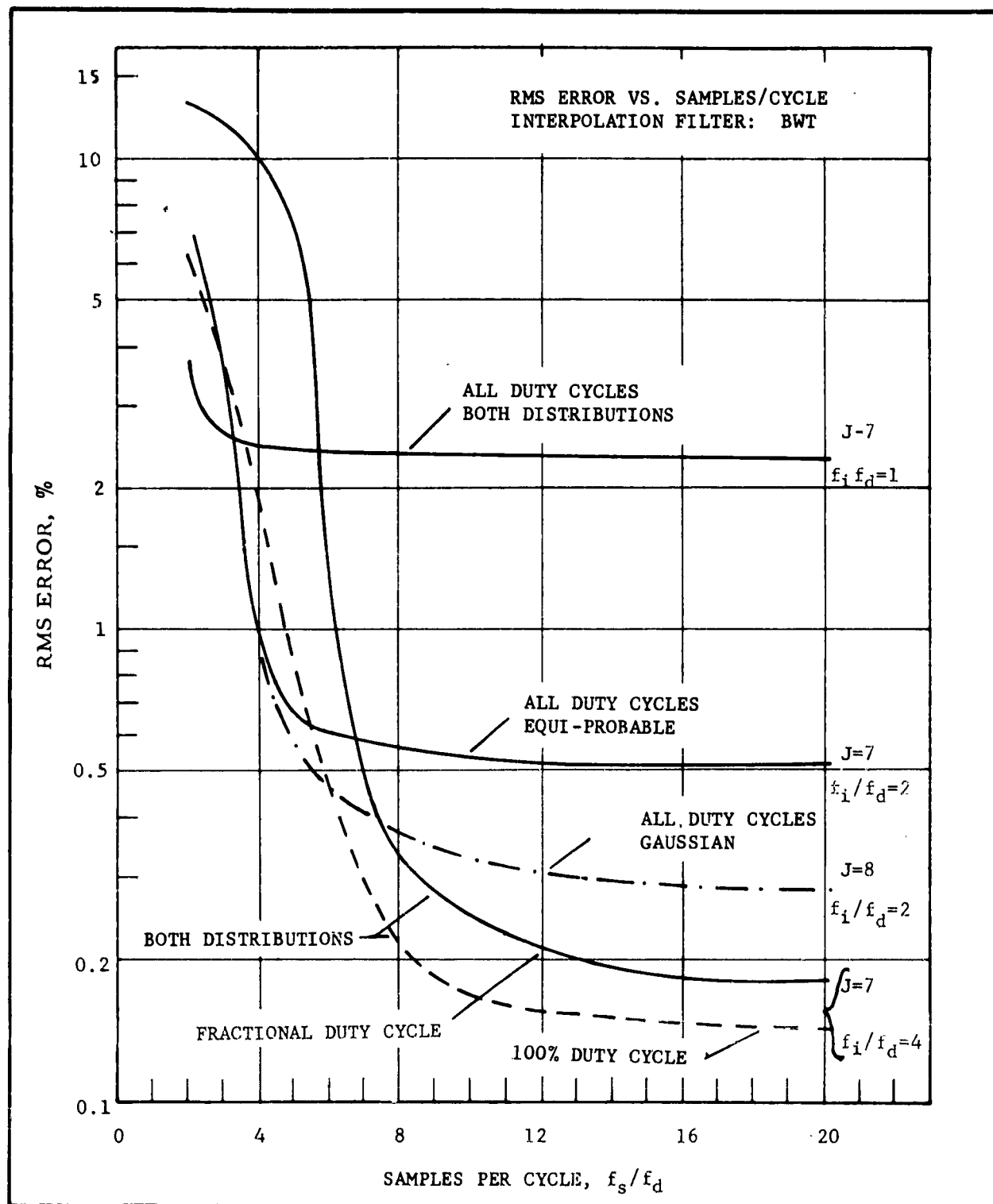


FIG. 4-16 BUTTERWORTH SHAPED DATA CURVES AVERAGED WITH  
RESPECT TO SAMPLE PULSEWIDTH

Separate averaging was performed for  $f_i/f_s = 2$ , since the data source spectral cutoff rates differ. Here the higher cutoff rate reaches a lower minimum error as expected. For  $f_i/f_d = 4$  an average was included in the figure for two cases: 1) fractional and 2) 100% duty cycle because a significant difference was present. This can be attributed to the difference between the fractional duty cycle sampling and the 100% duty cycle sampling techniques.

Figure 4-17 gives the rms error versus samples per cycle for a data cutoff rate of 30 db/oct. ( $J=5$ ) with the BWT filter, and the parameters:  $f_i/f_d = 2$  and  $t_1 f_i = 0.02$ . The results for the 100% duty cycle pulsetrain are plotted in the same figure for comparison. When these curves are compared with Figures 4-10 and 4-12, it is apparent that the data cutoff rate is a sensitive parameter affecting both aliasing and distortion errors. In Figure 4-17 the rms error increased by a factor of 2.8 over that for Figure 4-12 for 100% duty cycle sampling for the parameter  $f_s/f_d$  greater than 10, while the increase is a factor of 1.6 for  $t_1 f_i = 0.02$  over that shown in Figure 4-10. Distortion error takes effect at small values of  $f_s/f_d$  in Figure 4-17 than for Figure 4-10 or 4-12. This causes the sharper corner at about 5 samples per cycle.

Figures 4-18 and 4-19 give the rms error versus samples per cycle for 24 and 36 db/oct. Butterworth interpolation filters. The two sets of curves in each figure are for data cutoff rates of 30 and 48 db/octave. Interpolation of  $t_1 f_i = 0.02$  and 100% duty cycle pulsetrains are shown for each data cutoff rate. The 100% duty cycle pulsetrain gives the best results for aliasing with the 24 db/oct. interpolation filter while  $t_1 f_i = 0.02$  is best for the 36 db/oct. interpolation filter. The difference in observed distortion error is not significant. It can be seen that the greater data cutoff rate allows a smaller rms error for a fixed samples per cycle as expected. Comparison of the three pairs of curves for 30 db/oct. data cutoff shows that the error is fairly insensitive to the interpolation filter response. The BWT filter performs best at low samples per cycle,  $f_s/f_d$ , due to its greater selectivity as noted earlier. The 36 db/oct. Butterworth response offers better performance at high values of  $f_s/f_d$  due to reduced distortion error. Performance is still quite good with the 24 db/oct. filter and this would be a useful design for low frequency interpolation when an RC filter is desired.

Figure 4-20 presents the rms error vs. samples per cycle for a 24 db/oct. Gaussian interpolation filter with 100% duty cycle pulsetrain. The data cutoff rate is 48 db/oct. and  $f_i/f_d = 1$  and 2. The Gaussian filter provides poorer interpolation than any of the other three filters suggesting that amplitude response is of more importance than phase linearity.

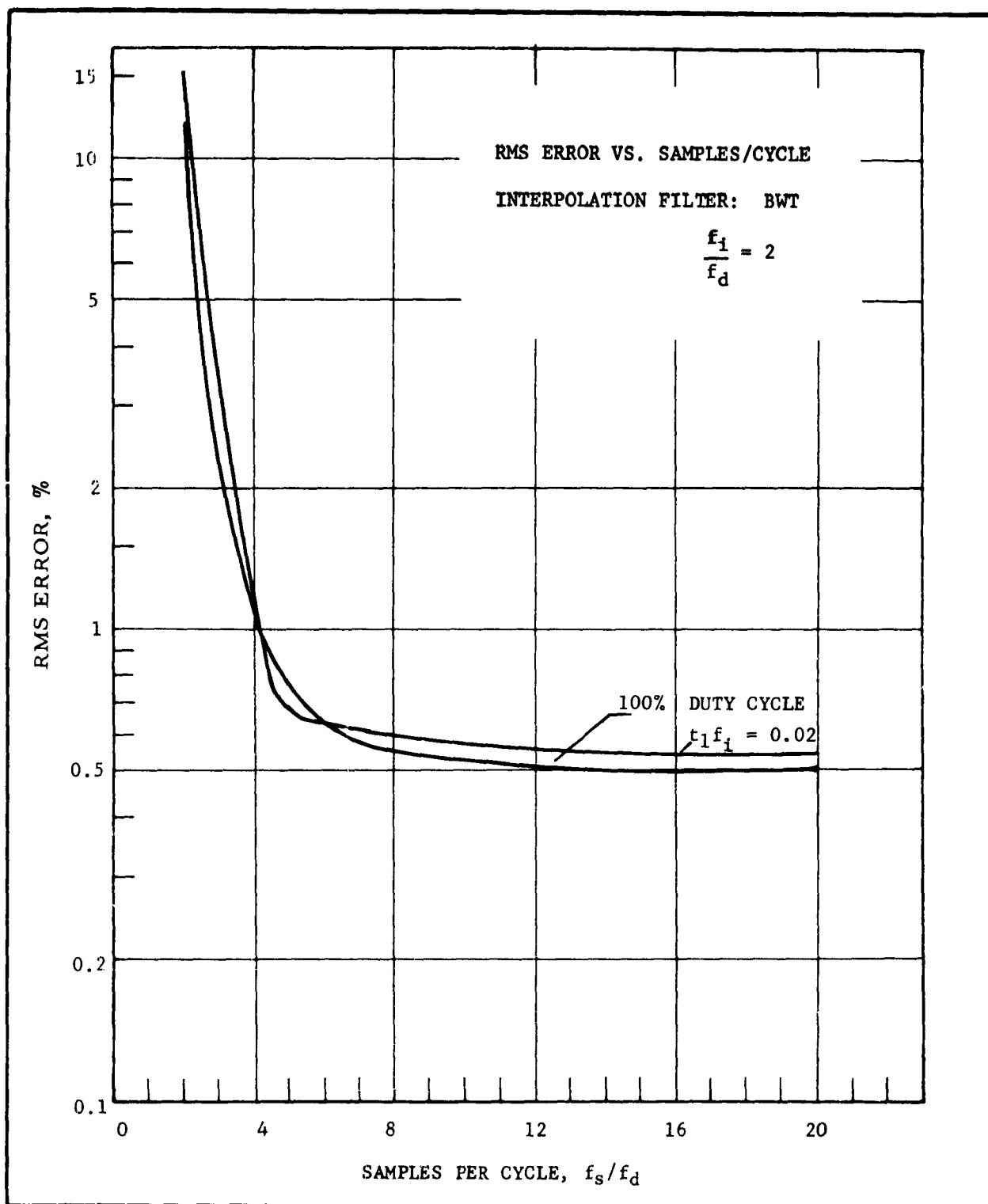


FIG. 4-17 BUTTERWORTH SHAPED DATA, GAUSSIAN PROBABILITY DISTRIBUTION,  $J=5$

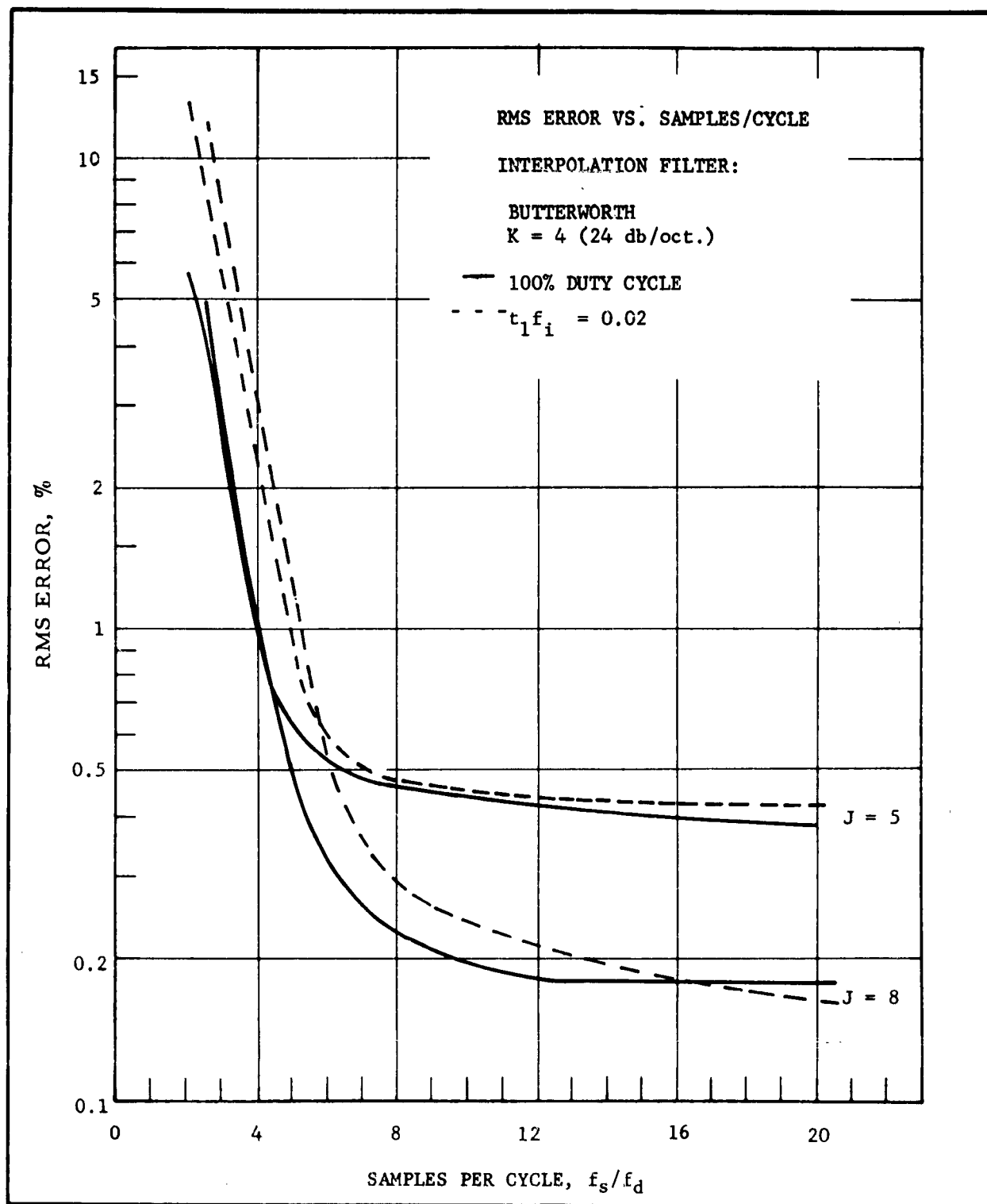


FIG. 4-18 · BUTTERWORTH SHAPED DATA, GAUSSIAN PROBABILITY DISTRIBUTION,  $f_i/f_d=2$ ,  $K=4$

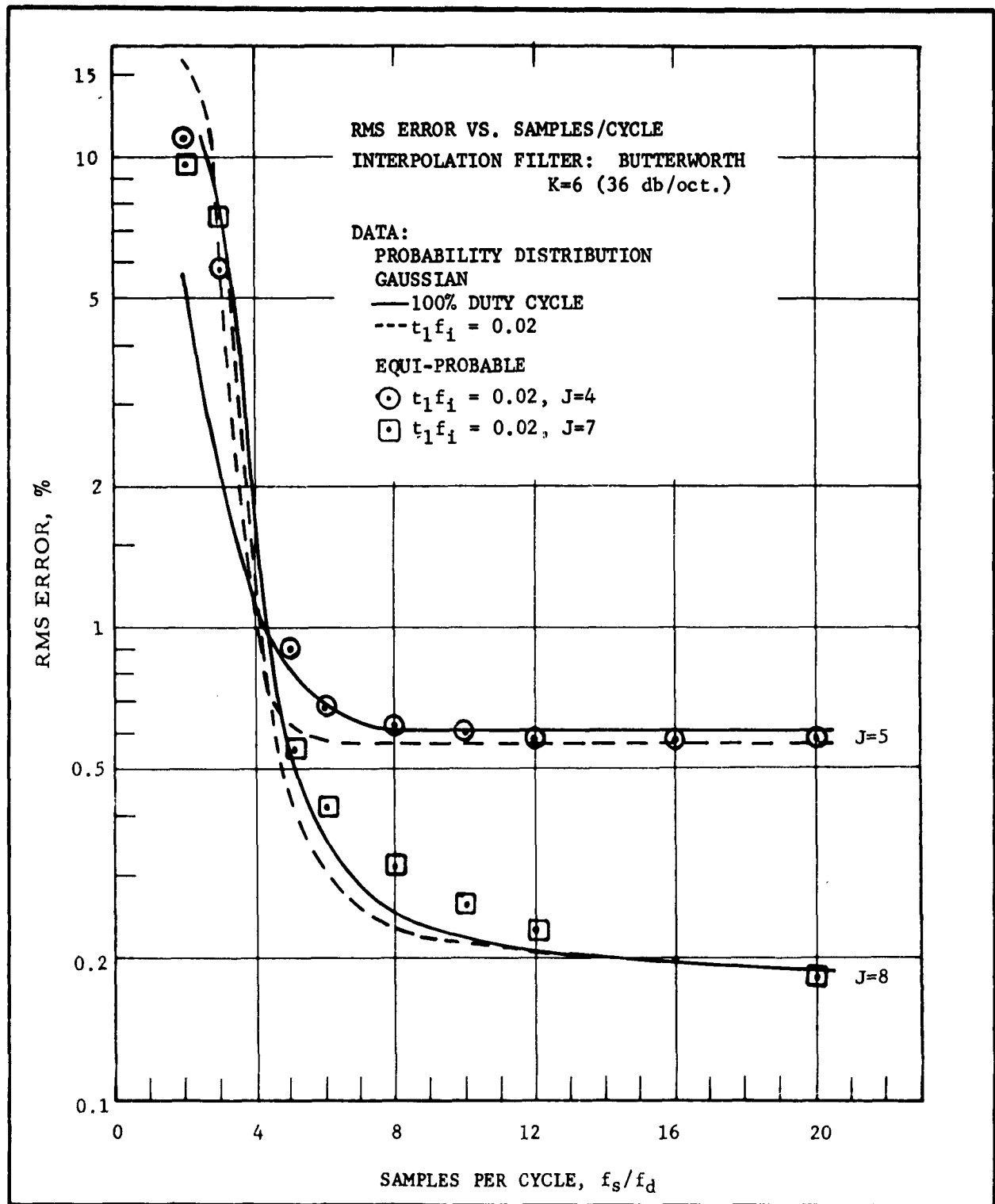


FIG. 4-19 BUTTERWORTH SHAPED DATA, GAUSSIAN AND EQUI-PROBABLE AMPLITUDE PROBABILITY DISTRIBUTION,  $f_i/f_d = 2$ . K = 6

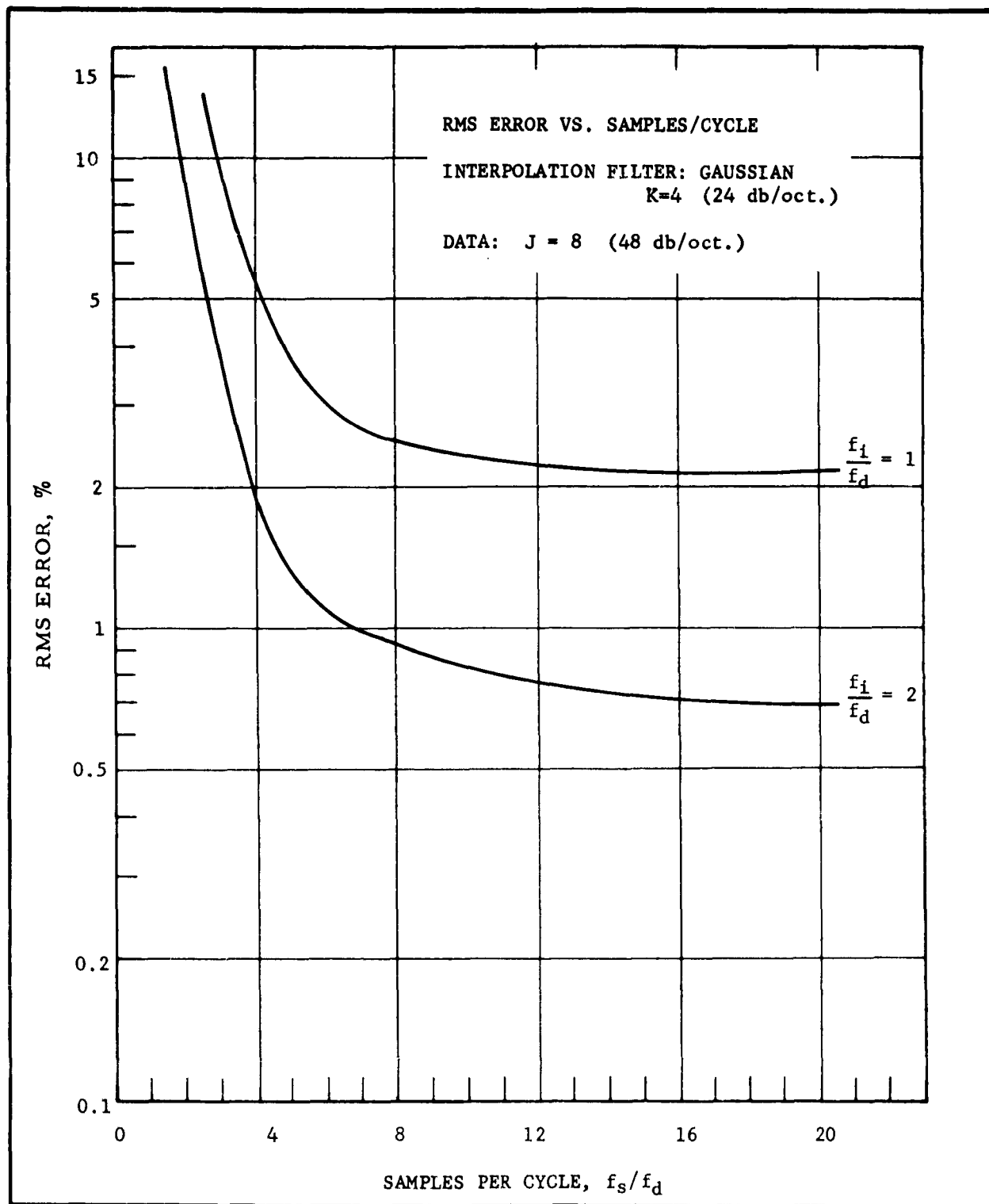


FIG. 4-20 BUTTERWORTH SHAPED DATA, GAUSSIAN PROBABILITY DISTRIBUTION, 100% DUTY CYCLE

### One Sinewave plus Butterworth Gaussian Data Test Results

Figures 4-21 through 4-24 show the test results for a data signal comprising a sinewave plus Butterworth shaped Gaussian noise.

The tests were conducted for:

- 1) various values of the ratio of the data cutoff frequency to the sinewave frequency,  $f_d/f_1$
- 2) two values in db of the ratio of the sinewave voltage to the noise voltage,  $A_S/A_N = 0$  and 12 db
- 3)  $t_1 f_1 = 0.02$  pulsewidth and 100% duty cycle pulsewidth.

The BWT interpolation filter was used throughout these tests.

It will be noticed that for ratios of sinewave to noise voltage of 12 db the test results are similar to the single sinewave test results. At ratios of zero db test results reflect the influence of the Butterworth noise in that the minimum rms error is higher.

The 100% duty cycle interpolation competes favorably with the  $t_1 f_1 = 0.02$  pulsewidth case. In some cases,  $f_d/f_1 = 2$ , the 100% duty cycle pulsewidth gives the best results. For  $f_d/f_1 = 1$  the  $t_1 f_1 = 0.02$  pulsewidth sampling is better. However, the differences are never large.

In general, as the sinewave is reduced in frequency lower rms error is achieved for a fixed sample per cycle of the Gaussian noise cutoff frequency. This is due to the fact that the sinewave is the predominant data and as its frequency is reduced the samples per cycle of the sinewave increases.

### Three Sinewaves plus Butterworth Gaussian Data Test Results

Figures 4-25 through 4-28 show results for three sinewaves plus Butterworth shaped Gaussian noise. The sinewaves are located at various points in the data spectrum:  $f_d/f_1 = 1$ ,  $f_d/f_2 = 1.5$ ,  $f_d/f_3 = 2$ . The db ratio of the sinewave to noise voltage is variable from figure to figure. The two curves in each figure are for  $t_1 f_1 = 0.02$  pulsewidth and 100% duty cycle pulsewidth.



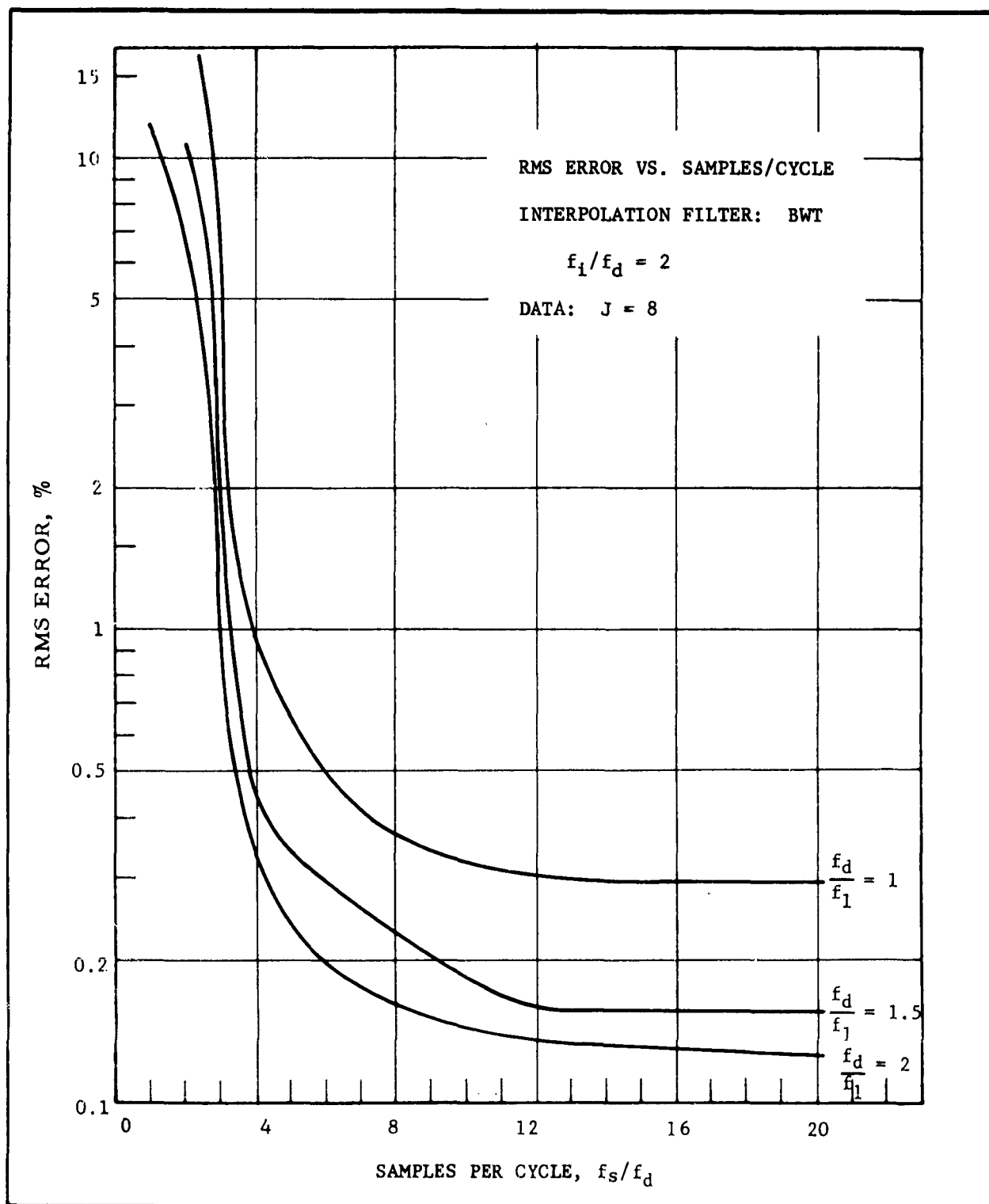


FIG. 4-21 BUTTERWORTH PLUS SINEWAVE DATA, 100% DUTY CYCLE,  $A_S/A_N = 12$  db.

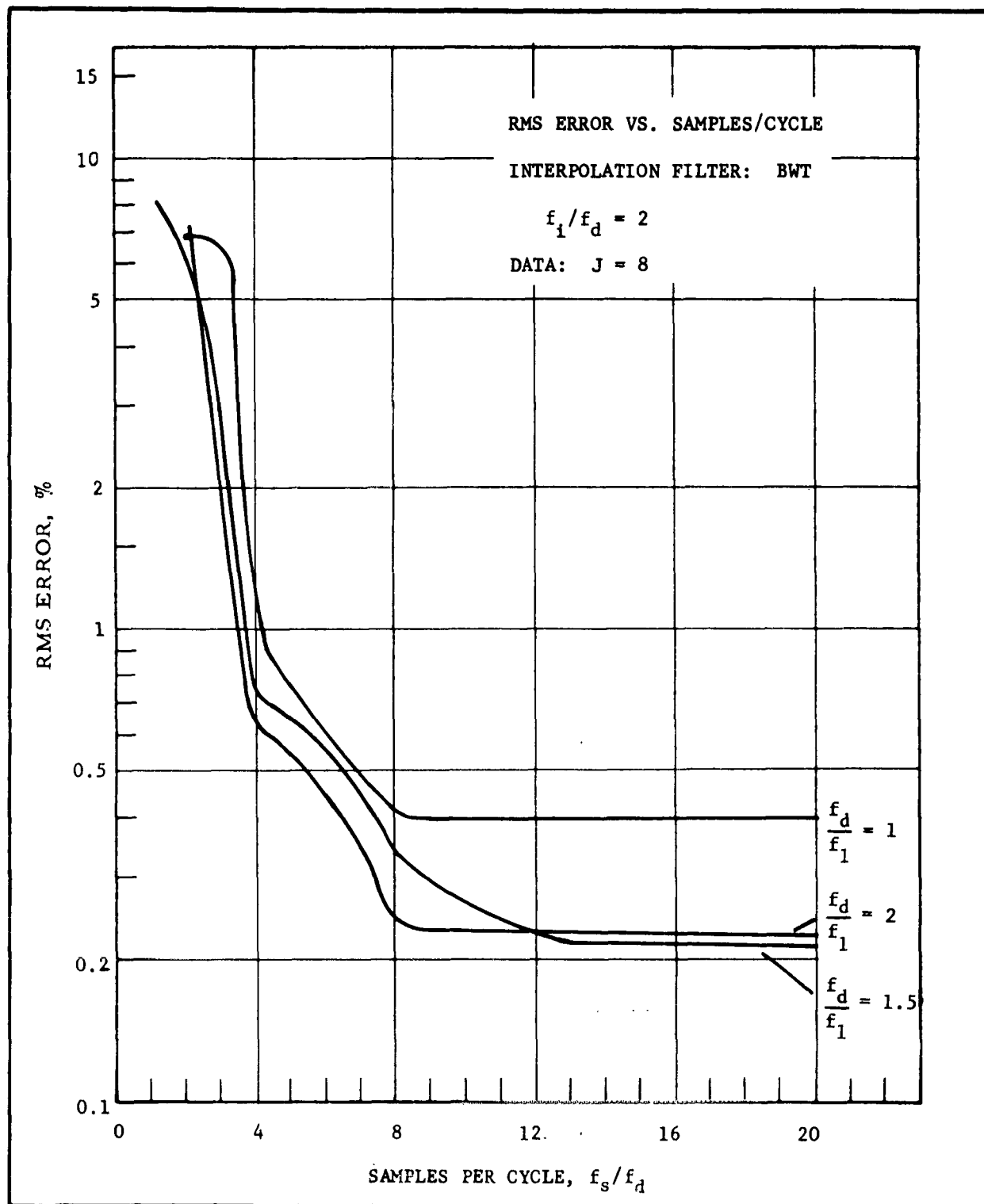


FIG. 4-22 BUTTERWORTH PLUS SINEWAVE DATA, 100% DUTY CYCLE,  $A_S/A_N = 0$  db

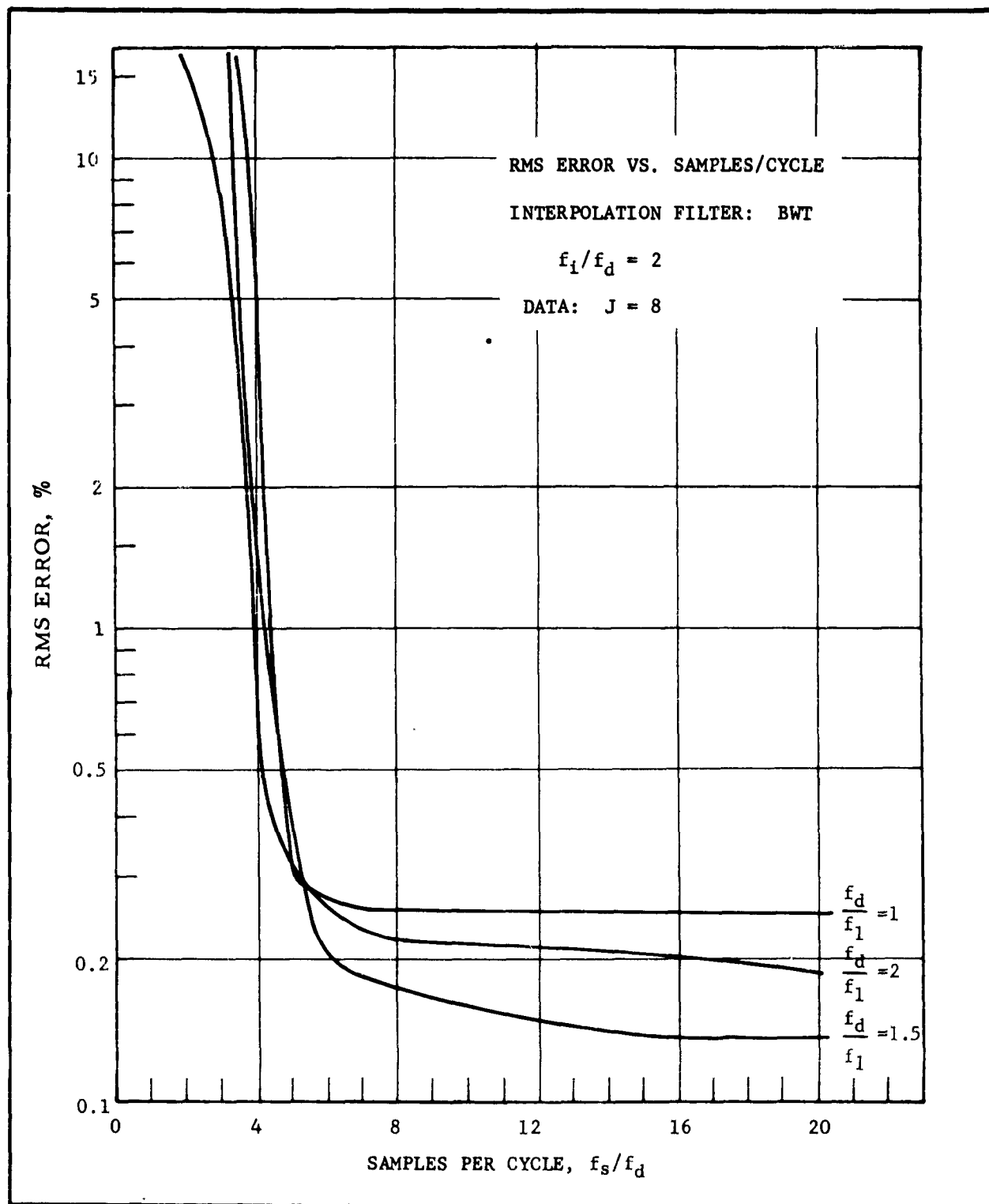


FIG. 4-23 BUTTERWORTH PLUS SINEWAVE DATA,  $t_1 f_1 = 0.02$ ,  $A_S/A_N = 12$  db

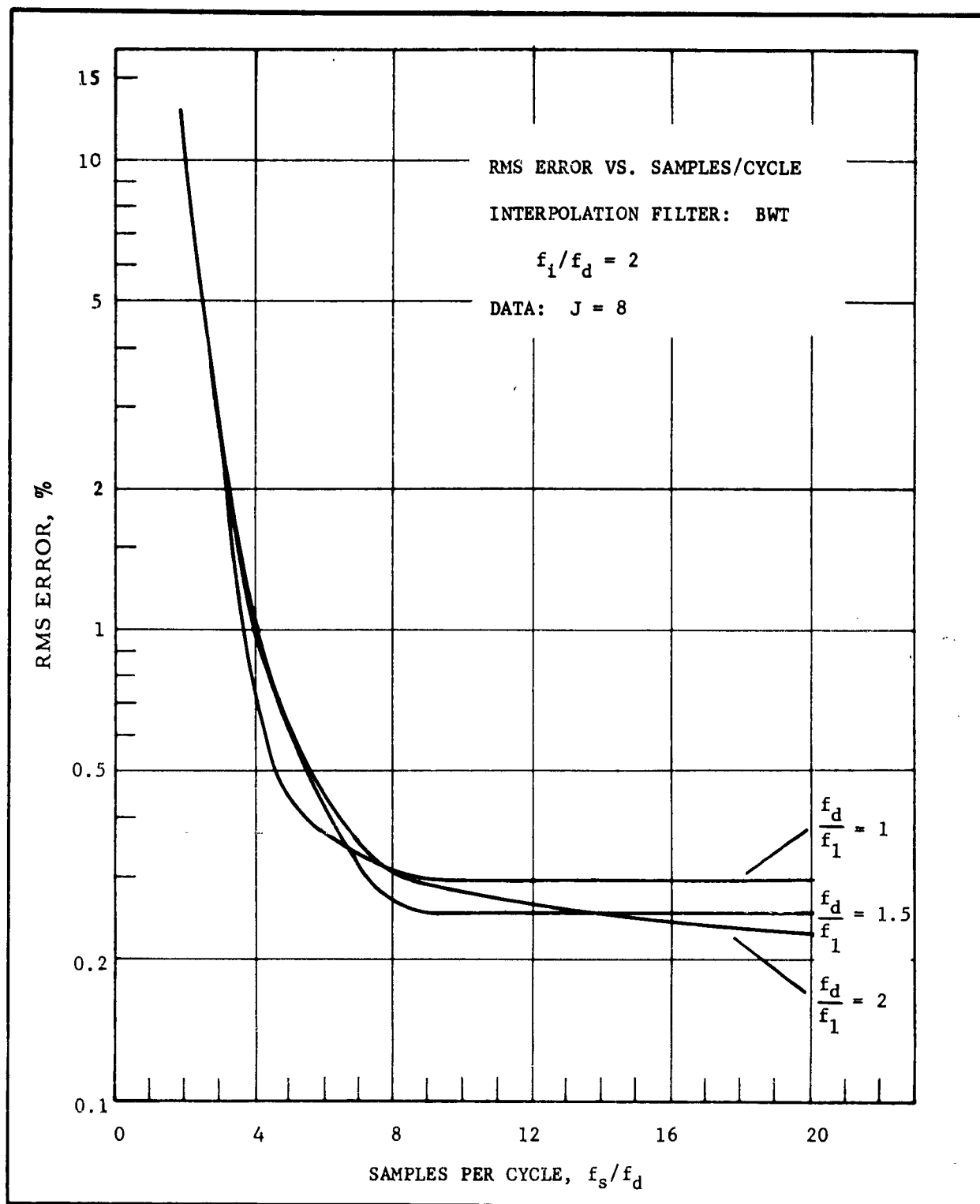


FIG. 4-24 BUTTERWORTH PLUS SINEWAVE DATA,  $t_1 f_i = 0.02$ ,  $A_S/A_N = 0$  db

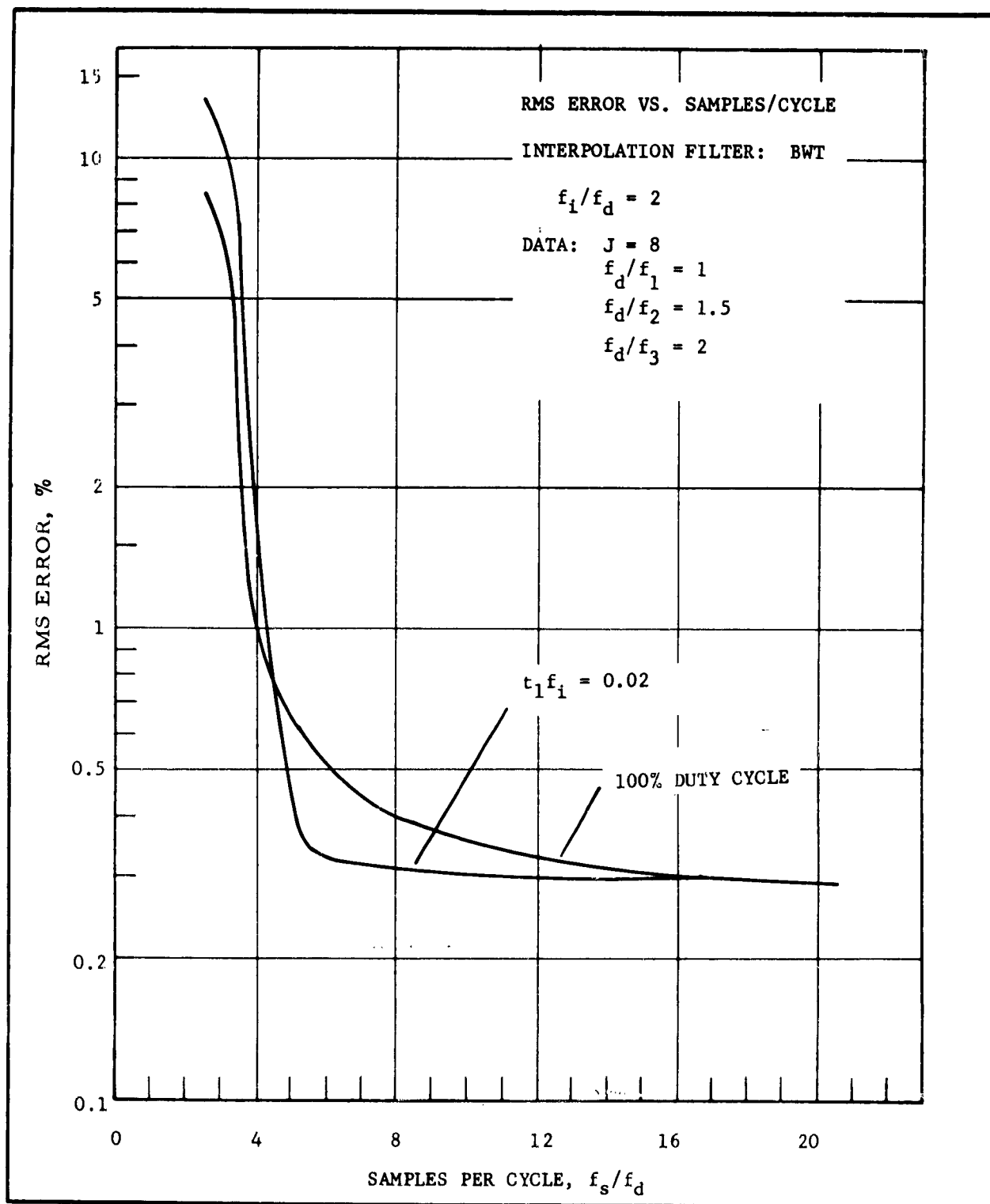


FIG. 4-25 BUTTERWORTH PLUS THREE SINEWAVES DATA,  $A_1/A_N=A_2/A_N=A_3/A_N=0$  db

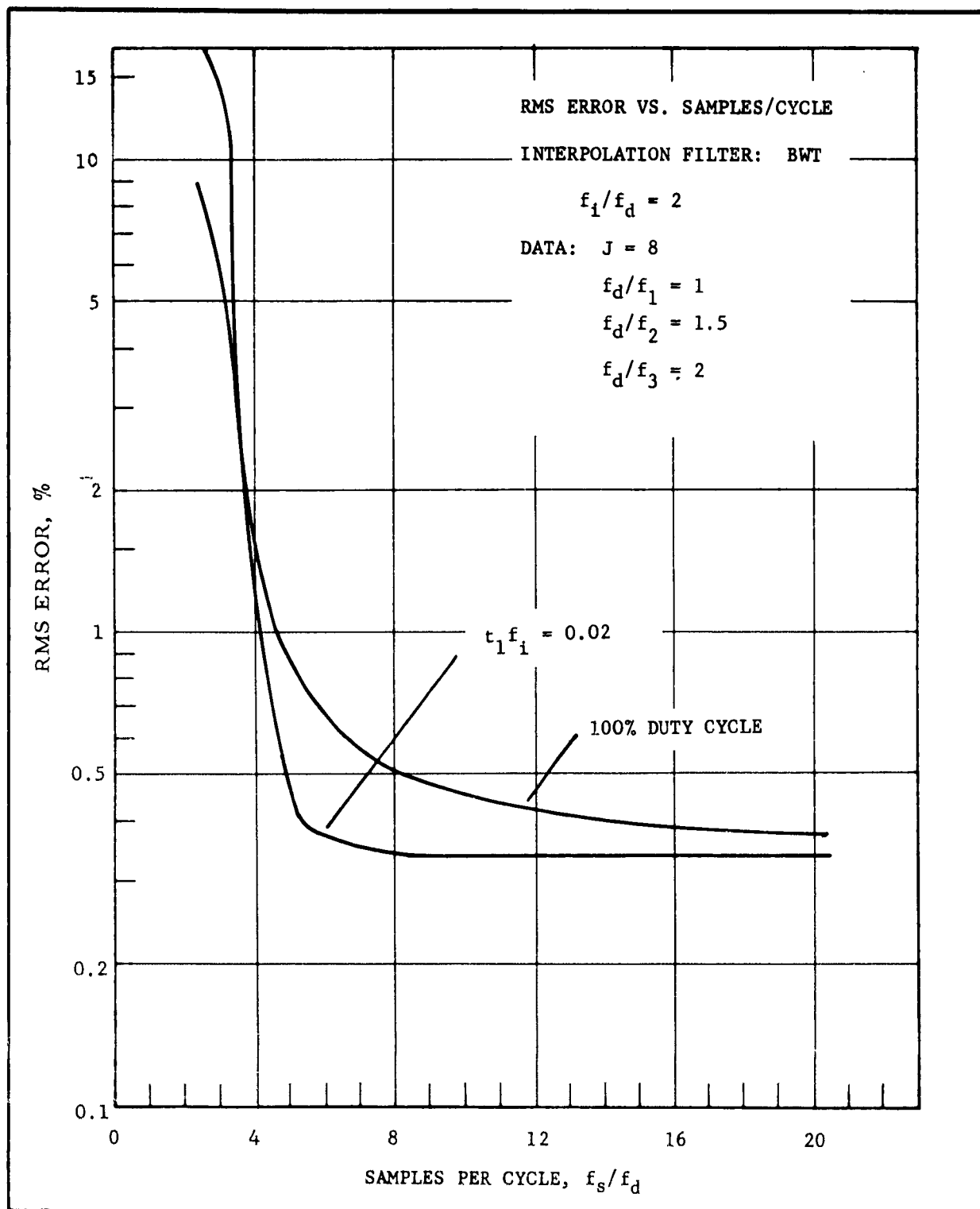


FIG. 4-26 BUTTERWORTH PLUS THREE SINEWAVES DATA,  $A_1/A_N = 6$  db,  $A_2/A_N = 0$  db,  $A_3/A_N = 12$  db

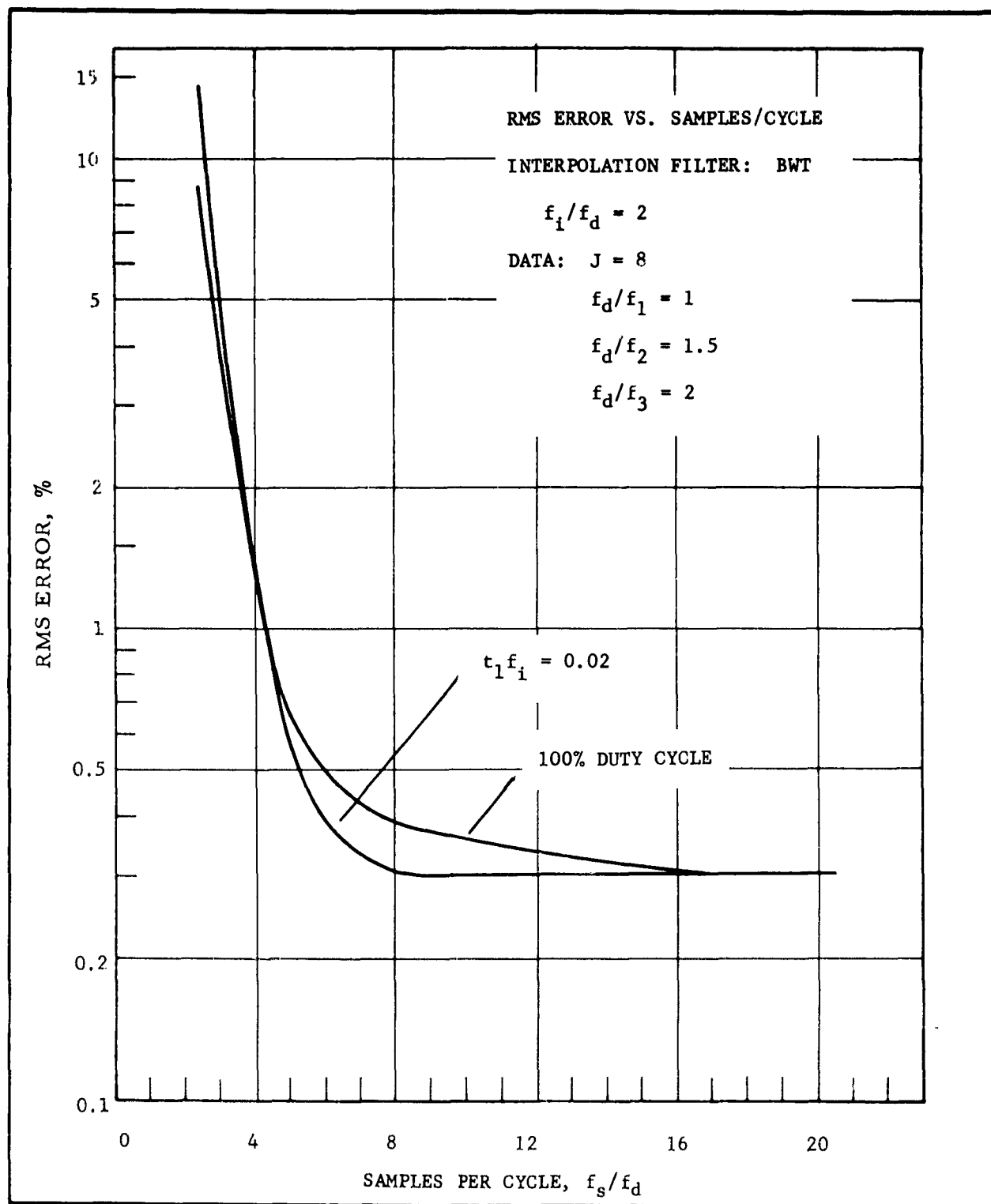


FIG. 4-27 BUTTERWORTH PLUS THREE SINEWAVES DATA,  $A_1/A_N=A_2/A_N=A_3/A_N=12$  db

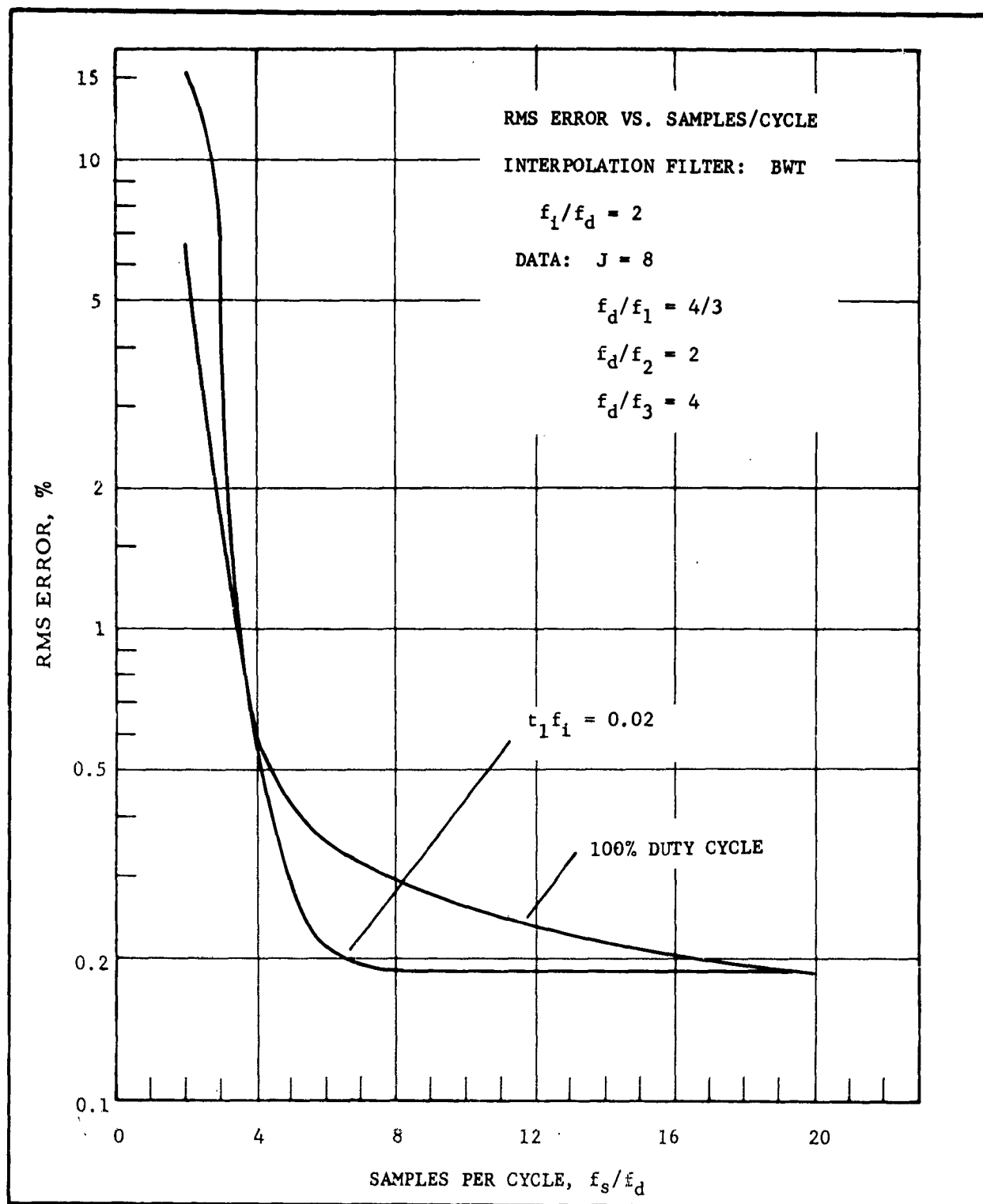


FIG. 4-28 BUTTERWORTH PLUS THREE SINEWAVES DATA,  
 $A_1/A_N=A_2/A_N=A_3/A_N=12$  db;  $f_1/f_d = 2$



Figures 4-25 and 4-27 are nearly the same. It follows that even for the zero db case the noise is relatively unimportant in determining the error. Figure 4-28 displays lower rms errors for a given sample per cycle of the data cutoff frequency since the sinewave frequencies have been lowered.

#### Step Type Butterworth Gaussian Data

The test results and the spectrum are presented in Figure 4-29. The results show that the low frequency data is predominant in determining the aliasing error. As the ratio of  $A_1$  to  $A_2$  is decreased the results will approach that for Butterworth Gaussian data.

#### Bandpass Data

Figure 4-30 shows the results for bandpass data with two pairs of upper and lower cutoff frequencies. Values of  $t_1 f_i = 0.02$  and 100% pulse-width were used. The BWT interpolation filter was used. Best results were obtained when the low frequency data signal was increased.

Some bandpass interpolation tests not reported were tried briefly, but performance was poorer than for lowpass interpolation.

#### 4.3.3 Time Function Photographs and Spectral Measurements

The following data is included to illustrate the effects observed in performance of the experimental tests and typical power spectral density measurements taken during the course of the program.

##### Time Function Photographs

Figure 4-31 provides a comparison of the data, 100% duty cycle pulsetrain, and the BWT interpolation filter output waveforms for equiprobable amplitude data. The delay between the data and interpolation filter output is accounted for by the analog error comparator.

Figure 4-32 is a comparison of the data and BWT interpolation filter output waveforms for Gaussian data and fractional duty cycle pulsetrain. In Figure 4-32 the aliasing spectrum feedthrough is quite evident in the second photograph from the top, and contributes significantly to the error.

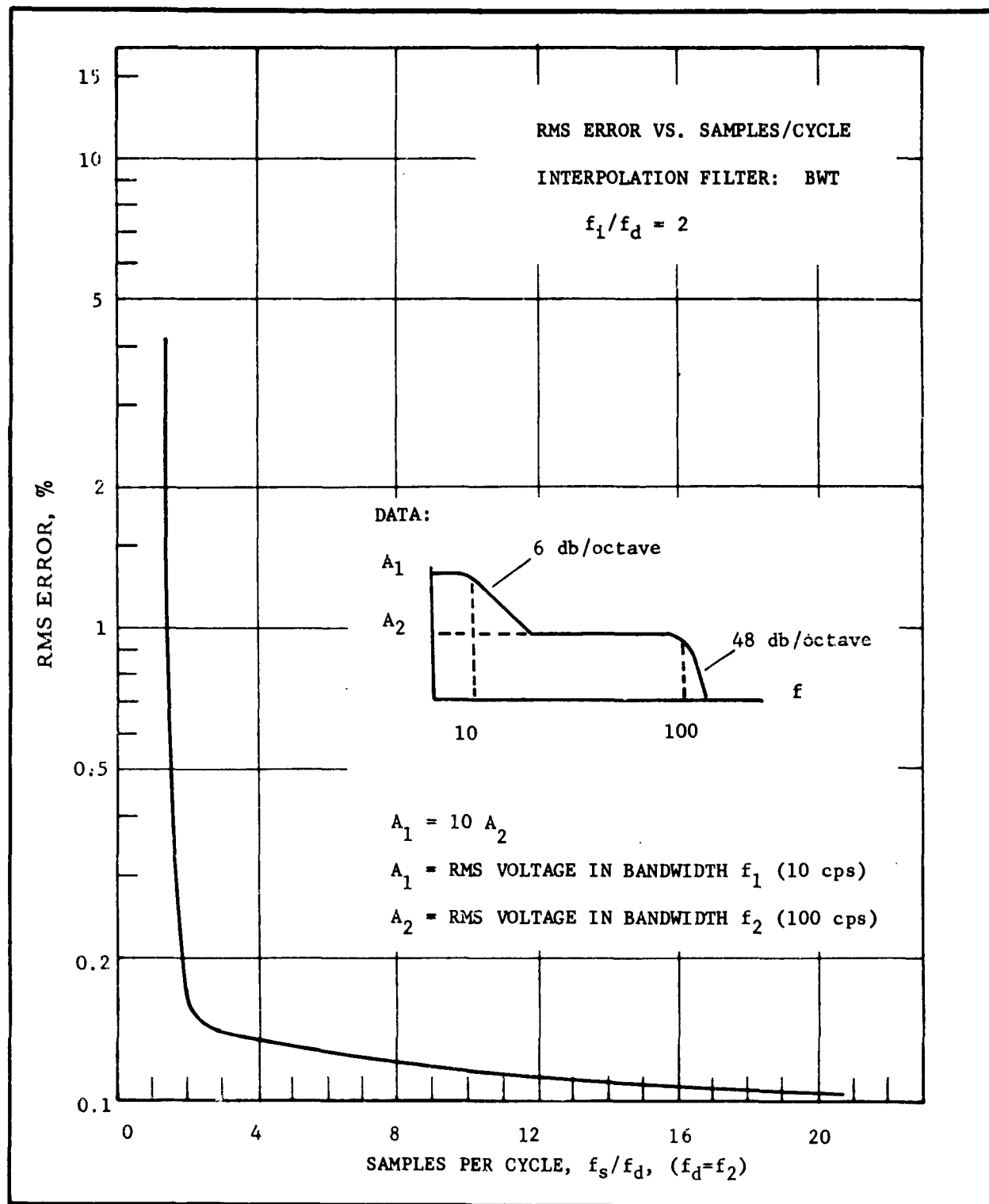


FIG. 4-29 CONTINUOUS WITH STEP BUTTERWORTH SHAPED  
GAUSSIAN DATA, 100% DUTY CYCLE

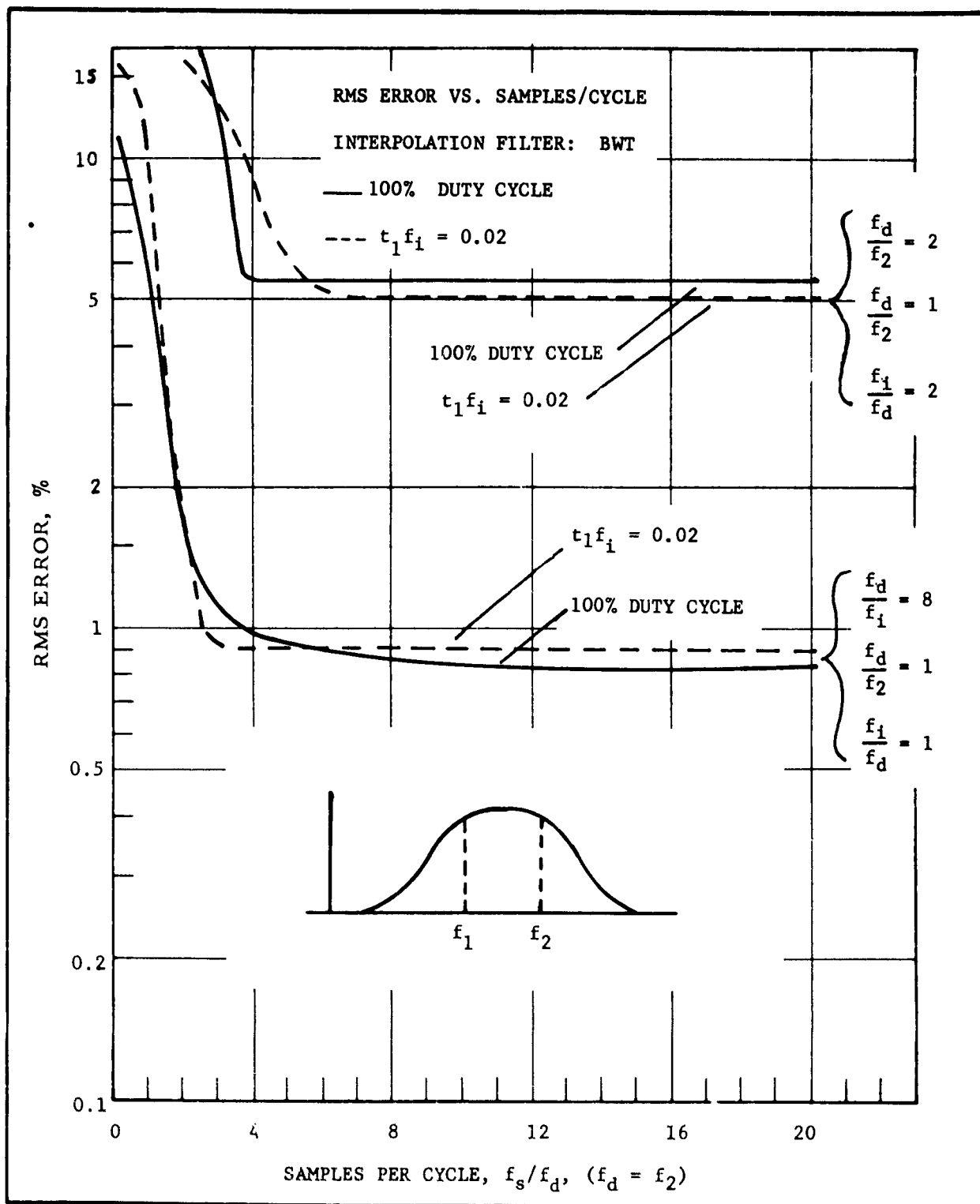
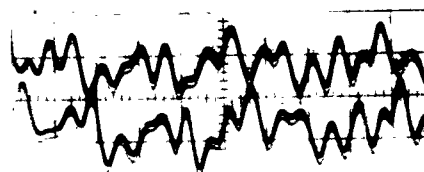
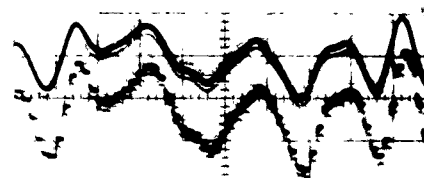


FIG. 4-30 BANDPASS GAUSSIAN DATA WITH 24 db/oct. SLOPES



INTERPOLATION FILTER OUTPUT  
DATA

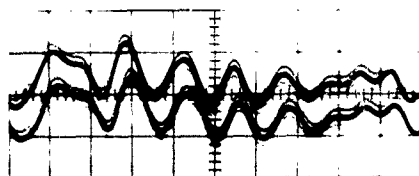


DATA

SAMPLED DATA OUTPUT

$J=7$ ,  $f_i/f_d=1$ ,  $f_s/f_d=6$ , RMS ERROR = 2.8%

FIG. 4-31 PHOTOGRAPHS OF DATA, BWT INTERPOLATION FILTER OUTPUT,  
AND SAMPLER OUTPUT. EQUI-PROBABLE AMPLITUDE  
DISTRIBUTION. 100% DUTY CYCLE

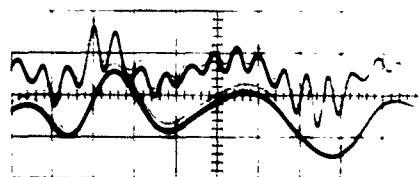


$J=7, f_1/f_d=4$

INTERPOLATION FILTER OUTPUT

DATA

$f_s/f_d=14$ , RMS ERROR = 0.2%

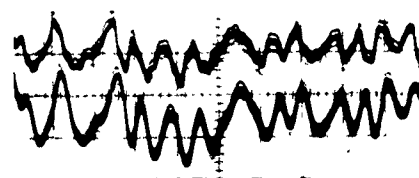


$J=7, f_1/f_d=4$

INTERPOLATION FILTER OUTPUT

DATA

$f_s/f_d=4$ , RMS ERROR = 9.4%



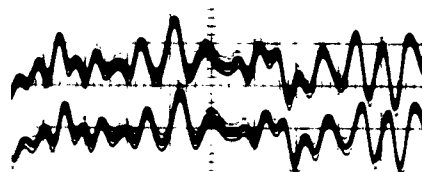
$J=8, f_1/f_d=2$

INTERPOLATION FILTER OUTPUT

DATA

$f_s/f_d=3$ , RMS ERROR = 2.6%

FIG. 4-32 PHOTOGRAPHS OF DATA AND BWT INTERPOLATION FILTER OUTPUT.  
GAUSSIAN PROBABILITY DISTRIBUTION  $t_1 f_1=0.02$ .

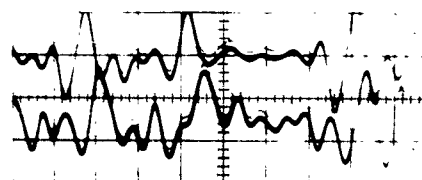


$J=8, f_1/f_d=2$

INTERPOLATION FILTER OUTPUT

DATA

$f_s/f_d=14$ , RMS ERROR = 0.84%

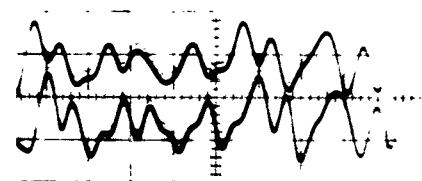


$J=7, f_1/f_d=1$

INTERPOLATION FILTER OUTPUT

DATA

$f_s/f_d=2$ , RMS ERROR = 4.25%



$J=7, f_1/f_d=1$

INTERPOLATION FILTER OUTPUT

DATA

$f_s/f_d=8$ , RMS ERROR = 3.75%

FIG. 4-32 PHOTOGRAPHS OF DATA AND BWT INTERPOLATION FILTER OUTPUT.  
GAUSSIAN PROBABILITY DISTRIBUTION  $t_1 f_1=0.02$ .

### Spectral Measurements

The accompanying spectral measurements have been recorded using a B&K Audio Frequency Spectrum Recorder Type 3311 which consists of AF Spectrometer Type 2111 and Level Recorder Type 2304. It is designed for the automatic recording of spectrograms, and has a frequency range of 50 cps - 35 kcps. The bandpass filters are either full octave or 1/3 octave wide, a constant percentage of the center frequency, which produces a positive 6 db/oct. change in slope in all spectra analyzed.

This slope is readily seen in Figure 4-33. The fact that the bandwidth is broad means that the resulting spectral measurements are lacking in detail. This is evident in Figure 4-33 for the equi-probable amplitude noise source which has a  $\sin(x)/x$  spectrum with the first null at 4000 cps. This spectrum is essentially flat up to 200 cps.

The spectra of interest in the single channel system are shown in Figure 4-34. That portion of the spectrum which contributes to aliasing is readily seen as that portion above 500 cps in the Sampled Data Spectrum.

Figure 4-35 shows comparable spectra in the single channel system for the equi-probable amplitude data source.

The Sigmatron noise generator provides three bandwidth selections - 1000, 100, and 10 cps. When the data bandwidth was 200 cps the 1000 cps bandwidth was used and the resulting cutoff rate was that due to the filter, 42 db/oct. For a data bandwidth of 100 cps the Sigmatron noise generator bandwidth was set at 100 cps in order to provide sufficient signal at the data filter output and the cutoff rate of the noise generator at 100 cps is approximately 6 db/oct. Combining this cutoff with that of the filter results in an overall rolloff of 48 db/oct. These cutoff rates were measured with a General Radio Company Wave Analyzer, Type 736-A and are shown in Figure 4-36. The Sigmatron noise generator output for 100 cps bandwidth setting was measured as well as the filtered output using the SKL Model 308 filter. When a data bandwidth of 50 cps was desired the 100 cps Sigmatron bandwidth was used and the resulting data cutoff rate was again 42 db/oct. This problem was not encountered for equi-probable amplitude distribution noise since the 3 db noise bandwidth was approximately ten times the largest data bandwidth.

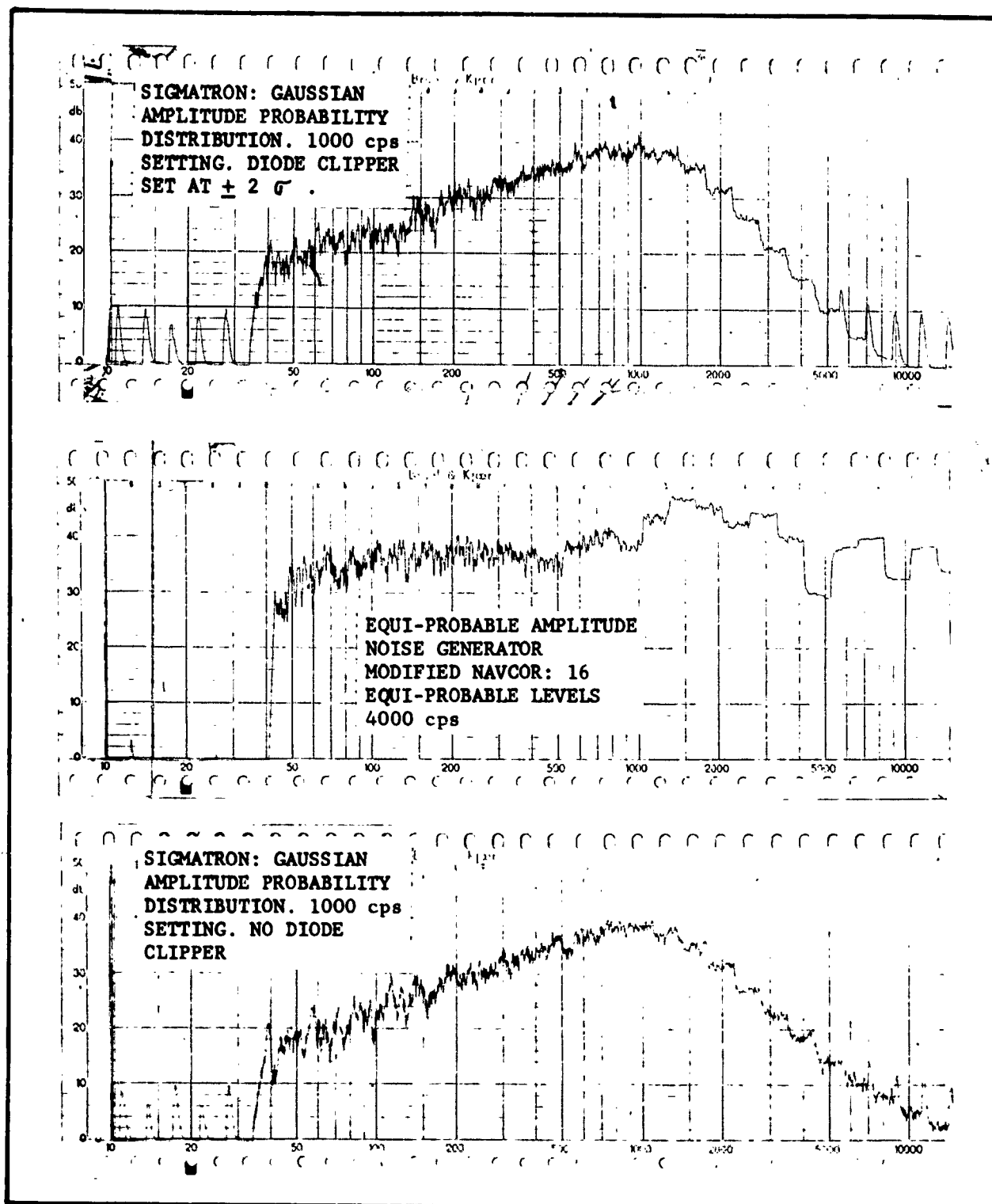


FIG. 4-33 SPECTRA OF NOISE SOURCES



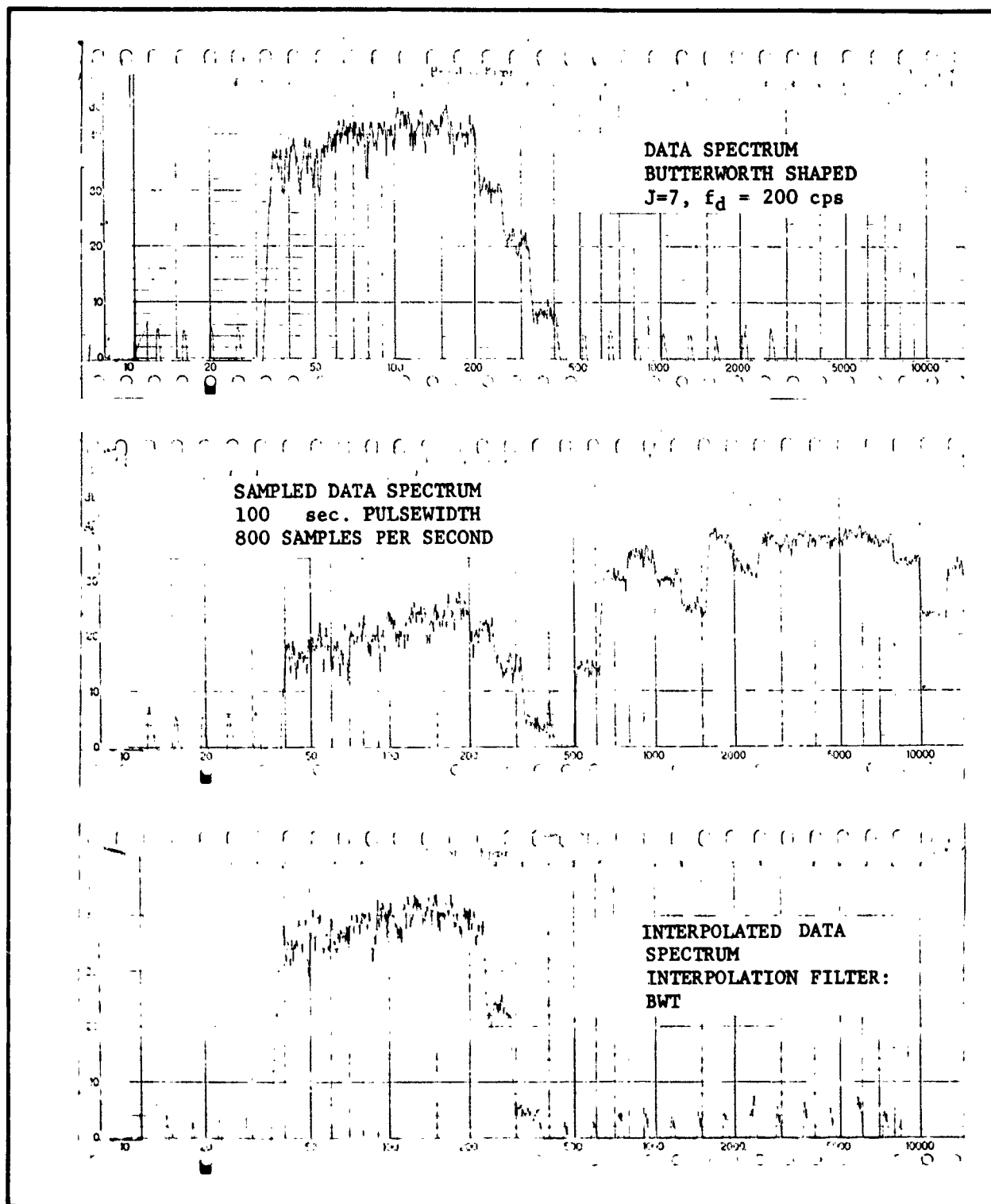


FIG. 4-34 SINGLE CHANNEL SYSTEM SPECTRA,  
DATA: GAUSSIAN AMPLITUDE  
PROBABILITY DISTRIBUTION

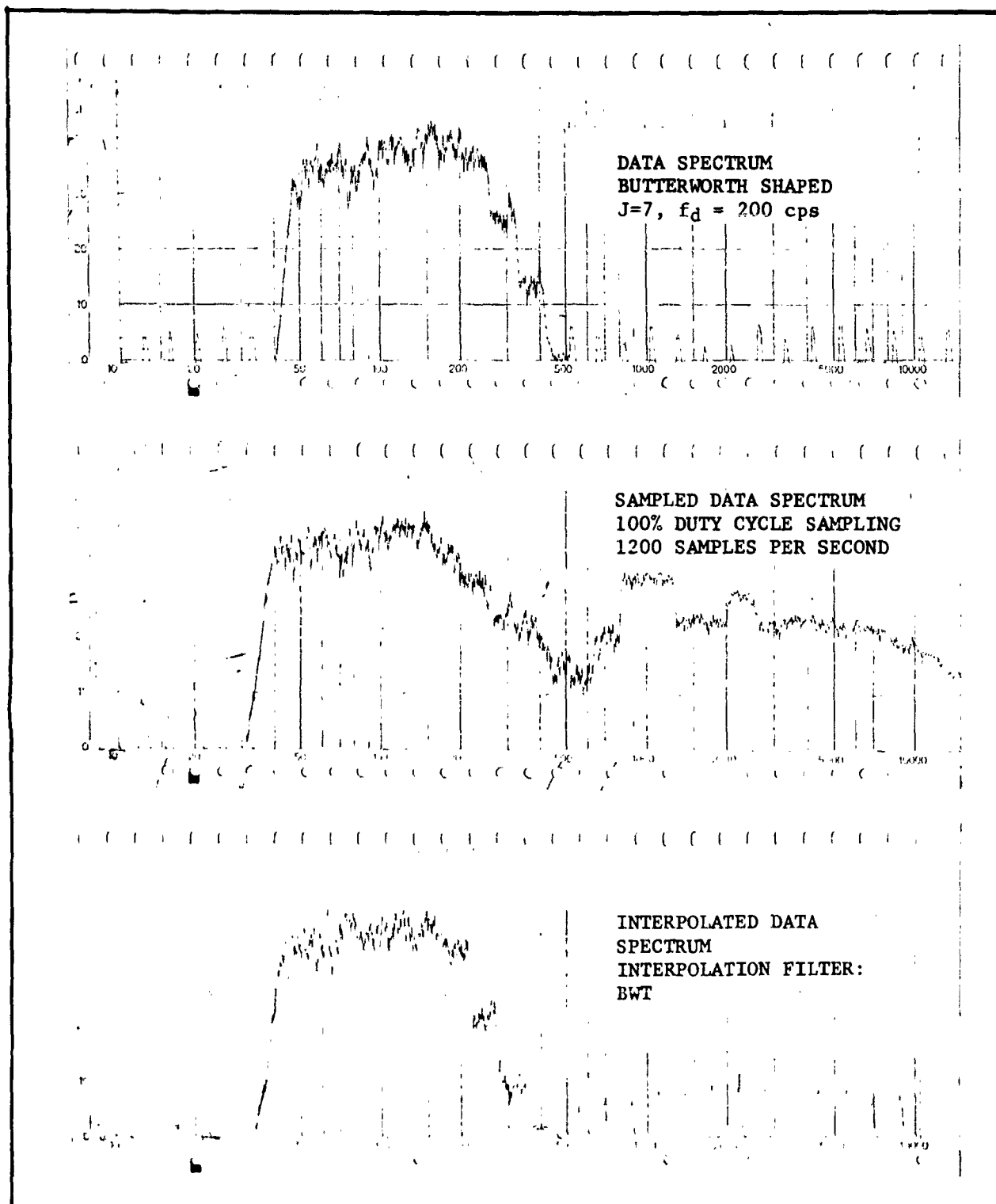


FIG. 4-35 SINGLE CHANNEL SYSTEM SPECTRA,  
 DATA: EQUI-PROBABLE AMPLITUDE  
 PROBABILITY DISTRIBUTION

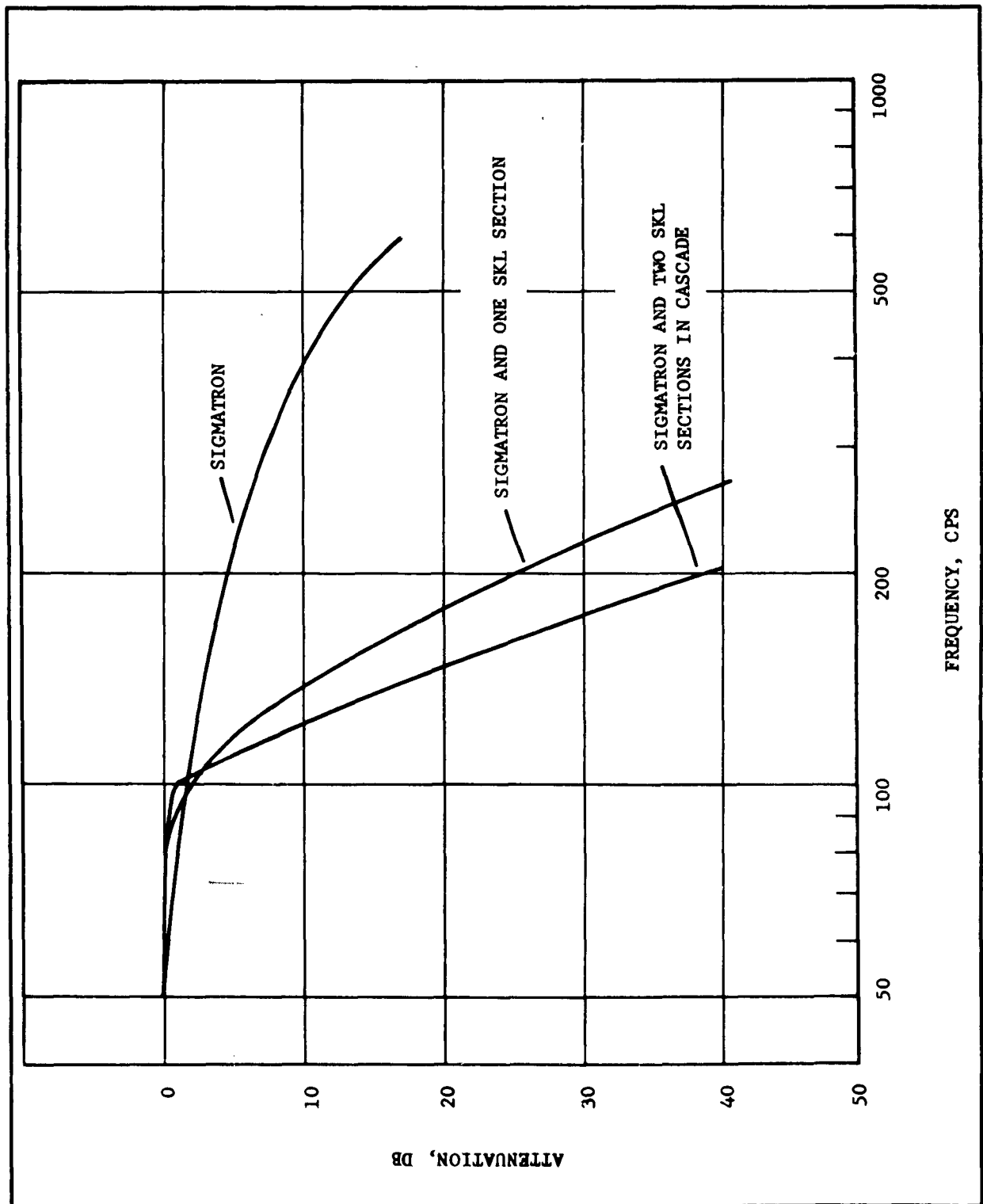


FIG. 4-36 SPECTRA OF BUTTERWORTH SHAPED DATA,  
GAUSSIAN AMPLITUDE PROBABILITY DISTRIBUTION

#### 4.4 MULTI-CHANNEL SYSTEM TESTS

##### 4.4.1 System Description

The general system block diagram and description is given in Figure 5-1 Section 5. A brief description of the system operation is given here.

The test setup is similar to that used for the PAM-FM tests described in Reference 1, Volume III. The same subcarrier equipment was used as an RF carrier. All tests were performed with 150  $\mu$  second pulse-width sampling constituting 60% of the pulse period for driving the interpolation filter. The analog error comparator was activated only by the data channel being measured with modulation on all other channels removed to permit ready determination of the crosstalk error. No pulse detector was used. The equivalent function was performed by the interpolation filter since the wide sample pulsewidths including noise were fed to the lowpass interpolation filter which discriminated against the noise by performing an integrating action similar to that performed by an integrating pulse detector. The position of the decommutator gate within the pulse period was also adjustable. The position was chosen to give the minimum system residual error reading. This position was approximately at the center of the pulse.

##### 4.4.2 Test Results

The multi-channel tests served to establish that overall system error could be obtained by combining interpolation error determined from single channel tests with the other error sources consisting primarily of interference and crosstalk. Error due to interference and crosstalk were obtained during the telemetry system study reported in Reference 1. This was verified for the P/M-FM system.

The carrier system was set up as follows:

- 1) Receiver bandwidth,  $B = 12$  kcps
- 2) System pulse rate,  $F_s = 4$  kcps
- 3)  $M = B/F_s = 3$
- 4) Channel sampling frequency,  $f_s = 500$  cps

- 5) Peak deviation =  $\pm 4.5$  kcps
- 6) No premodulation filtering
- 7) Lowpass filter following discriminator = 6 kcps
- 8) Data - Butterworth, Gaussian noise
- 9) Interpolation Filter - Butterworth

Four tests were conducted with this setup. Slope of the data and the interpolation filter were selected and tests conducted for variable samples per cycle. The rms error was measured as a function of S/N, the signal to noise ratio, measured preceding the discriminator. The results of these tests are shown in Figures 4-37 through 4-40. Calculated results are also shown.

The calculated results were obtained by adding the mean-square interpolation error for the single channel tests to the mean-square pulse error with the residual equipment error removed from the values of  $S/k_1 F_S^{1/2}$  obtained from Figure II-6-17, Reference 1, Volume II reproduced in Figure 4-41. The rms error was obtained by taking the square root of this sum. The agreement obtained is very good in most cases. This method allows the overall system performance to be calculated for any of the time-division multiplexed systems under a wide range of operating conditions and signal-to-noise ratios by using the single channel interpolation error in conjunction with the system performance determined from Reference 1 or from other data.

#### 4.4.3 Time Function Photographs and Spectral Measurements

##### Time Function Photographs

Figure 4-42 shows multiple sweep oscilloscope waveforms at the 8 channel multiplexer output. The top photograph shows several frames with all channels modulated; the next photograph has an expanded sweep rate to show detail as does the bottom photograph where only one channel is modulated.

Figure 4-43 shows the decommutator input and output waveforms with and without adjacent channel modulation. It can be seen that the output waveform is a gated portion of the input waveform.

##### Spectral Measurements

Spectra were observed at various points in the system and were found to appear similar to those shown for the single channel tests at the corresponding points. Carrier and multiplex output spectra were checked and are as reported in Reference 1.

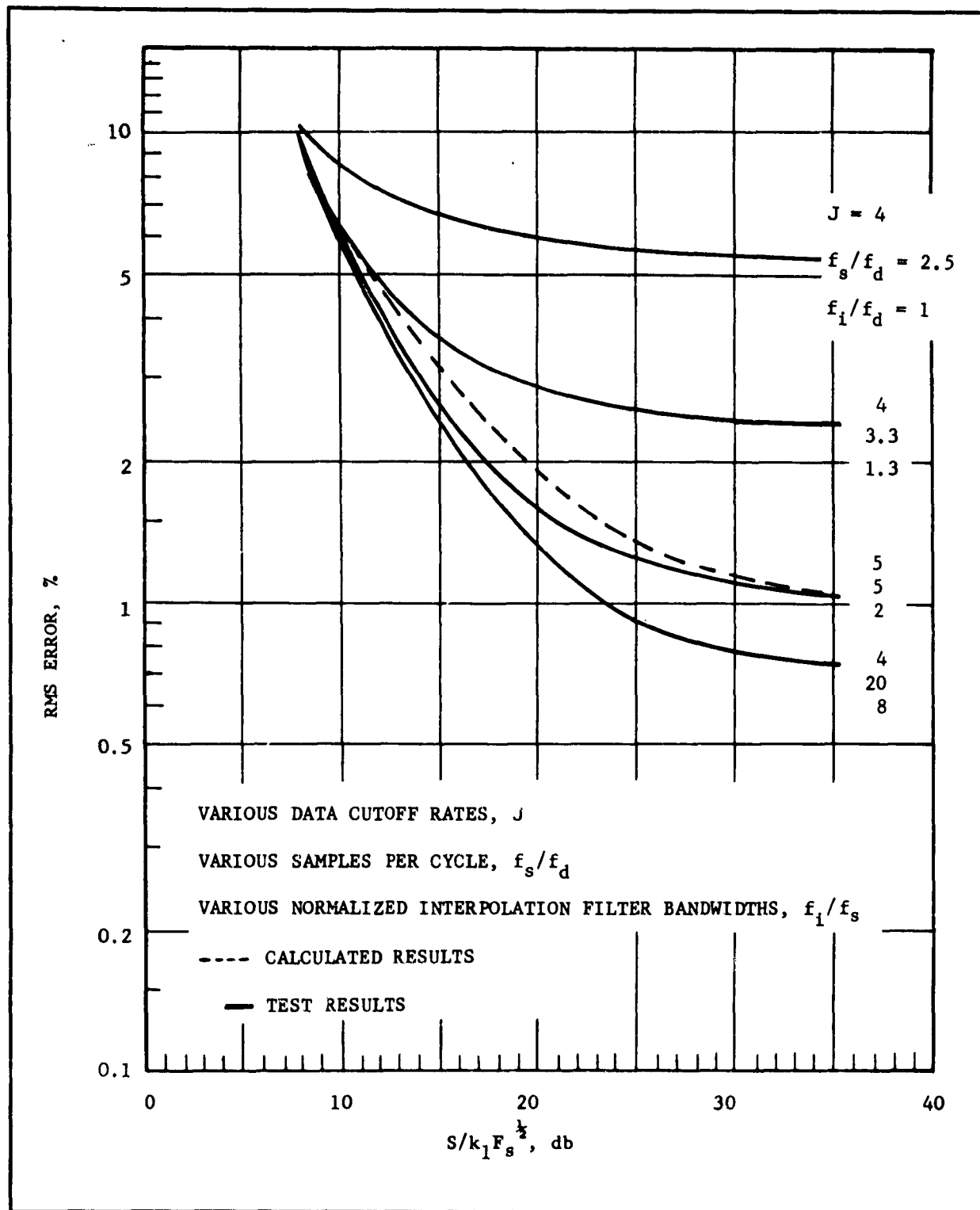


FIG. 4-37 RMS ERROR VS.  $S/k_1 F_s^{1/2}$ . INTERPOLATION FILTER: BUTTERWORTH, 24 db/oct. DATA: BUTTERWORTH,  $J = 4$  AND 5

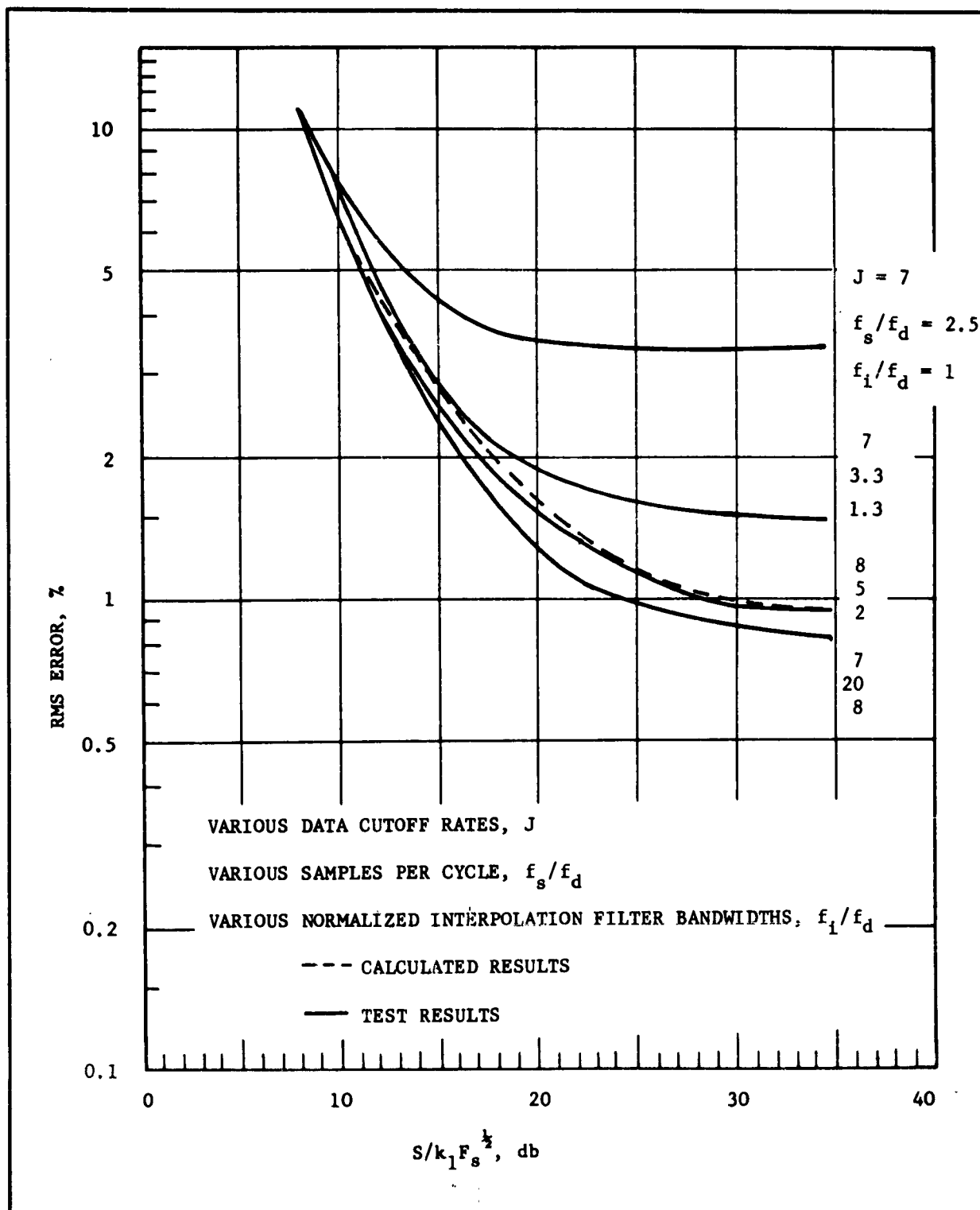


FIG. 4-38 RMS ERROR VS.  $S/k_1 F_s^{1/2}$ . INTERPOLATION FILTER: BUTTERWORTH, 24 db/oct. DATA: BUTTERWORTH, J = 7 AND 8

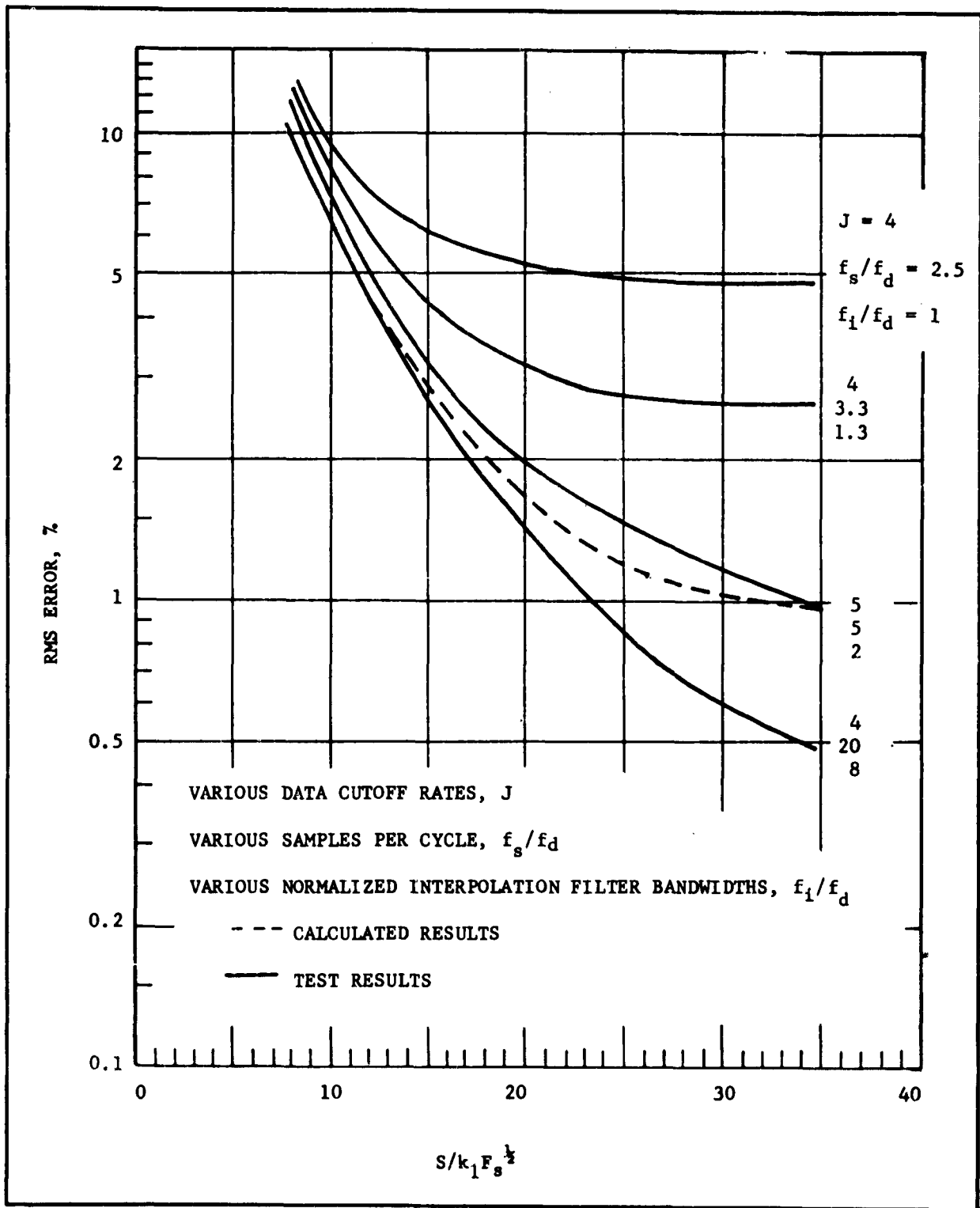


FIG. 4-39 RMS ERROR VS.  $S/k_1 F_s^{1/2}$ . INTERPOLATION FILTER: BUTTERWORTH, 36 db/oct. DATA: BUTTERWORTH,  $J = 4$  AND 5



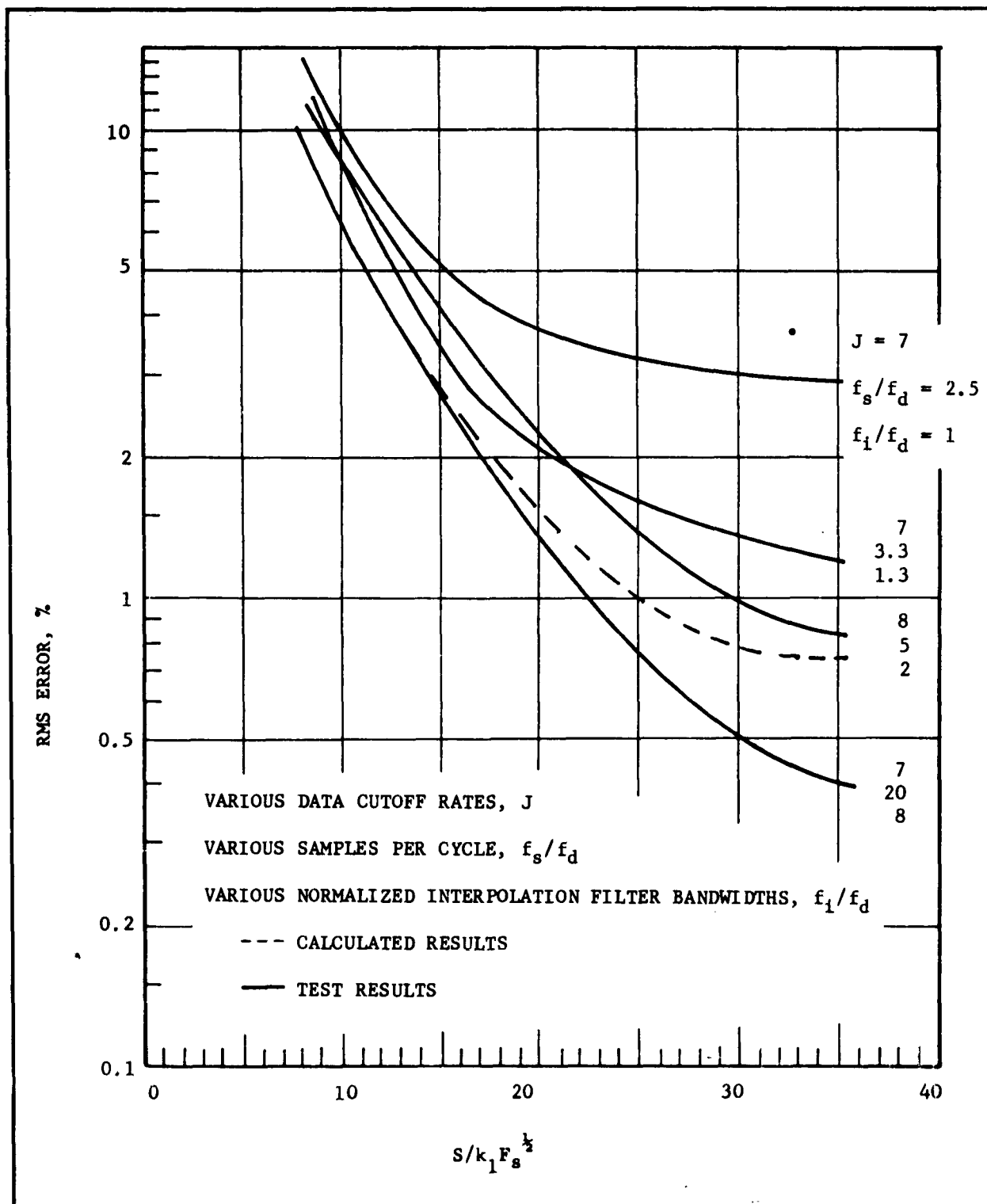


FIG. 4-40 RMS ERROR VS.  $S/k_1 F_s^{1/2}$ . INTERPOLATION FILTER: BUTTERWORTH, 36 db/oct. DATA: BUTTERWORTH,  $J = 7$  AND 8

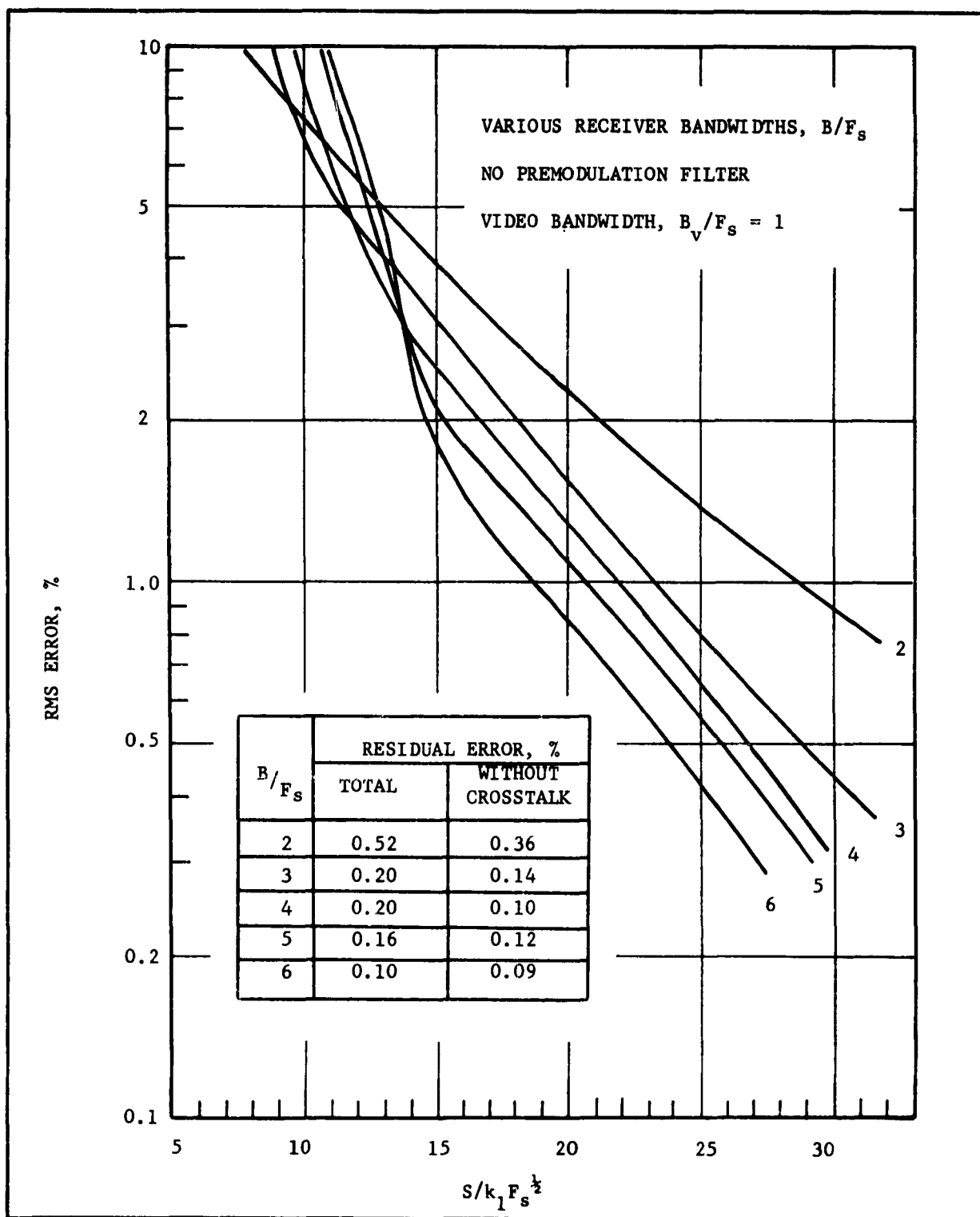
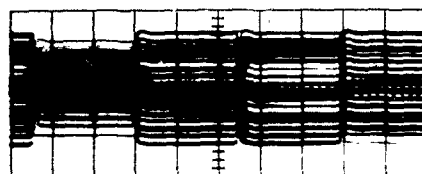


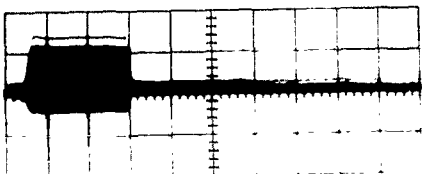
FIG. 4-41 PAM-FM. RMS ERROR VS.  $S/k_1 F_s^{1/2}$ . RMS DEVIATION,  $f_D/1/2B = 0.4$ .



2½ FRAMES  
ALL 8 CHANNELS MODULATED



½ FRAME  
ALL 8 CHANNELS MODULATED



½ FRAME  
1 CHANNEL MODULATED

FIG. 4-42 PHOTOGRAPHS OF MULTIPLEXER OUTPUT WAVEFORM

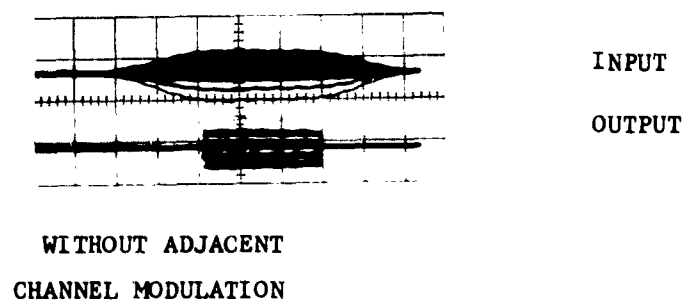
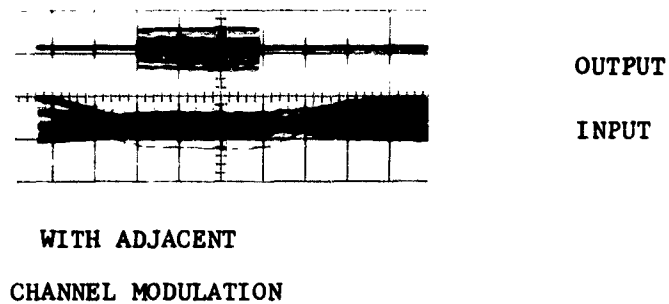


FIG. 4-43 PHOTOGRAPHS OF DECOMMUTATOR INPUT AND OUTPUT WAVEFORMS

## SECTION 5

### TEST EQUIPMENT

#### 5.1 INTRODUCTION

The test equipment designed to measure experimentally the aliasing error in telemetry systems is described in this section. The general test setup will be presented in Section 5.2. This will include the single channel and multi-channel descriptions. Section 5.3 will discuss the equipment making up the telemetry system. The analog error comparator is described in Section 5.4, and the accuracy with which measurements were obtained is evaluated in Section 5.5.

Many of the basic elements of the system, the analog error comparator, and the evaluation of the accuracy of measurements have been previously discussed in reference 1, Volume III. Reference will be made to this volume frequently. Therefore, it will be referred to simply as "reference 1".

The majority of the equipment used for this contract was transferred from the Telemetry System Study, Contract No. DA-36-039-SC-73182, DA Project No. 3-16-00-300. Two additional pieces of equipment were designed for this project; 1) an 8-channel electronic multiplexer, and 2) an electronic decommutator. These are described in Section 5.3.

#### 5.2 GENERAL TEST SETUP

The setup for measuring errors due to aliasing and interpolation for a single-channel or time-division multiplex sampled data system is shown in Figure 5-1. Basically the setup provides an assembly of a typical telemetry system including a signal source which simulates the telemetry

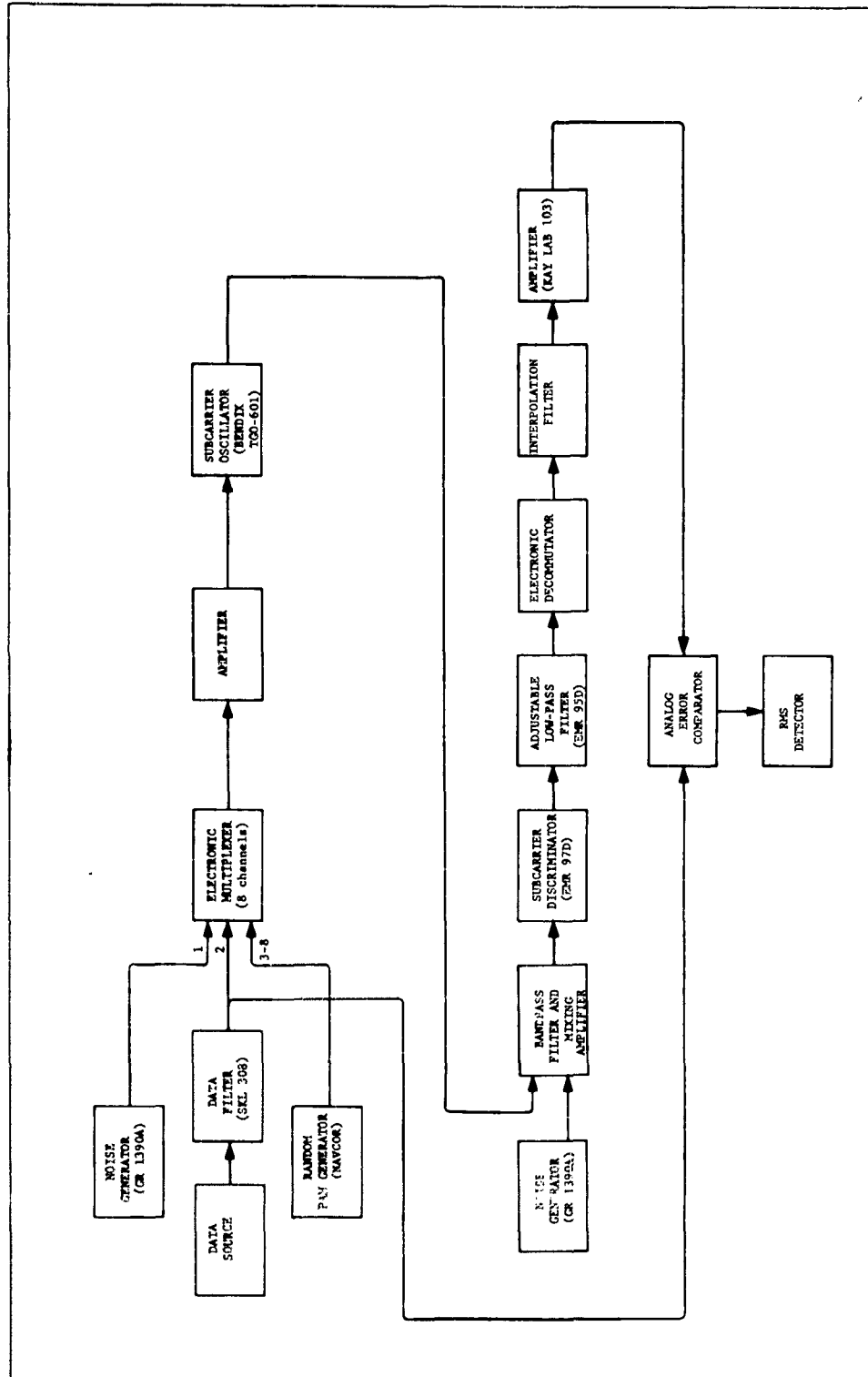


FIG. 5-1 BLOCK DIAGRAM - GENERAL TEST SETUP

data, sources of interference, monitoring equipment, and an analog error comparator.

The test setup provided for adjustment of significant parameters in order that a thorough evaluation could be accomplished. Signal simulators are multiplexed to provide the modulating wave to the telemetry system. The duty cycle of the multiplexer and decommutator output can be varied. The error measurement made by the analog error comparator is accomplished by comparing the signal simulator output with the interpolation filter output. The data signal is taken to be the data filter output since the filter was utilized to simulate typical data spectra by shaping broadband noise sources.

In order to evaluate the effects of crosstalk three signals can be multiplexed at the input to the communication link. Separate data signals modulate the measured channel and the multiplexed channel preceding the measured channel. The third signal is a quasi-random PAM pulsetrain filling up the 6 remaining channel positions. Separate control of the channel preceding the measured channel allows determination of crosstalk effects.

The single channel sampled data system is obtained by omitting the multiplexer and the carrier equipment. The experimental setup consisted of the following elements in tandem: data source, data filter, decommutator, interpolation filter, and amplifier. The error measurements were made as before by comparing the data filter output with the amplified interpolation filter output.

### 5.3 SYSTEM EQUIPMENT

The majority of the equipment used for the aliasing project has been discussed in reference 1. Rather than repeating descriptions of basic elements they will be itemized and the reader may obtain a detailed description there.

#### 5.3.1 Signal Simulators

- 1) Random Noise Generator, Model GR 1390-A, General Radio Co. (Gaussian Amplitude Probability Distribution).
- 2) Random Signal Generator, Sigmatron, Model GA-1000, Intercontinental Dynamics Corporation, (Gaussian Amplitude Probability Distribution).

- 3) Sinewave Oscillator, Model HP-200CD, Hewlett-Packard Co.
- 4) Random Noise Generator, Modified Navcor Equipment, (Equal Amplitude Probability Distribution).

#### 5.3.2 Data Filter

- 1) Variable Filter, Model 308, Spencer Kennedy Laboratories, Inc.

The frequency response for this filter is shown in Figures 5-2 and 5-3 for one and two sections in cascade respectively.

A frequency response curve is shown for each of the data bandwidths considered in the experimental test program. The cutoff rates were determined at the 30 db attenuation point. One section of the filter gives a cutoff rate of 24 db/oct., while two sections in cascade provide a 42 db/oct. cutoff rate (the specifications quote 48 db/oct.).

#### 5.3.3 Multiplexer

##### General Description

The multiplexer provides a PAM wave of either 50% or 100% duty cycle. Between pulses the 50% duty cycle wave returns to zero or to any desired pedestal level.

Three independent signal sources may be multiplexed to provide eight PAM pulses per frame. Channels 1 and 2 are independent, while channels 3 through 8 are strapped at the input. Channel 2 is used for test.

An external sine wave clock controls the PAM pulse rate. The multiplexer will operate at rates from 500 to 5000 pulses per second. Full scale PAM output amplitude is  $\pm 2.5$  volts. A frame sync pulse is provided for the decommutator.

The multiplexer is shown in block form on Fig. 5-4.



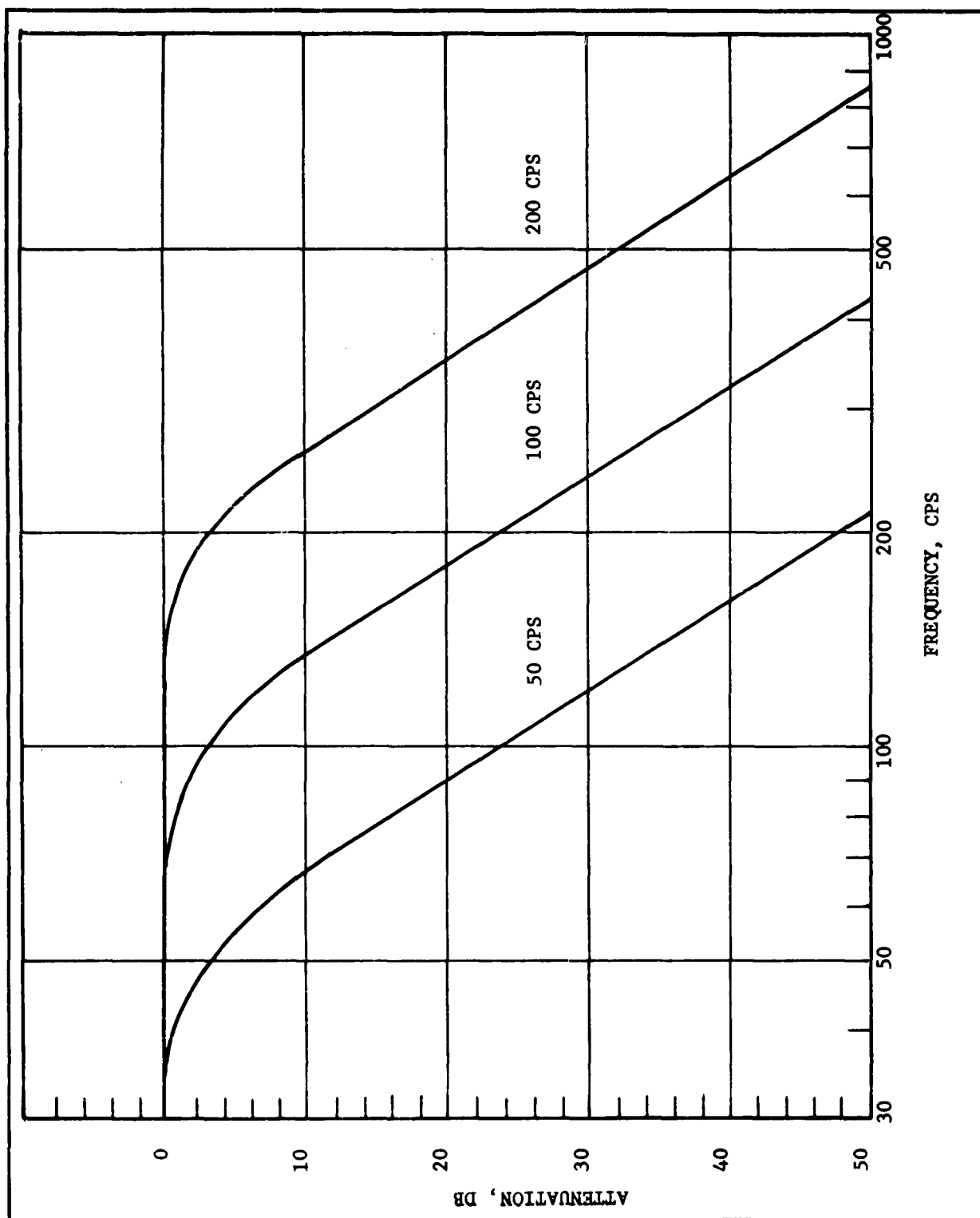


FIG. 5-2 FILTER RESPONSE - SKL MODEL 308, 24 DB/OCT.

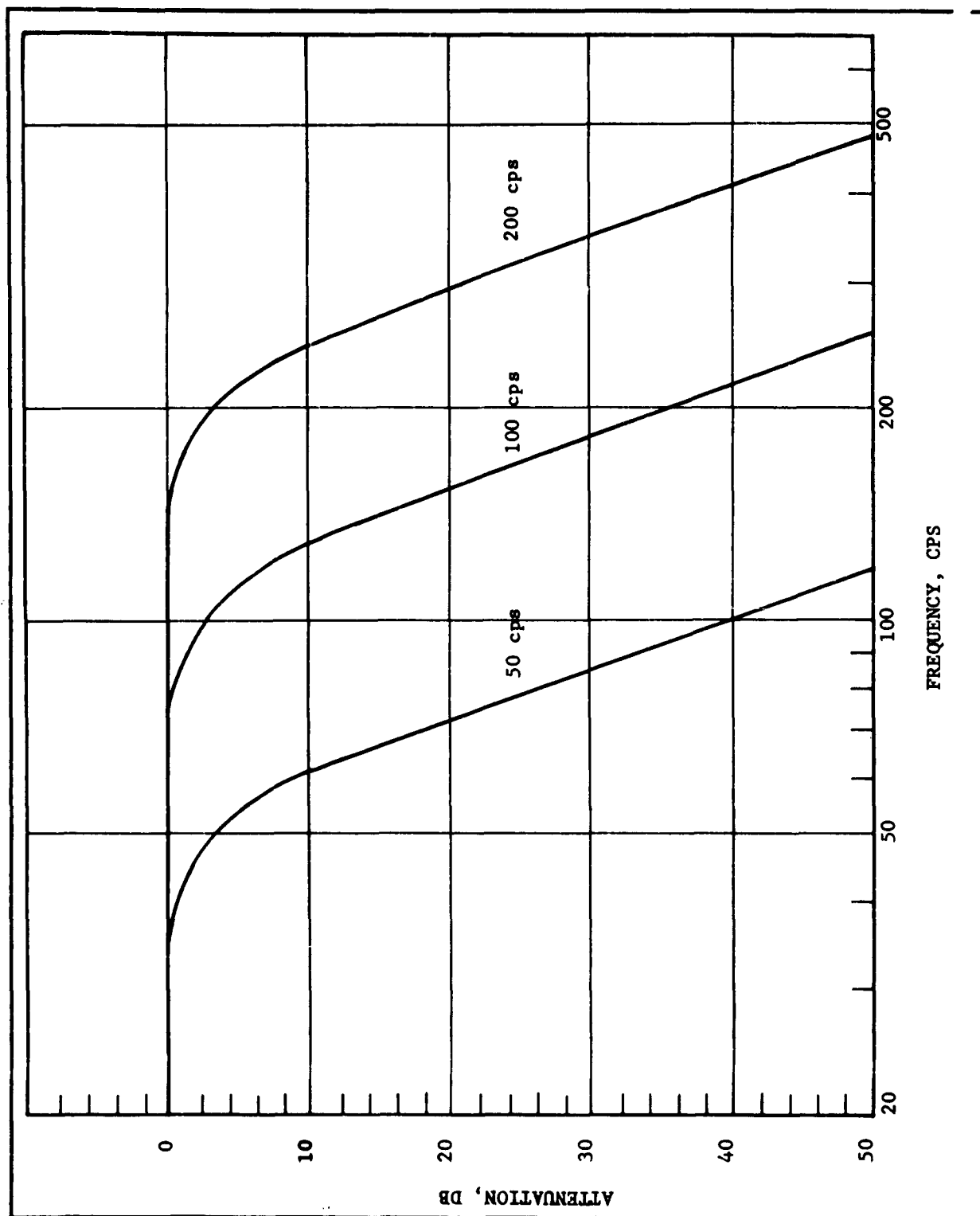


FIG. 5-3 FILTER RESPONSE - SKL MODEL 308, 42 DB/OCT.

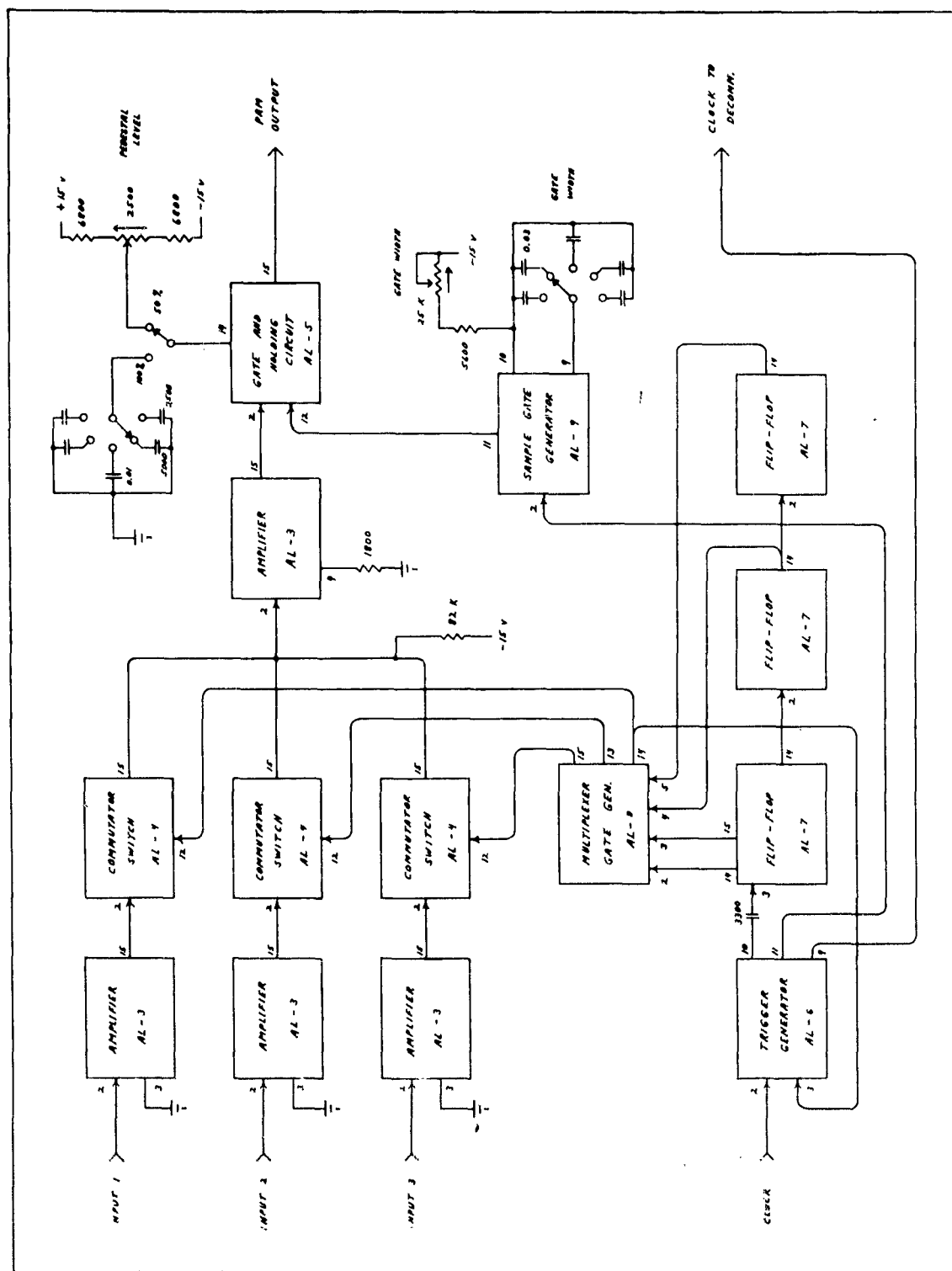


FIG. 5-4 MULTIPLEXER BLOCK DIAGRAM, AL-1

### Circuit Description

Figures 5-5 through 5-11 show circuit details schematically.

The input amplifier, Fig. 5-5, is an operational type. Two inputs are provided so that it may be connected to invert or not invert the signal. In the multiplexer no signal inversion takes place between input and output.

The commutator switch, Fig. 5-6, is of the series type. The gating transistors are driven to saturation so the effective series impedance is low. The ratio of the off to the on impedance is greater than  $10^5$ . This type of switch causes a bias current in the input circuit so it must be driven by a low impedance source. The operational amplifier is satisfactory for this.

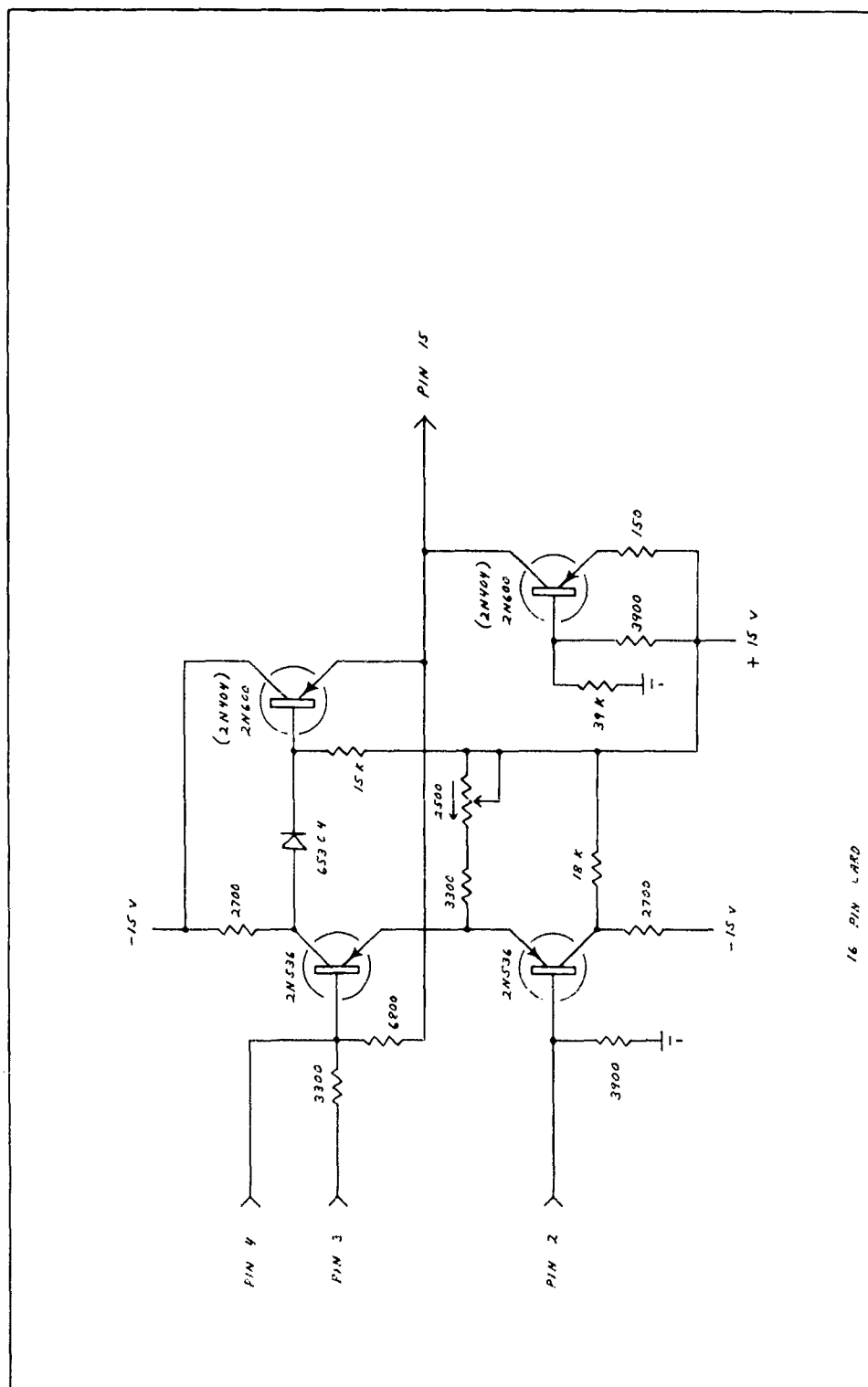
The outputs of the three commutator switches are combined at the input of another operational amplifier. The multiplexed signals are then sent to the gate and holding circuit, Fig. 5-7. If a PAM wave of 100% duty cycle is required, the signal is sampled for approximately  $20 \mu$  sec during each channel period and then held until the next sample. A non-return to zero PAM wave is generated. If a 50% duty cycle wave is required, the sample time is extended to one-half of the channel period but no holding action is performed. During the time between samples the PAM wave returns to an adjustable pedestal value. The gate and holding circuit contains a series gate and an output amplifier.

The remainder of the multiplexer generates the timing waves that control the commutator gates and the output gate.

A trigger generator, Fig. 5-8, provides sharp pulses to drive the counter. An inductive kickback pulse generator is used. One output pulse is generated per cycle of input from the sine wave clock.

A binary counter, consisting of three flip flops (Fig. 5-9), provides three waves which are combined in the multiplexer gate generator, Fig. 5-10, to generate the three sequential timing waves to control the commutator switches. The control wave for Channel 1 is also amplified and used as a frame sync pulse for decommutation. The amplifier for this is shown on Fig. 5-8.

An additional timing wave is generated by the sample gate generator, Fig. 5-11. The sampling gate is delayed approximately  $50 \mu$  sec from the beginning of each channel period to ensure that the commutator switching transients have died away before sampling of the combined wave takes place.



16 PIN LARD

FIG. 5-5 AMPLIFIER, AL-3

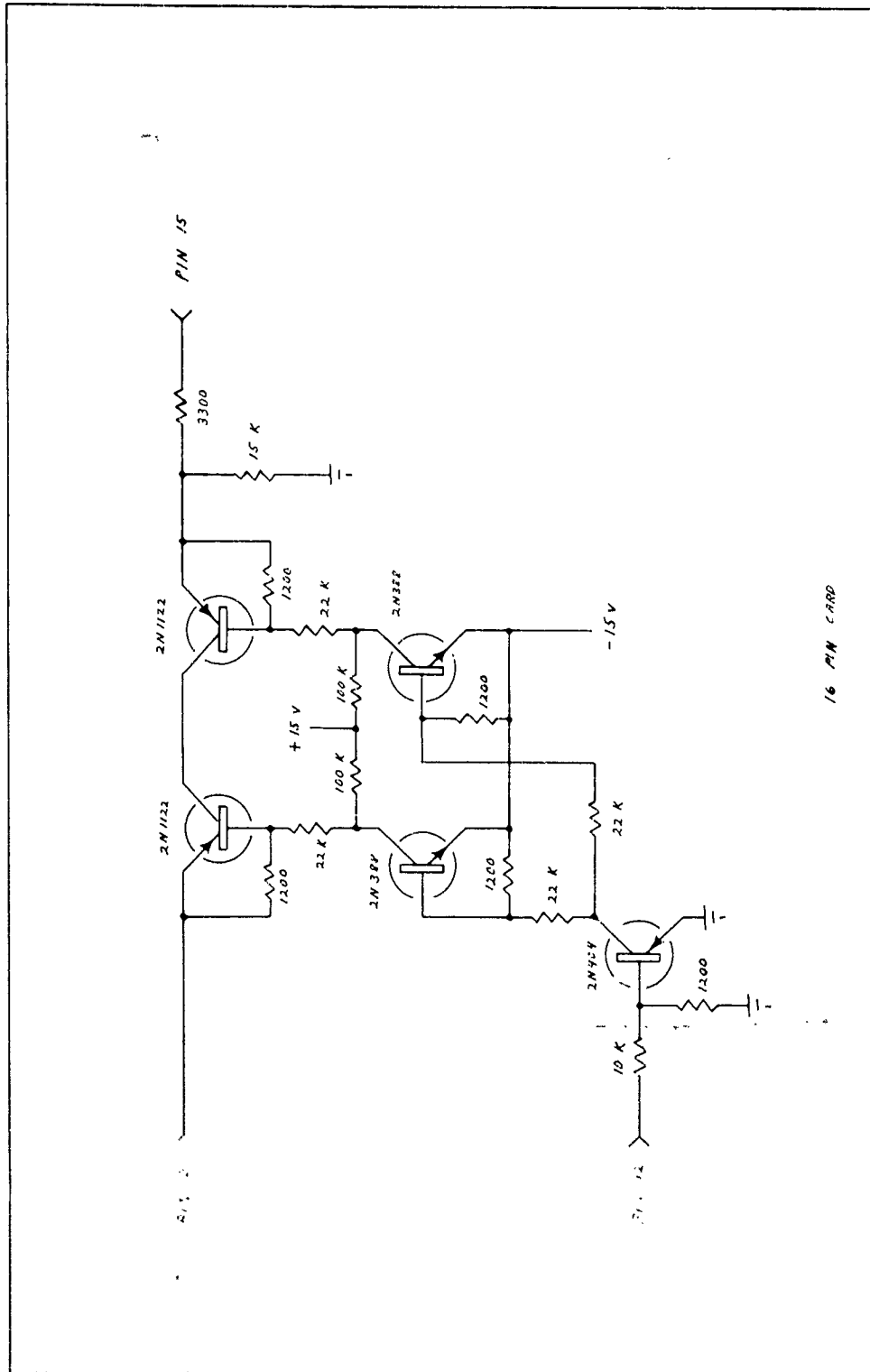


FIG. 5-6 COMMUTATOR SWITCH, AL-4



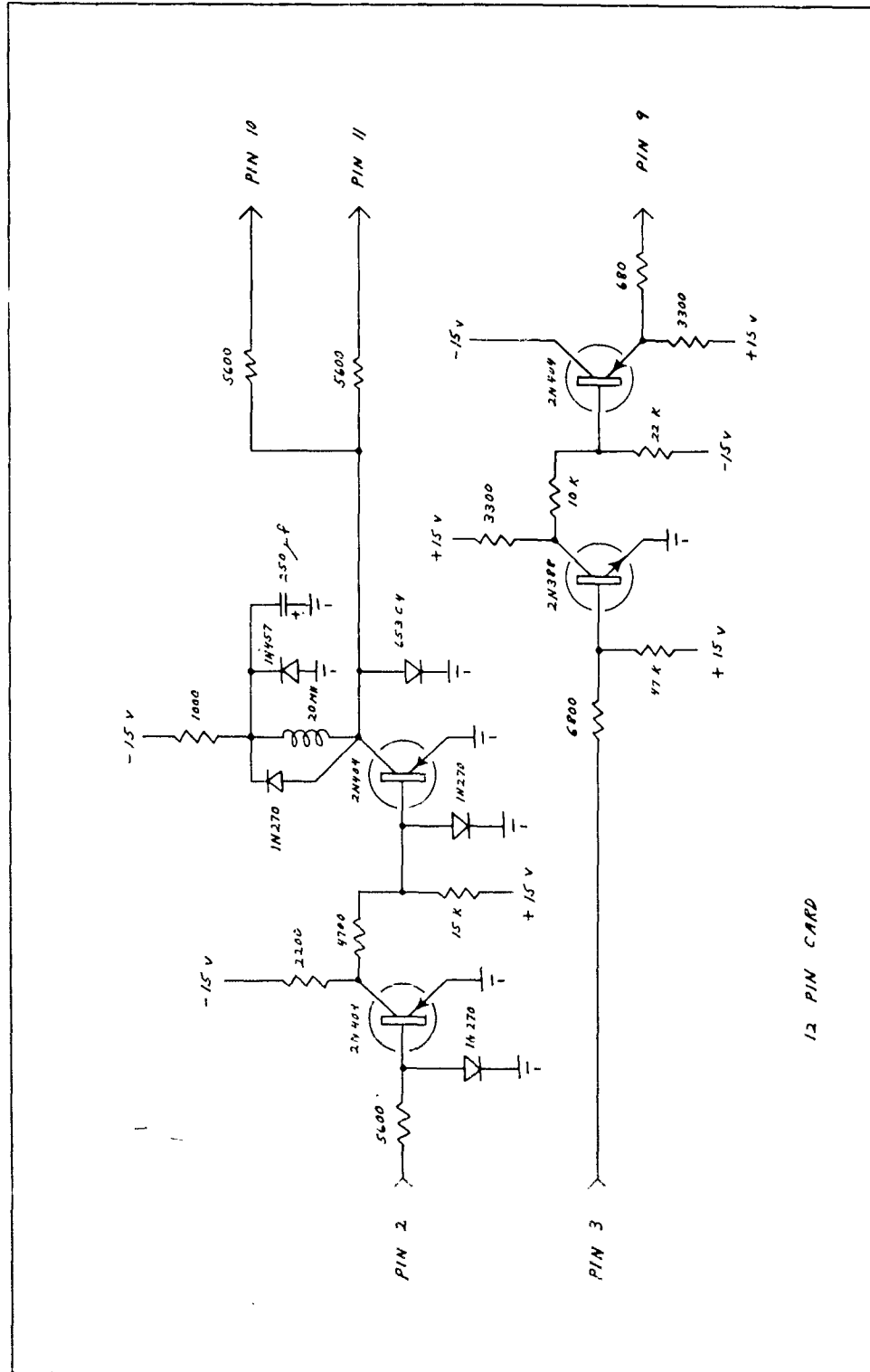


FIG. 5-8 TRIGGER GENERATOR, AL-6



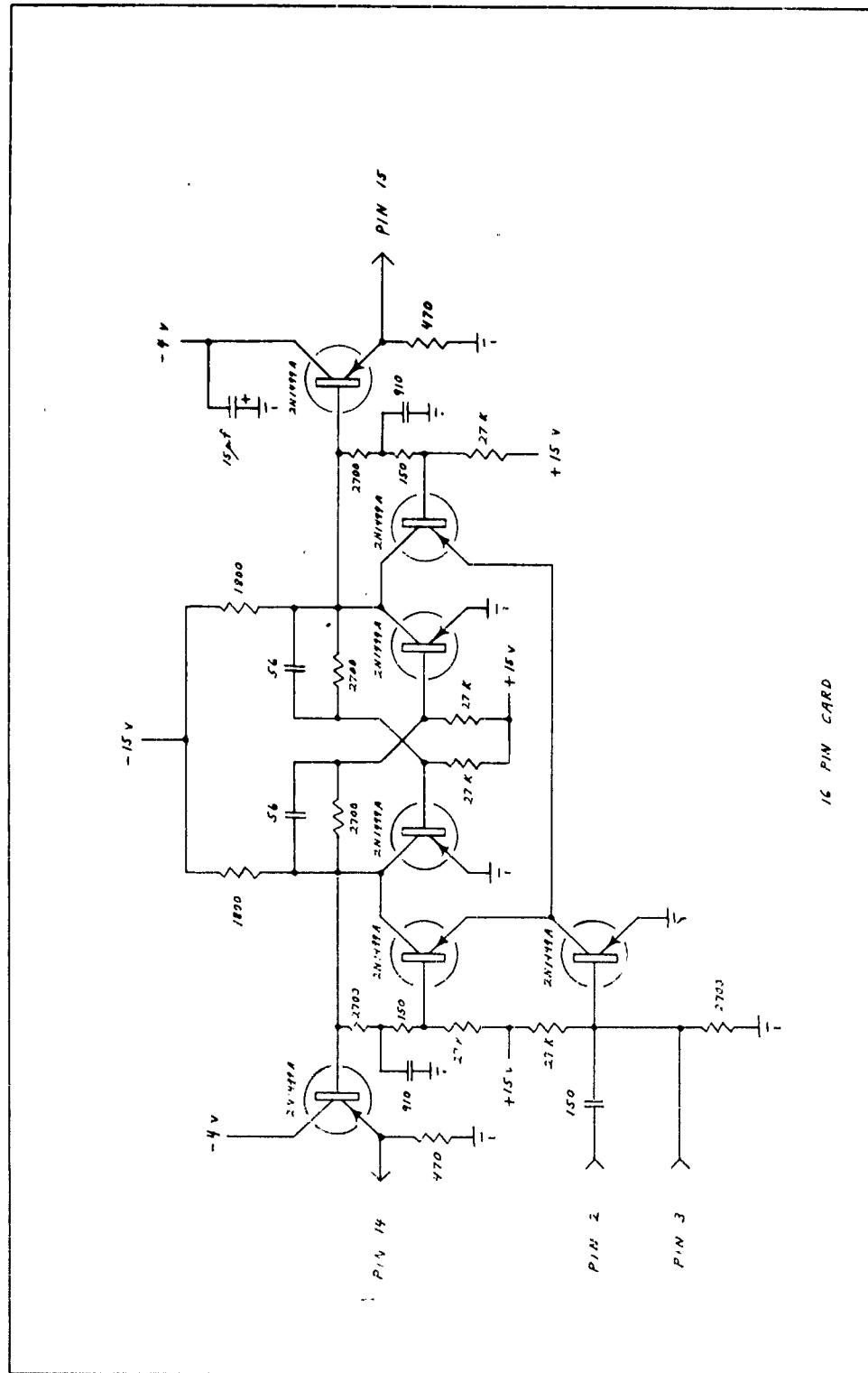


FIG. 5-9 FLIP-FLOP, AL-7

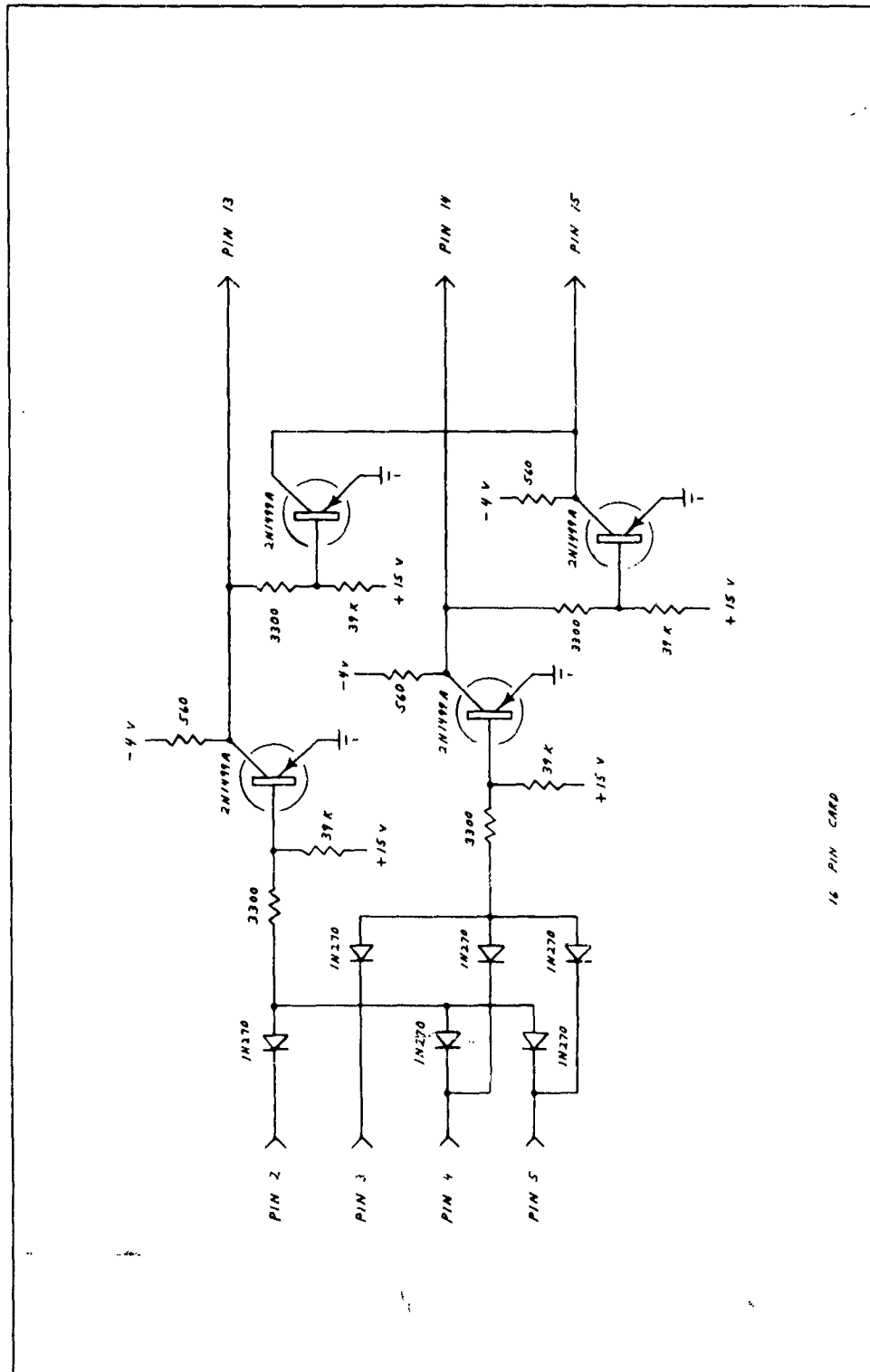
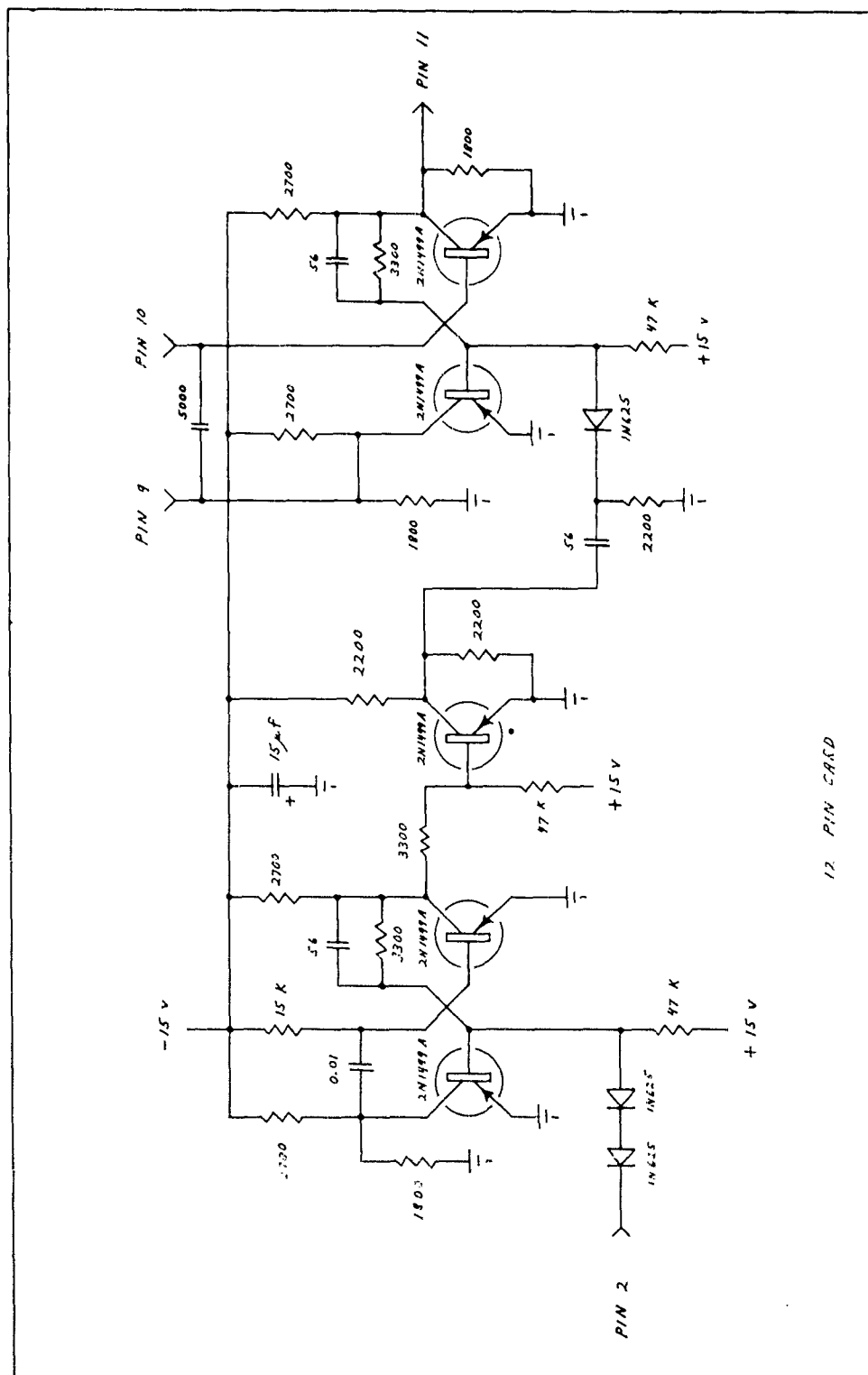


FIG. 5-10 MULTIPLEXER GATE GENERATOR, AL-8



Three control functions are provided on the multiplexer: duty cycle, pedestal level, and sample pulse duration.

#### Operating Adjustments

1. Set the clock generator to a frequency corresponding to the required channel rate. The clock wave amplitude must be at least 10 volts rms.
2. Adjust the input signal levels so that the amplitude of the output PAM wave is  $\pm 2.5$  volts full scale on each channel.
3. Set the duty cycle selector switch to the 50% position. Adjust the coarse and vernier gate width controls for the required gate width. If 100% duty cycle PAM is required adjust the width controls for a 20  $\mu$  sec gate and then switch to 100% duty cycle.
4. If 50% duty cycle PAM is required, adjust the pedestal level control for the desired pedestal level.

#### 5.3.4 Communication Link

The communication link shown in Figure 5-1 consists of the following:

- 1) Amplifier
- 2) Subcarrier Oscillator, Bendix TGO-601
- 3) Bandpass Filter and Mixing Amplifier
- 4) Subcarrier Discriminator, EMR 97D
- 5) Adjustable Lowpass Filter, EMR 95D

See Reference 1 for equipment descriptions.

#### 5.3.5 Decommutator

##### General Description

The decommutator provides a means of separating the desired channel from the remainder of the multiplexed PAM wave. Either of two output gates may be used. One provides a variable aperture sample with return to zero and the other a short sample which is held.

Two delay circuits are provided. One delays the input PAM wave so that the analog error comparator may be used to measure the error between the input and output of the decommutator. The other delays the frame sync pulse from the multiplexer and can be adjusted so that the decommutator gate operates at the proper time.

A frequency divider is provided to select only every second, third, or fourth frame sync pulse in case the analog error comparator is to be operated synchronously with the multiplexer at high pulse rates. The divider is not used when the analog error comparator samples asynchronously.

Controls are provided to adjust the input bias, the output bias, the sampling pulse delay, and the sampling pulsewidth.

The decommutator block diagram is shown in Figure 5-12.



### Circuit Description

Figures 5-13 through 5-18 show circuit details schematically.

The delay network, Fig. 5-13, is an 11-pole maximally flat time delay type. It has a 1 db bandwidth of 500 cps, which is several times the maximum data bandwidth, and a time delay of approximately  $600 \mu$  sec required for proper operation of the error comparator. In the multichannel tests the delay network is removed because the carrier system supplies this delay.

An amplifier, Fig. 5-5, drives the decommutator gate. A switch permits polarity inversion of the PAM wave if it is required. This amplifier is the same as those used in the multiplexer.

The first type of decommutator gate, Fig. 5-14, provides variable aperture gating of the PAM wave.

It contains an amplifier capable of driving a 2k ohm LC interpolation filter. The gating circuit is similar to that in the commutator switch in the multiplexer. The gate output returns to zero or to a selected bias value after sampling. The second type of gate, Fig. 5-15, is similar except that it provides a holding circuit which maintains the output at the previous sample level until the next sample begins.

The remainder of the decommutator circuitry provides a sample gate pulse to the decommutator gate at the proper time.

The trigger generator, Fig. 5-16, generates sharp pulses from either a sine wave clock or from the frame sync pulse from the multiplexer.

The clock pulses are delayed by two adjustable one shot multivibrators, Fig. 5-17. A third one shot generates the sample gate pulse. Coarse and vernier controls are provided for each function.

The frequency divider, Fig. 5-18, is a synchronized multivibrator. Pulses from the trigger generator are injected to lock the period of the multivibrator wave at an integral multiple of the period of the clock pulse. An injection sensitivity control and coarse and vernier frequency controls are provided.

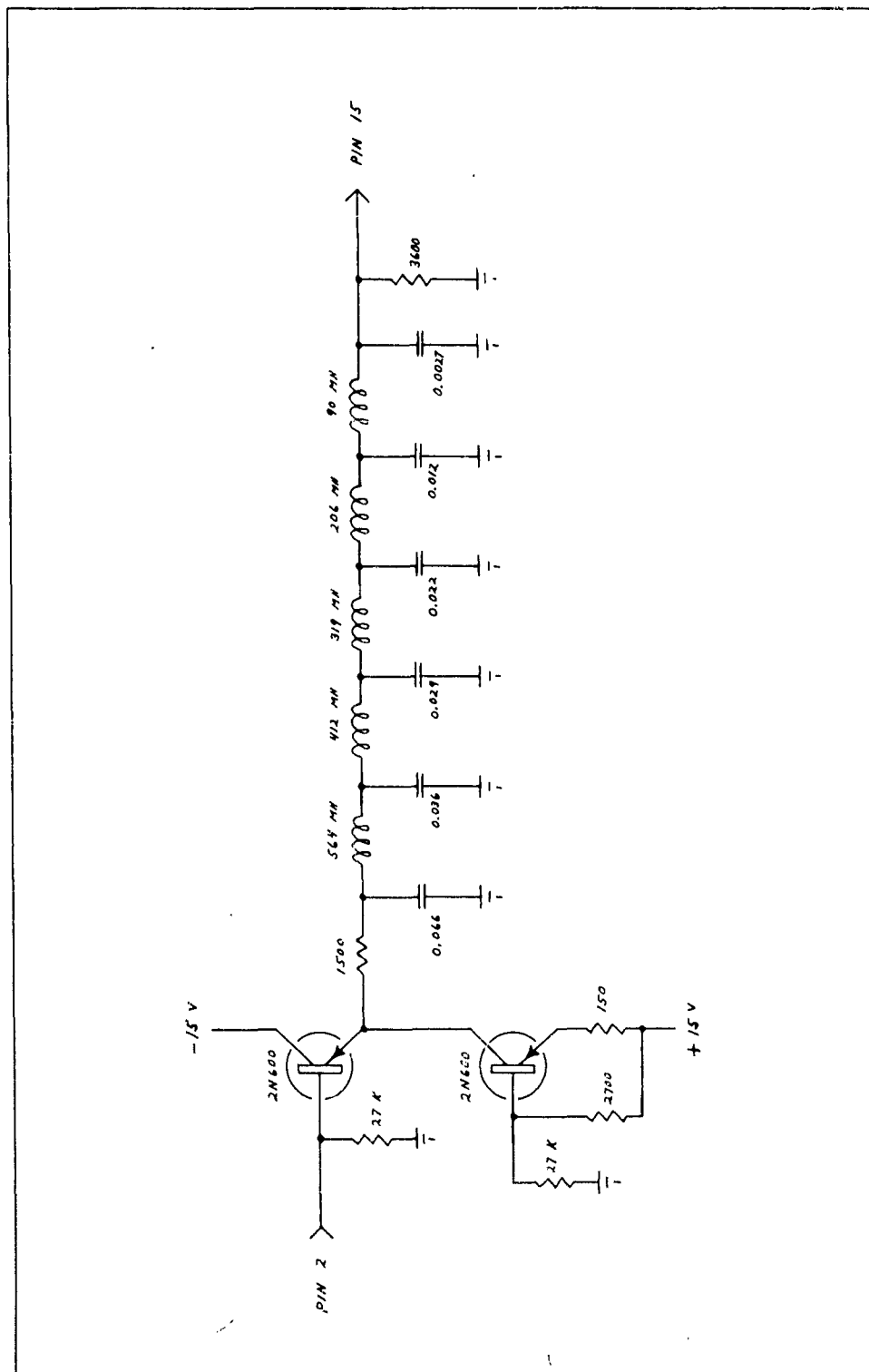


FIG. 5-13 DELAY NETWORK, AL-10



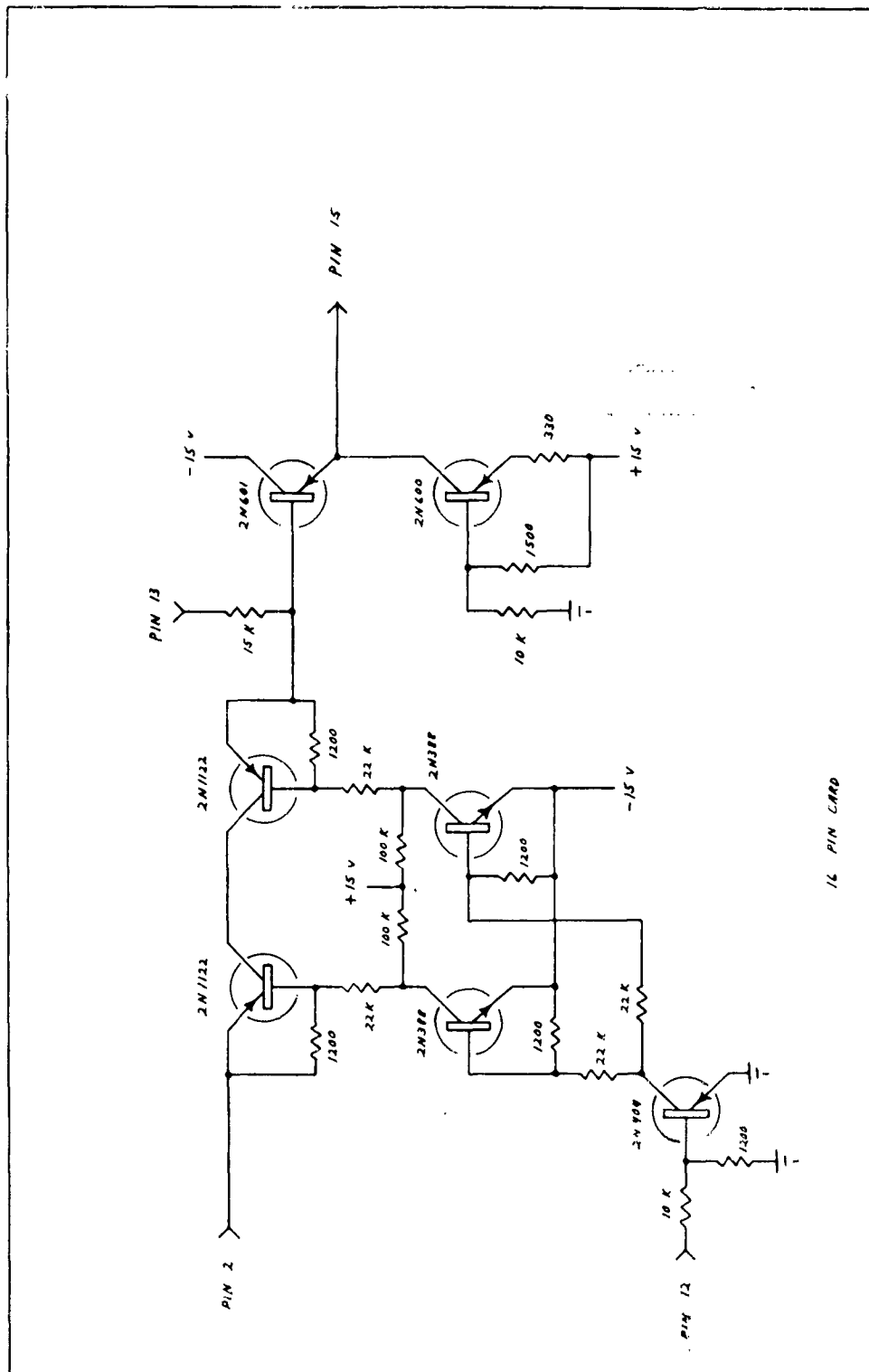


FIG. 5-14 DECOMMUTATOR GATE, AL-11

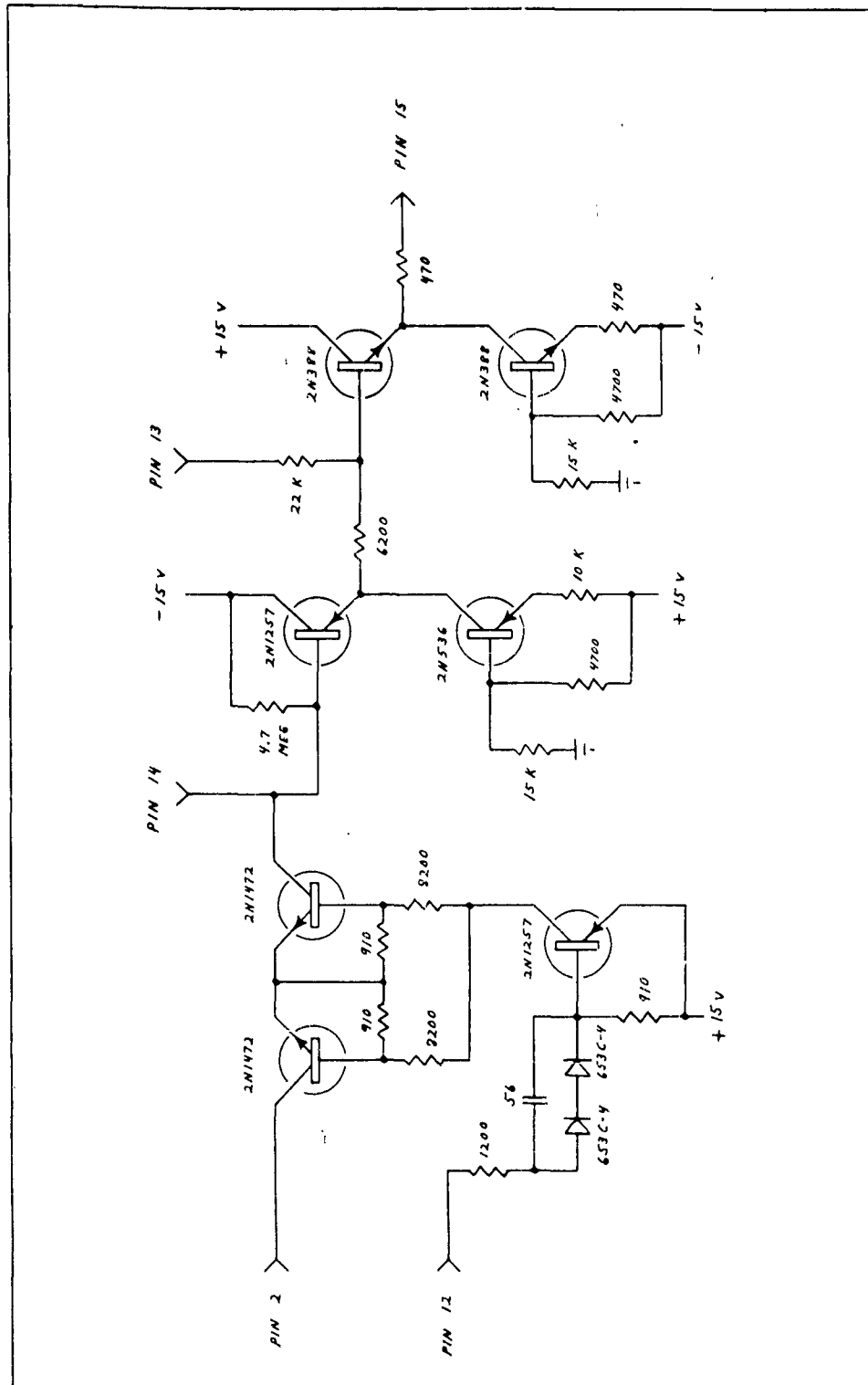


FIG. 5-15 DECOMMUTATOR GATE AND HOLDING CIRCUIT

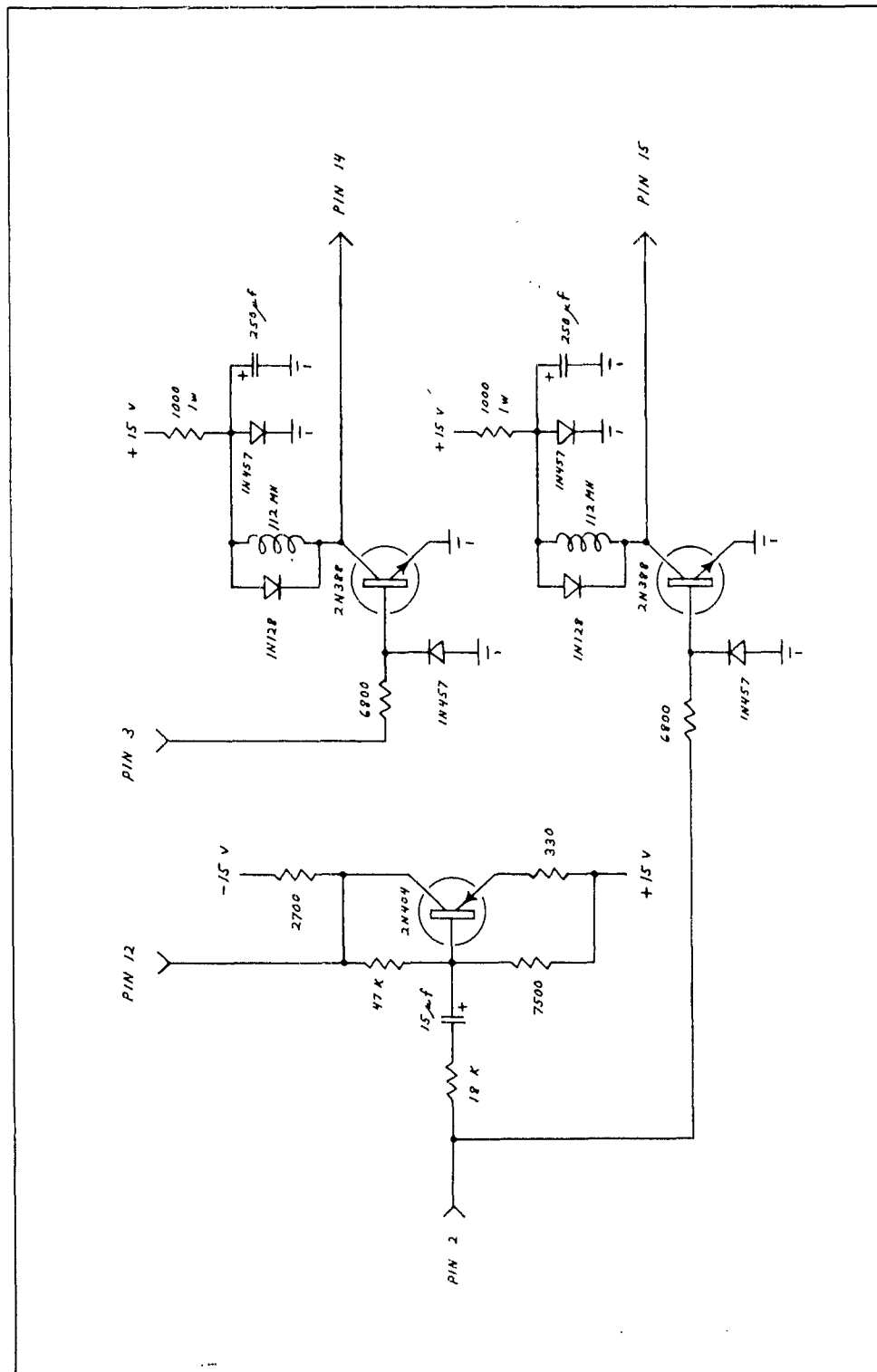


FIG. 5-16 TRIGGER GENERATOR, AL-13

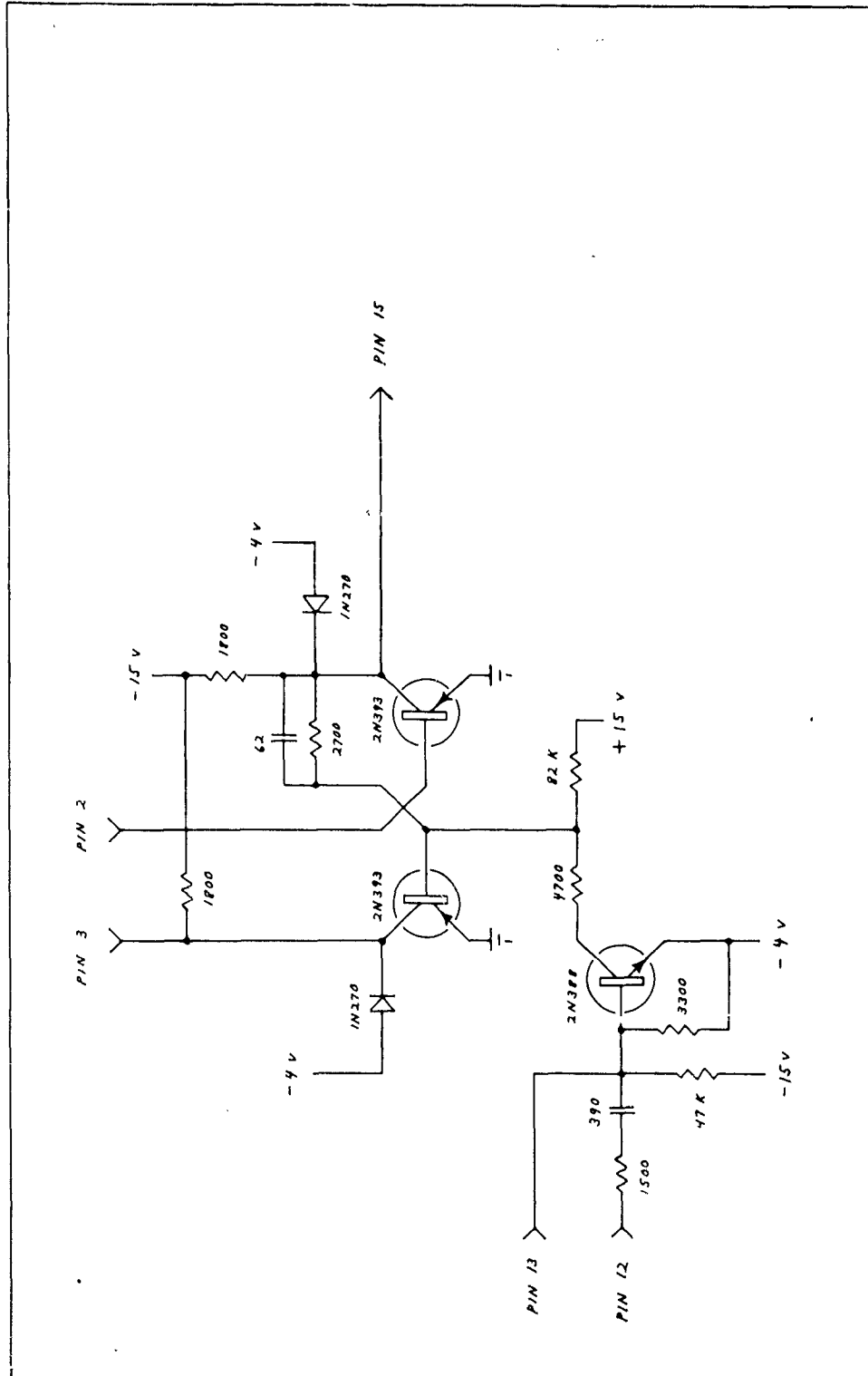


FIG. 5-17 GATE GENERATOR OR DELAY, AL-14

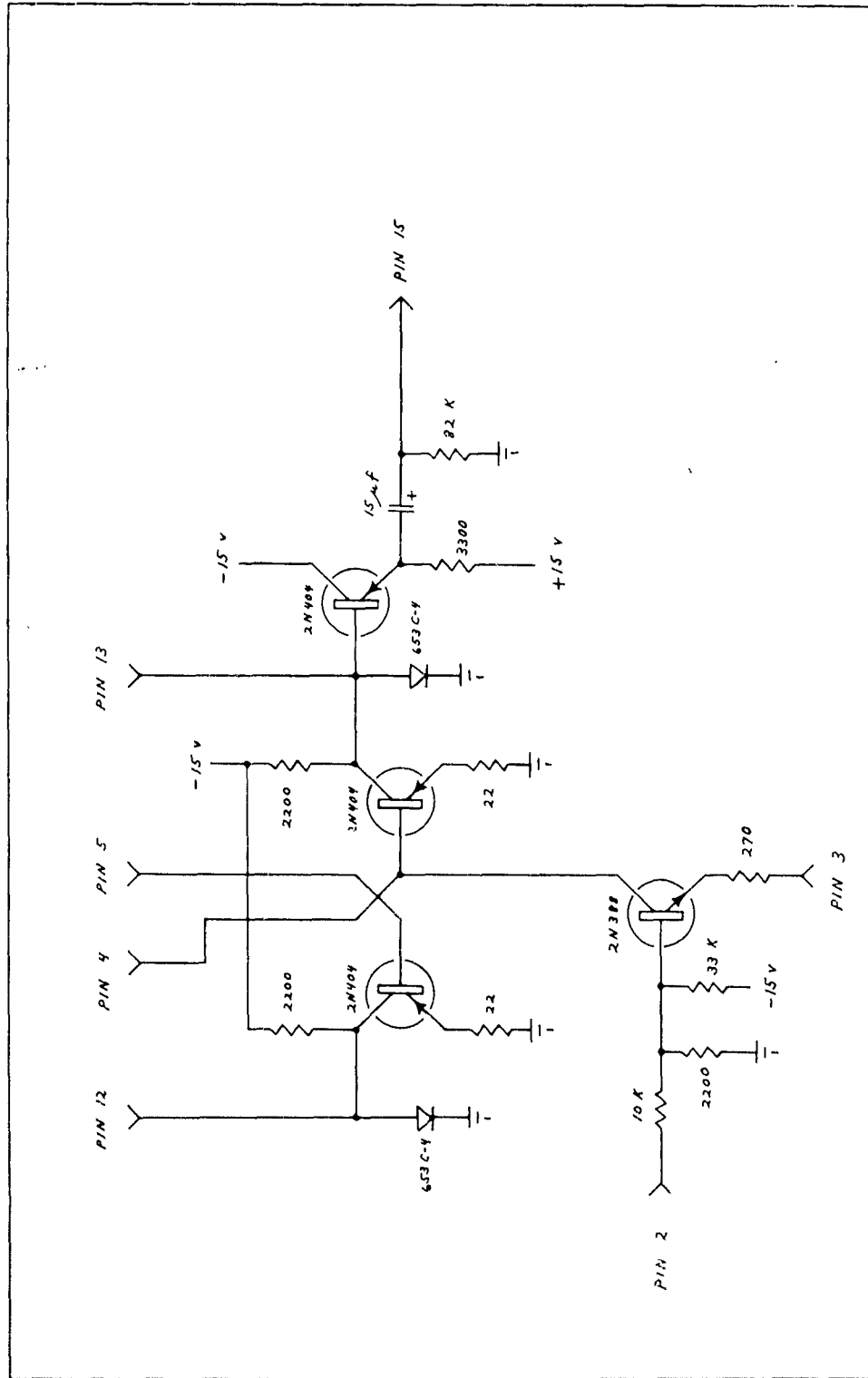


FIG. 5-18 FREQUENCY DIVIDER, AL-15

### Operating Adjustments

1. Adjust the sine wave clock (if frame sync from the multiplexer is not used) to the required sample frequency between 100 and 2000 cps. The amplitude must be at least 10 volts rms.
2. Observe the decommutator output with an oscilloscope. Adjust the amplifier bias and the PAM input level so that the decommutator output is  $\pm 2.5$  volts full scale.
3. Adjust the output bias control so that the output level between samples is zero.
4. Insert AL-11 in the decommutator gate socket. Adjust the sample gate width controls for the required aperture.
5. Adjust the sample delay controls so the gate is positioned properly in the frame for correct decommutation. If the holding circuit is desired, replace AL-11 with AL-12.
6. If synchronous operation of the analog error comparator is required, adjust the divider sensitivity and frequency controls until a stable wave is obtained at the desired frequency.

### 5.3.6 Interpolation Filters

Four interpolation filters were investigated. These are:

1) A 200 cps cutoff filter with a trap at 400 cps with the frequency response shown in Figure 5-19. This is a 6 element Butterworth filter with an added capacitor to form a trap with the center inductor. The resulting cutoff rate is approximately 60 db/oct. at the 30 db attenuation point.

2) A Gaussian interpolation filter with a final cutoff rate of approximately 24 db/oct. The frequency response is shown in Figure 5-20.

3) A 4-pole Butterworth filter with the frequency response shown in Figure 5-21.

4) A 6-pole Butterworth filter with the frequency response shown in Figure 5-22.

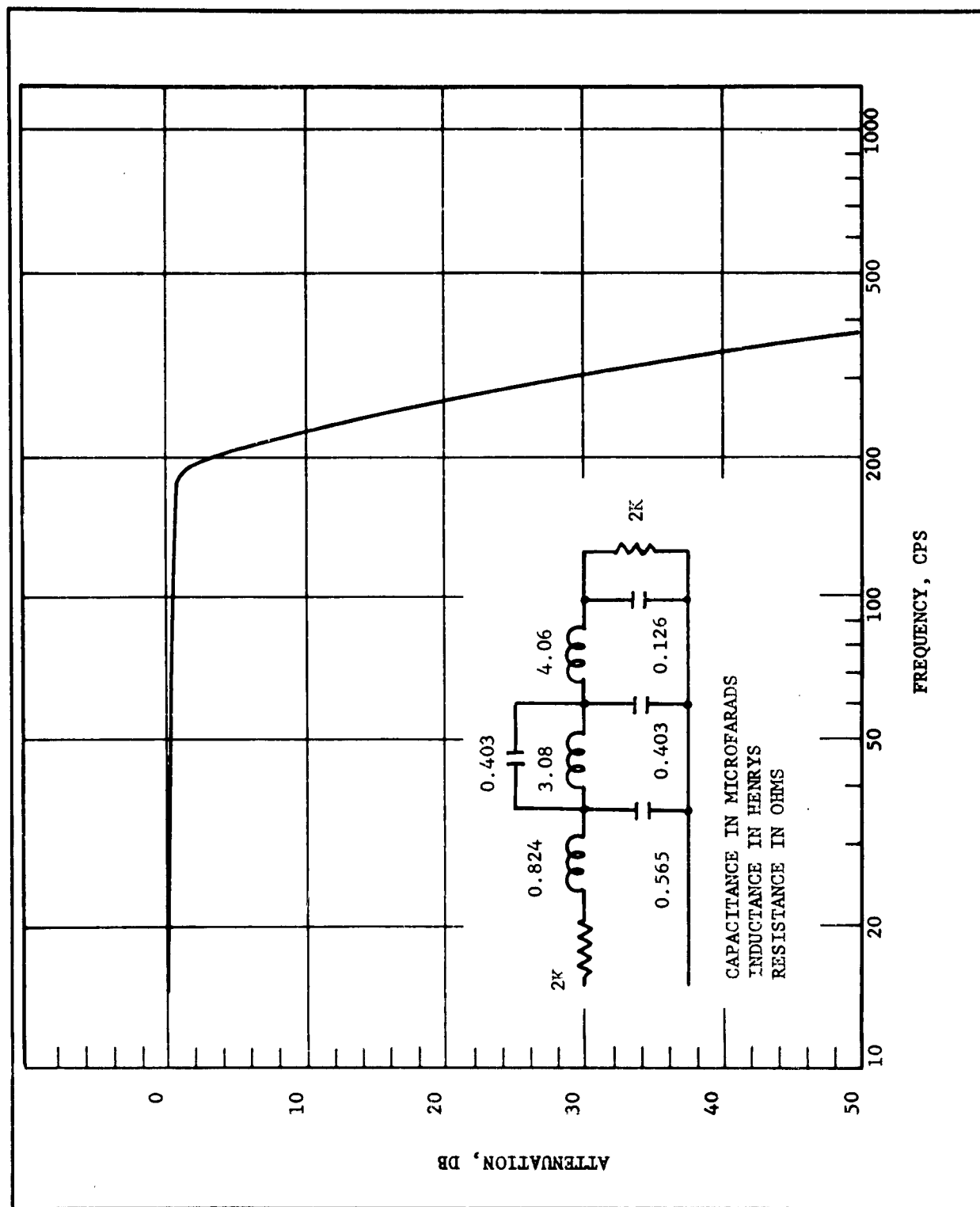


FIG. 5-19 FILTER RESPONSE - BWT, 60 DB/OCT.



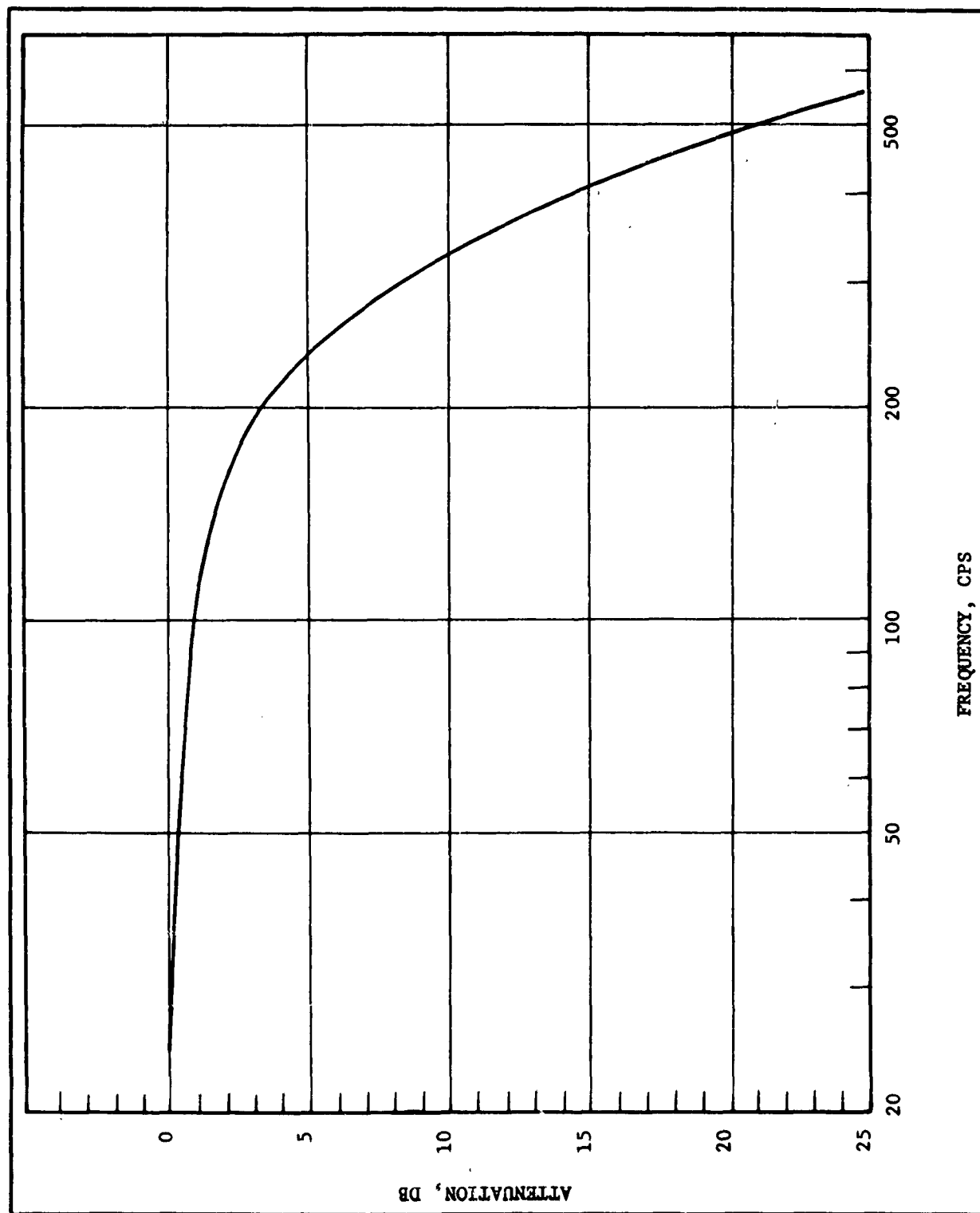


FIG. 5-20 FILTER RESPONSE - EMR 95D, GAUSSIAN CHARACTERISTIC, 24 DB/OCT.

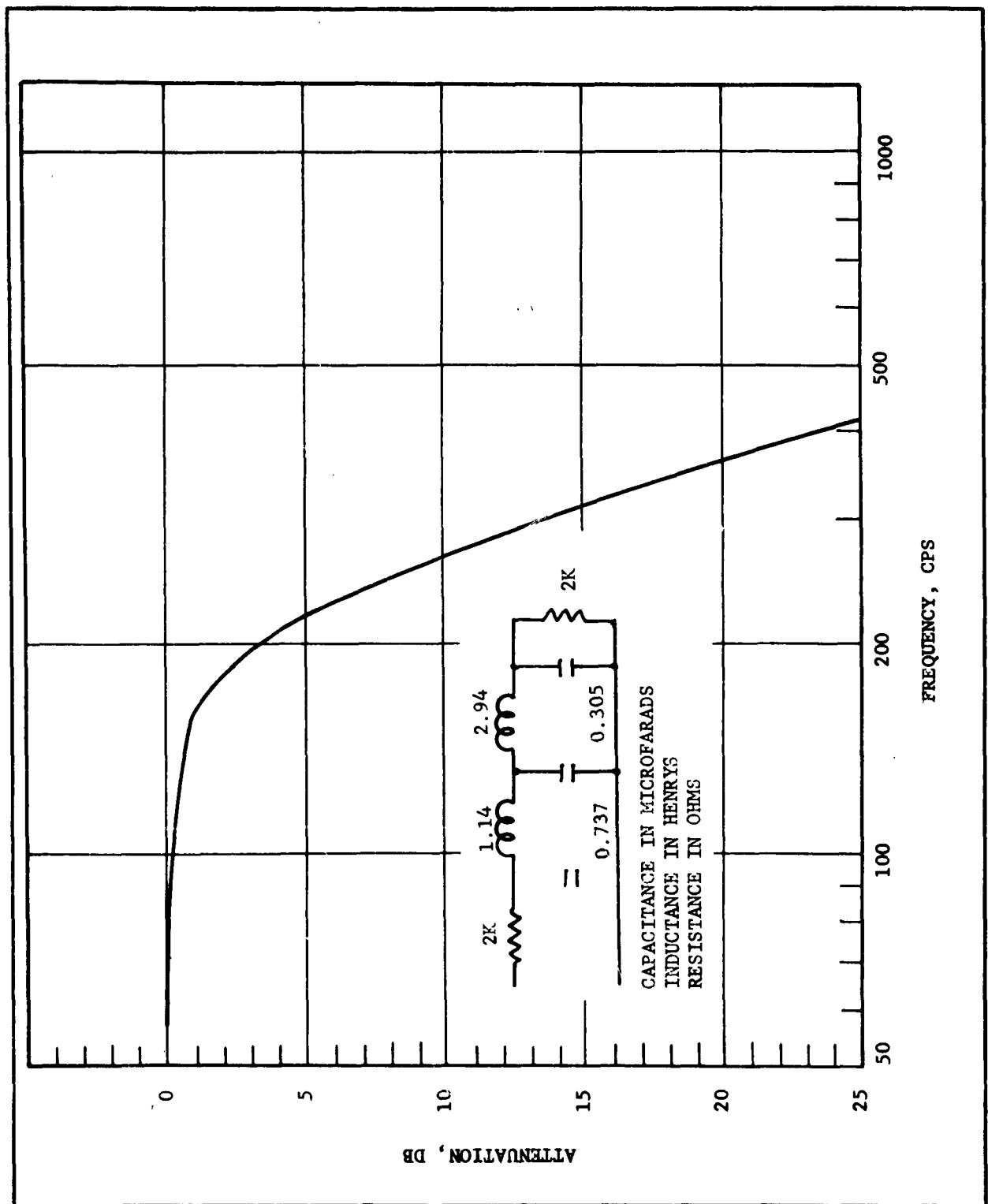


FIG. 5-21 FILTER RESPONSE - 4-POLE BUTTERWORTH FILTER, 24 DB/OCT.

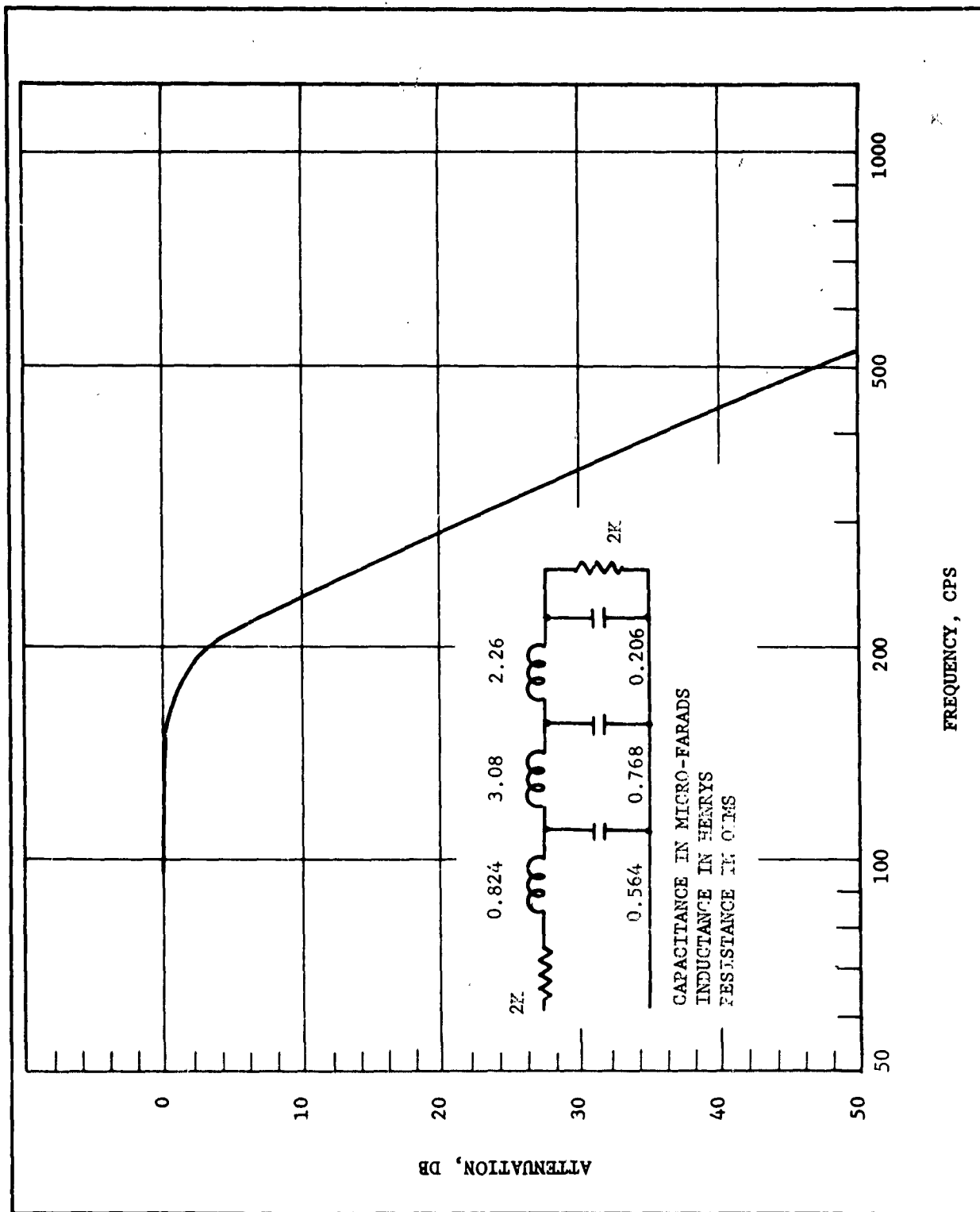


FIG. 5-22 FILTER RESPONSE - 6-POLE BUTTERWORTH FILTER, 36 DB/OCT.

#### 5.4 ANALOG ERROR COMPARATOR

Figure 5-23 shows the comparator in block form. A detailed description is given in reference 1, Vol. III. It is basically a device for sampling two analog signals and comparing their amplitudes. The sampling is done serially. The amplitude differences are indicated in terms of both average and rms value.

The following sequence of operations takes place in the analog error comparator:

- A. The sampling switch connects the follow and hold to the reference analog signal.
- B. A hold pulse causes the follow and hold unit to hold its output signal constant for 200  $\mu$  sec. (sample A).
- C. A convert pulse causes the Adage A/D converter to convert sample A into digital form (parallel binary).
- D. A store pulse causes the A/D converter to put this binary number into a storage register.
- E. The sampling switch connects the follow and hold unit to the output of the telemetering system.
- F. A second hold pulse causes the follow and hold unit to hold its output signal constant for 200  $\mu$  sec. (sample B).
- G. A second convert pulse causes the A/D converter to subtract sample B from the analog of Sample A, convert the difference to digital form, and present it as a parallel binary number at the output terminals.
- H. A dump and store pulse clears the storage register in the D/A converter and enters the binary number from the A/D converter.
- J. A dump pulse clears the storage register in the A/D converter.

This completes the sequence of operation of the analog error comparator. It is capable of making up to 2000 comparisons per second.

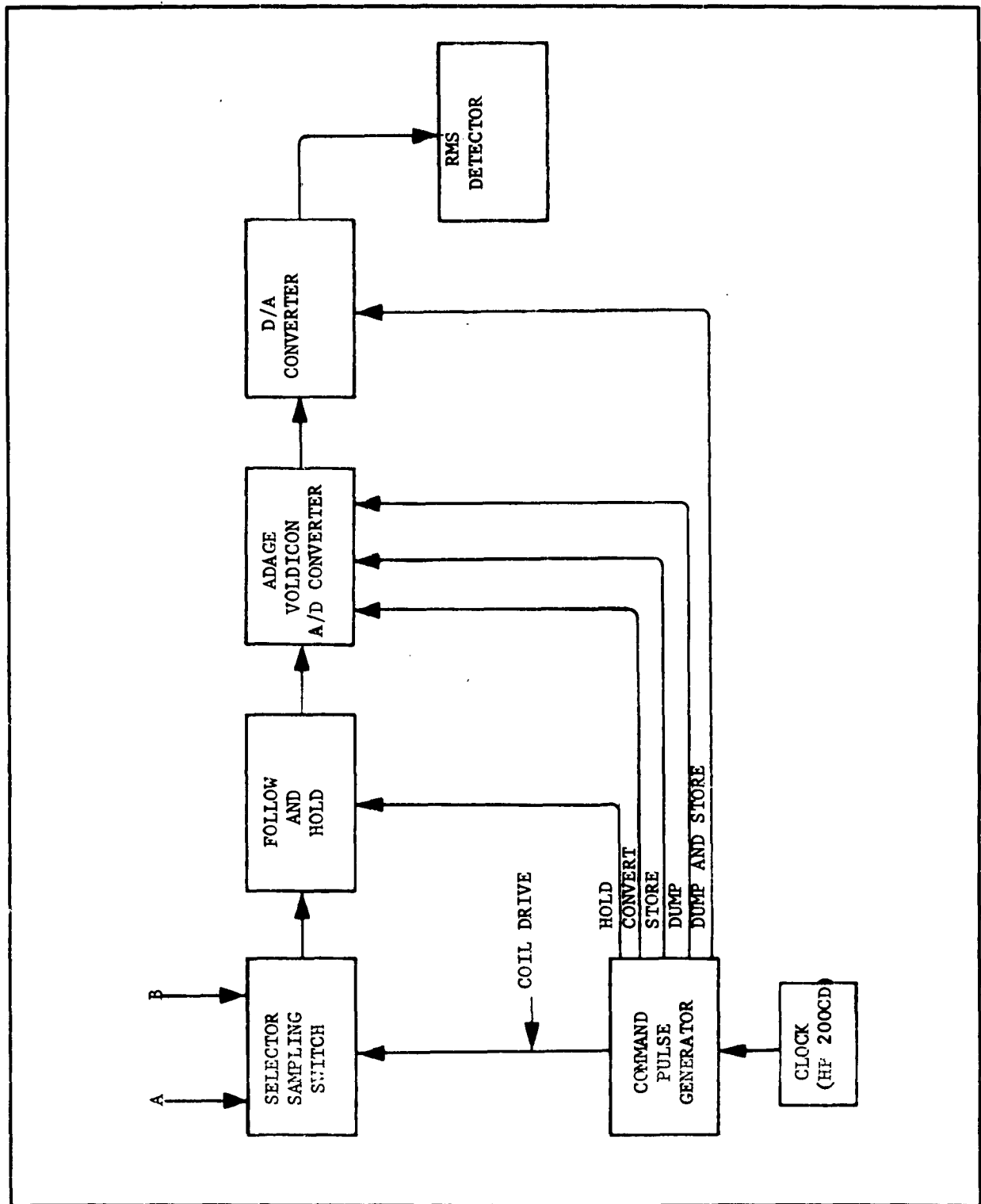


FIGURE 5-23 BLOCK DIAGRAM - ANALOG ERROR COMPARATOR

The time between the A and B samples is determined by a sine wave clock. The clock frequency is adjusted so that the period of one clock cycle equals the time delay in the telemetering system.

#### 5.5 ACCURACY OF MEASUREMENTS

Overall accuracy and limitations are discussed in reference 1 Volume III.

The overall measurement accuracy for the Aliasing tests are considered to be within the limits shown below:

<u>Measurement</u>	<u>Limiting Accuracy</u>
Rms error	5% (0.05% resolution)
S/N	1 db
Spectrum amplitude	3 db

## SECTION 6

### CONCLUSIONS AND RECOMMENDATIONS

Conclusions and recommendations derived from this study are summarized below:

#### 6.1 CONCLUSIONS

##### 6.1.1 Determination of Typical Data Spectra

- 1) Satisfactory spectral models have been derived for representing typical spectral data characteristics.
- 2) Practical application of the spectral models requires additional information on the part of the system designer. This information consists of an understanding of the basic mechanisms generating the data spectra to permit specification of the bandwidth and spectral shapes of the data spectra by the designer.

##### 6.1.2 Analysis

- 1) The analysis and numerical computations of selected examples agreed closely with experimental data.
- 2) Additional numerical computations to predict aliasing and interpolation distortion errors should be undertaken. These computations should be based on the spectral models derived in this study and should take into account a broad class of interpolation filters to provide a number of different filter types to instrumentation engineers for reconstructing data.

3) An analytical investigation supplemented by implementation of a practical technique for obtaining "alias-free" sampling should be undertaken. This investigation should be supplemented by experimental test and evaluation.

#### 6.1.3 Laboratory Measurements

1) The experimental test program conducted in this study has provided proven operating parameters for a time-division telemetry system which guarantees a minimum standard of performance.

2) Techniques for improving this performance should be investigated experimentally, especially in determining the error mechanisms which limit the ultimate accuracy of sampled data systems. The range of accuracies which should be investigated lie in the region of .05 to .25% rms.

#### 6.1.4 Operating Parameters

The most salient factor in controlling interpolation error is the spectral characteristic of the signal to be sampled. This, of course, was well known and is borne out by the results of this study. This means that to optimize the system parameters the data spectrum must be known and design information such as given in Section 4 must be utilized for the specific data spectrum being sampled. However, when the data spectrum is not accurately known many specific recommendations can be made to aid the system design based upon the results of this study.

A very important result of this work is the determination of which parameters are sensitive in controlling aliasing and interpolation errors, and which are insensitive. The fact that performance is insensitive to some parameters makes the design information in Section 3 and 4 more universally applicable.

The following conclusions relating to operating parameters can be enumerated:

1) The aliasing error is primarily dependent upon the data spectrum and upon  $f_s/f_d$  (the samples per cycle of data). If  $f_s/f_d$  is to be minimized, minimizing the required power and bandwidth, the data spectrum must be accurately known.

2) The amplitude probability distribution of the data does not affect the aliasing error (or distortion error which is due to amplitude and time delay variation with frequency).



3) It is the high frequency region of the data spectrum which is of most importance (unless this region is very low in relative energy) which often allows simplifying the spectral type for ordinary low-pass interpolation. For continuous data spectra the high frequency skirt or rolloff characteristic is very important.

4) The interpolation error is relatively insensitive to the interpolation filter characteristic for the low-pass types examined with selectivity from 24 to 60 db/oct. The most selective filter performs best at low samples per cycle, 2 to 3 or 4, while the 36 db/oct. Butterworth type is about optimum for higher  $f_s/f_d$  due to reduced distortion error. The Gaussian characteristic is inferior to the Butterworth for interpolation. The 24 db/oct. Butterworth filter performed well enough for many applications and would be useful for low frequency interpolation where a relatively simple R-C mechanization is desired.

5) The interpolation error is insensitive to the duty cycle of the interpolated pulsetrain, even from short pulses to 100% duty cycle for the same interpolation filters. The 100% duty cycle signal supplies much more energy to the interpolation filter minimizing the effects of system noise. It also minimizes the modulation effects of possible pulse jitter. This waveform will therefore improve the performance of most practical systems by reducing these noise sources.

6) In most applications, especially when the interpolation error must be 1% or better, a minimum  $f_s/f_d$  of 3 or higher will be required. For  $f_s/f_d \geq 3$  the interpolation filter cutoff,  $f_i$ , should be set for  $f_i/f_d$  of about 2 which minimizes the distortion error due to amplitude and phase effects.

## 6.2 RECOMMENDATIONS

The following recommendations are based on the conclusions cited in Section 6.1.

1) Investigation of the nature of the data sources should be made from the viewpoint of practical instrumentation applications. Such an investigation would consider typical data sources and methods of estimating the proper bandwidth and spectral shape to assign to the given data source. Consideration of data sources derived from deterministic as well as statistical processes and the common limitations imposed on the processes by physical considerations would lead to more realistic estimates of the spectrum of the data sources. A simple example of such estimation techniques would be to take velocity, acceleration and position limiting into account in the derivation of the spectrum generated

by a physical variable such as temperature, pressure, shaft positions, and so forth. The effects of data spectral filtering by pre-sampling filtering could then be more realistically evaluated and applied.

2) Computation of a family of parametric curves presenting rms error versus sampling rate for different spectral data models and filter types should be undertaken. This data should be based on selected sampling and reconstruction techniques representing the best methods for practical instrumentation at the present time.

3) An experimental investigation of techniques to obtain "alias-free" sampling should be undertaken.

4) Techniques for performing more accurate data sampling, processing of the sampled data value into a suitable carrier waveform, and recovery of the processed data sample before the interpolation process is performed should be undertaken to extend the accuracy of data recovery into the accuracy region of .05 to .25% rms.

## APPENDIX 1

### PAM MULTIPLEX SYSTEM ANALYSIS

#### A1-1 SUMMARY OF RESULTS

This Appendix includes the following results applicable to the design of a PAM multiplex system:

- a) A simplified system model including the effects of finite bandwidth, finite sampling width, aliasing, crosstalk, and noise developed for an N-channel system.
- b) A general expression for total mean square error due to all the effects in a) is obtained.
- c) An error minimization procedure is carried out for the special case in which all channels are identical and a signal power constraint is imposed.
- d) Expressions for optimum transfer functions, both realizable and non-realizable, are obtained for the data filter and the interpolation filter. In general, these transfer functions are bandlimited and can only be approximated in the practical case.
- e) Optimum sampling rate is specified in terms of the filter transfer functions.
- f) Optimum sampling delay is specified in terms of the video filters and the design of these filters to reduce crosstalk is mentioned.

## A1-2 SYSTEM MODEL AND NOTATION

The basic system model which was assumed for purposes of analysis is shown in Figure A1-1. This model includes  $N$  input channels and one output channel.

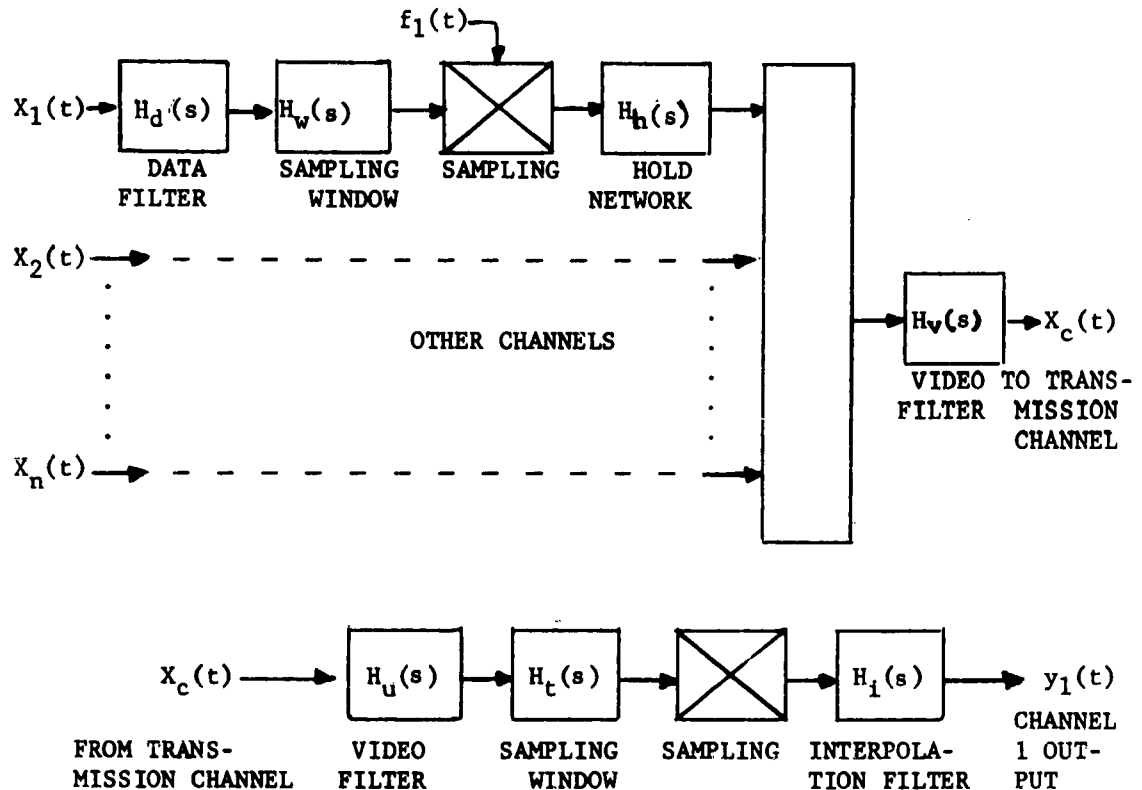


FIG. A1-1 BLOCK DIAGRAM OF  $N$  CHANNEL PAM SYSTEM

The various transfer functions associated with one channel of this model are discussed in detail below. Although corresponding transfer functions for the other channels would frequently be the same, this condition is not required in the present analysis. It may also be noted that modulation to an RF signal and back again is not considered.

$H_d(s)$  = The data filter shapes the signal spectrum to an optimum form. This transfer function is assumed to be capable of adjustment.

$H_w(s)$  = The sampling window makes it possible to consider a finite sample width. Typically, this would be the transfer function for a finite-memory integrator in which the integration time is the desired sample width,  $T_s$ . Thus, for this case

$$H_w(s) = \frac{1 - e^{-sT_s}}{s}$$

If instantaneous samples are taken, then

$$H_w(s) = 1$$

$f_1(t)$  = The actual sampling operation is represented by multiplying the channel signal by a periodic sequence of impulses and holding the product for a specified time interval. For the  $n$ th channel the sampling function becomes

$$f_1(t) = \sum_{k=-\infty}^{\infty} \delta(t + nt_1 - kT_1), \quad n = 1, 2, \dots, N$$

Where  $T_1$  is the sampling interval, per channel, and  $t_1$  is the interval between sampling instants in adjacent channels.

$H_h(s)$  = The hold network would usually generate rectangular pulses from the impulses. If the pulse width is  $t_1$  (largest possible value) then

$$H_h(s) = \frac{1 - e^{-st_1}}{s}$$

$H_v(s)$  = The video filter smooths the boxcar sequence coming from the summing circuit in order to reduce the channel bandwidth. The minimum bandwidth is determined by crosstalk considerations.

$H_u(s)$  = The video filter at the receiver input is similar to the one above and is used to reduce the noise into the sampling circuits.

$H_t(s)$  = This sampling window again makes it possible to consider a finite sample width, if desired. Its form would be similar to  $H_w(s)$ .

$f_2(t)$  = The receiver sampling function is another periodic sequence of impulses given by

$$f_2(t) = \sum_{k=-\infty}^{\infty} \delta(t - \tau + nt_1 - KT_1), n = 1, 2, \dots, N$$

Where  $\tau$  is the sampling delay needed to compensate for the delay in the transmission channel.

$H_1(s)$  = The interpolation filter converts the reconstructed samples into the output signal. This transfer function is assumed to be capable of adjustment.

In addition to the system components discussed above, noise will be introduced into the system in the transmission channel. This noise will be assumed to be additive.

### A1-3 MODEL SIMPLIFICATION

For purposes of notational simplicity it is desirable to represent any one channel of the system in the more compact form shown in Figure A1-2. The transfer functions in this model may be expressed in terms of those

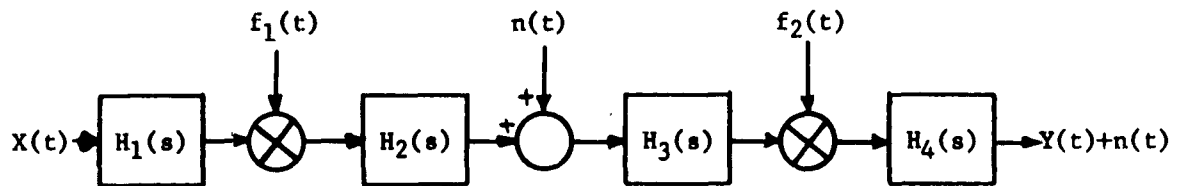


FIG. A1-2 SIMPLIFIED BLOCK DIAGRAM FOR A SINGLE CHANNEL

in Section A1-2 by the following set of relations:

$$H_1(s) = H_d(s) H_w(s)$$

$$H_2(s) = H_h(s) H_v(s)$$

$$H_3(s) = H_u(s) H_t(s)$$

$$H_4(s) = H_f(s)$$

In addition, noise  $n(t)$  has been added in the transmission channel. This noise is assumed to have a spectral density of  $\Phi_{nn}(s)$  which may be white compared to the system bandwidth.

When considering the signal component,  $X(t)$ , only, the double sampling operation can be replaced by a single sampling operation in order to achieve even greater simplicity. This simplification, which can be justified rigorously, can also be obtained heuristically by noting that the outputs of both multipliers are sequences of impulses. Hence, the second multiplier and the transfer function between it and the first can be replaced by pure attenuation and delay only. The resulting block diagram is shown in Figure A1-3.

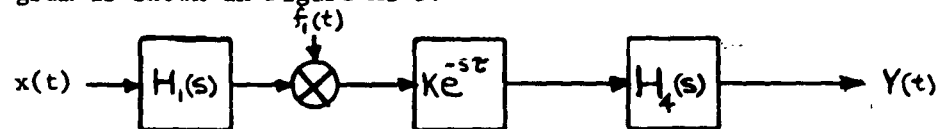


FIG. A1-3 SIMPLIFIED BLOCK DIAGRAM FOR SIGNAL ONLY

The attenuation factor  $K$  is simply the magnitude of the unit impulse response of  $H_2(s) H_3(s)$  evaluated at the receiver sampling times. Since these sampling times are delayed by  $\tau$  seconds, it follows that

$$K = \frac{1}{2\pi j} \int_{-j\infty}^{j\infty} H_2(s) H_3(s) e^{s\tau} ds \quad (1)$$

since this is just the inverse Laplace transform of the transfer function evaluated at the time  $\tau$ .

It will be shown later that this same simplification can be extended to consider crosstalk by using different values for  $\tau$ . However, the effects of noise cannot be considered in Figure A1-3 and it is necessary to use the form shown in Figure A1-2 for this purpose.

An assumption which is implicit in the use of Figure A1-3 is that the impulse response of  $H_2(s)H_3(s)$  is essentially zero at a time equal to the sampling interval  $T_1$ . Since small crosstalk requires that this impulse response be small at a time  $t_1 = \frac{T_1}{N}$ , it seems clear that assumption is extremely well justified.

#### A1-4 ERROR ANALYSIS

Errors of three types are considered in this analysis. These are designated as signal error, crosstalk, and noise. The signal error arises from three different sources. First, there is an error due to the finite bandwidth of the data filter and sampling window. Secondly, there is the aliasing error resulting from the spectrum folding of the sampling process. Finally, there is a reconstruction error resulting from imperfect interpolation. Since all of these signal error components depend upon the channel transfer functions and the sampling interval, it is neither necessary nor desirable to treat them separately.

For purposes of error analysis it will be assumed that the signal  $X(t)$  from the data source is a random function with a spectral density  $\Phi_{xx}(s)$ . The crosstalk and noise are also random functions and are assumed to be statistically independent of each other and of the signal.

If  $y(t)$  is the output from any channel due to the signal input to that channel only, then the signal error may be defined as

$$s(t) = x(t - t_0) - y(t) \quad (2)$$

The delay time  $t_0$  is introduced in order that delay in the channel not be interpreted as an error. The spectral density of this error may be written in terms of the spectral densities of  $x(t)$  and  $y(t)$  and the cross-spectral densities. Thus,

$$\Phi_{ss}(s) = \Phi_{xx}(s) + \Phi_{yy}(s) - e^{st_0} \Phi_{xy}(s) - e^{-st_0} \Phi_{yx}(s) \quad (3)$$

The spectral densities in (3) may be determined from the simplified block diagram of Figure A1-3. The only item of special concern is to correctly account for the effect of sampling. This may be done with the aid of Figure A1-4 which shows the multiplier only.



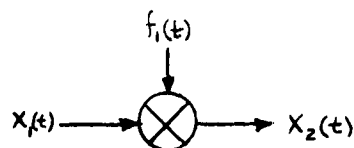


FIG. A1-4 MULTIPLIER WHICH IS EQUIVALENT TO SAMPLING

Since

$$X_2(t) = X_1(t)f_1(t) \quad (4)$$

the spectral density of  $X_2(t)$  is obtained by convolution. Thus,

$$\Phi_{22}(s) = \frac{1}{2\pi j} \int_{-j\infty}^{j\infty} \Phi_{11}(s-u) \Phi_{ff}(u) du \quad (5)$$

where

$$\Phi_{22}(s) = \text{spectral density of } X_2(t)$$

$$\Phi_{11}(s) = \text{spectral density of } X_1(t)$$

$$\Phi_{ff}(s) = \text{spectral density of } f_1(t)$$

Since the sampling function  $f_1(t)$  is a periodic sequence of unit impulses, its spectral density can be shown to be

$$\Phi_{ff}(s) = \frac{2\pi}{T_1} \sum_{n=-\infty}^{\infty} \delta(s - j \frac{2\pi n}{T_1}) \quad (6)$$

Substituting this function into (5) yields

$$\Phi_{22}(s) = \frac{1}{T_1} \sum_{n=-\infty}^{\infty} \Phi_{11}(s - j \frac{2\pi n}{T_1}) \quad (7)$$

Furthermore, it can be shown that cross-spectral density is

$$\Phi_{12}(s) = \frac{1}{T_1} \Phi_{11}(s) = \Phi_{21}^*(s) \quad (8)$$

where the asterisk denotes the complex conjugate.

Using (7), (8) and Figure A1-3, the signal error spectral density can be written as

$$\Phi_{ss}(s) = \Phi_{xx}(s) + \frac{k^2}{T_1^2} |H_4(s)|^2 \sum_{n=-\infty}^{\infty} \Phi_{xx}(s - j \frac{2\pi n}{T_1}) \left| H_1(s - j \frac{2\pi n}{T_1}) \right|^2 \quad (9)$$

$$- \frac{k}{T_1} e^{s(t_0 - \tau)} H_1(s) H_4(s) \Phi_{xx}(s) - \frac{k}{T_1} e^{-s(t_0 - \tau)} H_1(-s) H_4(-s) \Phi_{xx}(s)$$

The error due to crosstalk can be obtained by extending Figure A1-3 to include all channels. This extension is shown in Figure A1-5. The major difference

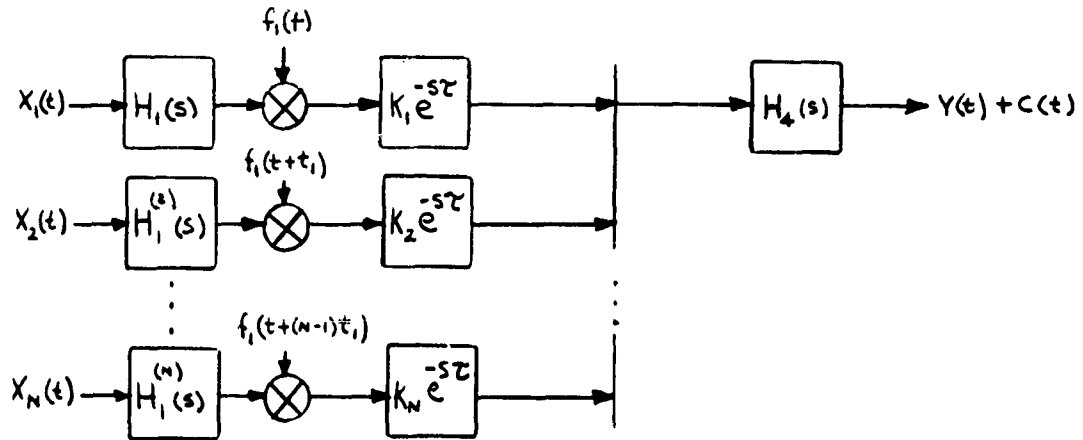


FIG. A1-5 BLOCK DIAGRAM FOR CROSSTALK ANALYSIS

among the various channels is the attenuation factor, which, for the kth channel, is

$$K_k = \frac{1}{2\pi j} \int_{-j\infty}^{j\infty} H_2^{(k)}(s) H_3^{(k)}(s) e^{s(\tau + (k-1)t_1)} ds \quad (10)$$

If  $y(t)$ , in Figure A1-5, is considered to be the output due to  $X_1(t)$  and  $c(t)$  is the crosstalk output due to all other inputs, then the spectral density of the crosstalk can be written as

$$\Phi_{ee}(s) = \frac{1}{T_1^2} |H_4(s)|^2 \sum_{k=2}^N K_k^2 \sum_{n=-\infty}^{\infty} \Phi_{kk}(s - j\frac{2\pi n}{T_1}) |H_1(s - j\frac{2\pi n}{T_1})|^{(k)} \quad (11)$$

where  $\Phi_{kk}(s)$  is the spectral density of  $X_k(t)$ .

The error due to noise can be obtained from the block diagram of Figure A1-6.

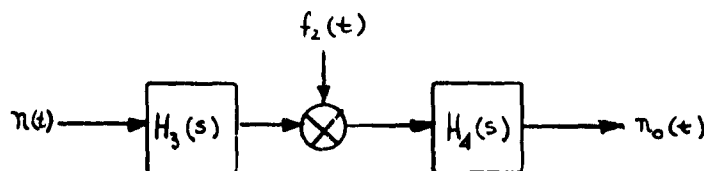


FIG. A1-6 BLOCK DIAGRAM FOR NOISE ANALYSIS

The similarity of this block diagram to Figure A1-3 makes it possible to write the spectral density of  $n_o(t)$  by analogy. Thus,

$$\Phi_{oo}(s) = \frac{1}{T_1^2} |H_4(s)|^2 \sum_{n=-\infty}^{\infty} \Phi_{nn}(s - j\frac{2\pi n}{T_1}) |H_3(s - j\frac{2\pi n}{T_1})|^2 \quad (12)$$

Usually the noise  $n(t)$  and the transfer function  $H_3(s)$  will both have a bandwidth which is large compared to the sampling frequency. In this case, the summation in (12) can be closely approximated by an integral. If this is done, the output noise spectral density can be written as

$$\Phi_{oo}(s) = \frac{1}{2\pi T_1} |H_4(s)|^2 \int_{-j\infty}^{j\infty} \Phi_{nn}(s) H_3(s) H_3(-s) ds \quad (13)$$

Since the various sources of error are statistically independent, their spectral densities can be added directly. Thus, the total mean square error can be obtained from

$$\overline{e^2} = \frac{1}{2\pi j} \int_{-j\infty}^{j\infty} [\Phi_{ss}(s) + \Phi_{ee}(s) + \Phi_{oo}(s)] ds \quad (14)$$

Upon combining some terms and simplifying the notation, this mean square error can be written as

$$\begin{aligned} \overline{e^2} = \frac{1}{2\pi j} \int_{-j\infty}^{j\infty} \left\{ \Phi_{xx}(s) - \frac{K_1}{T_1} \Phi_{xx}(s) \left[ e^{\frac{s(t_0-\tau)}{T_1}} H_1(s) H_4(s) + e^{\frac{-s(t_0-\tau)}{T_1}} H_1(-s) H_4(-s) \right] \right. \\ \left. + |H_4(s)|^2 \left[ \sum_{k=1}^N \sum_{n=-\infty}^{\infty} \frac{K_A^2}{T_1^2} \Phi_{AA}(s - j\frac{2\pi n}{T_1}) \left| H_1(s - j\frac{2\pi n}{T_1}) \right|^2 \right. \right. \\ \left. \left. + \frac{N_3}{T_1} \right] \right\} ds \end{aligned} \quad (15)$$

where

$$N_3 = \frac{1}{2\pi j} \int_{-j\infty}^{j\infty} \Phi_{nn}(s) H_3(s) H_3(-s) ds$$

It may be noted that  $N_3$  is the mean square value of noise into the receiver sampler.

Another quantity which will be needed in the remaining analysis is the mean square value of the signal into the receiver sampler. This mean square value is given by

$$S_3 = \frac{GB}{2\pi j T_1} \int_{-j\infty}^{j\infty} \Phi_{xx}(s) H_1(s) H_1(-s) ds \quad (16)$$

where

$$GB = \frac{1}{2\pi j} \int_{-j\infty}^{j\infty} [H_2(s) H_2(-s) H_3(s) H_3(-s)] ds$$

is the gain-bandwidth product of  $H_2(s) H_3(s)$

#### A1-5 ERROR MINIMIZATION

It is apparent from (15) that there are many different ways in which the error could be minimized. For purposes of the present analysis

it will be assumed that  $H_2(s)$ ,  $H_3(s)$ , and  $T_1$  are fixed and that  $H_1(s)$  and  $H_4(s)$  can be adjusted for minimum error. It will also be assumed that all channels are identical so that

$$\Phi_{kk}(s) = \Phi_{xx}(s) \quad k = 1, 2, \dots, N$$

$$H_1^{(k)}(s) = H_1(s)$$

$$H_2^{(k)}(s) H_3^{(k)}(s) = H_2(s) H_3(s)$$

The error minimization must also be carried out with a constraint on the average signal power. Without this constraint the effects of noise can be made negligible by simply increasing the signal power. Thus, it is necessary to minimize the function

$$I = \overline{e^2} + \lambda S_3 \quad (17)$$

where  $\lambda$  is the Lagrange multiplier which can be adjusted to satisfy the signal power constraint.

The notation can be further simplified by suppressing the integration variable  $s$  and letting

$$\Phi_{xx}(s) = \Phi_{xx} = \phi_x \phi_x^*$$

$$H_1(s) = H_1$$

$$H_1(-s) = H_1^*$$

$$H_1(s - j\frac{2\pi n}{T_1}) = H_{1n} \text{ etc.}$$

Furthermore, let

$$K_s^2 = \sum_{k=1}^N K_k^2$$

The integral  $I$  may now be written as

$$\begin{aligned} I = \frac{1}{2\pi j} \int_{-j\infty}^{j\infty} & \left[ \Phi_{xx} - \frac{K_1}{T_1} \Phi_{xx} (H_1 H_4 e^{s(t_0 - \tau)} + H_1^* H_4^* e^{-s(t_0 - \tau)}) \right. \\ & + \frac{K_s^2}{T_1^2} H_4 H_4^* \sum_n \Phi_{xxn} H_{1n} H_{1n}^* + \frac{N_3}{T_1} H_4 H_4^* \\ & \left. + \frac{\lambda 6B}{T_1} \Phi_{xx} H_1 H_1^* \right] ds \quad (18) \end{aligned}$$

Further work is simplified if the optimum value of  $t_0$  is chosen. It can be shown straightforwardly that

$$\frac{\partial I}{\partial t_0} = 0$$

when  $t_0 = \tau$ . This value of  $t_0$  will be assumed throughout the rest of the analysis.

The next step is to take a first variation of  $I$  with respect to  $H_4$ . Setting  $\delta I = 0$  and eliminating the redundant conjugate terms yields

$$\int_{-j\infty}^{j\infty} \delta H_4^* \left[ -\frac{k_1}{T_1} \Phi_{xx} H_1^* + \frac{K_s^2}{T_1^2} H_4 \sum_n \Phi_{xxn} H_{1n} H_{1n}^* + \frac{N_3}{T_1} H_4 \right] ds \quad (19)$$

from which

$$H_4 \left[ \frac{K_s^2}{T_1^2} \sum_n \Phi_{xxn} H_{1n} H_{1n}^* + \frac{N_3}{T_1} \right] = \frac{k_1}{T_1} \Phi_{xx} H_1^* \quad (20)$$

Before taking a variation with respect to  $H_1$ , it is convenient to make a change in variable in the portion of the integral containing  $H_{1n} H_{1n}^*$ . The resulting integral contains a summation over  $H_{4n} H_{4n}^*$ . Hence,

$$I = \frac{1}{2\pi j} \int_{-j\infty}^{j\infty} \left[ \Phi_{xx} - \frac{k_1}{T_1} \Phi_{xx} (H_1 H_4 + H_1^* H_4^*) + \frac{K_s^2}{T_1^2} \Phi_{xx} H_1 H_1^* \sum_n H_{4n} H_{4n}^* + \frac{N_3}{T_1} H_4 H_4^* + \frac{\lambda G B}{T_1} \Phi_{xx} H_1 H_1^* \right] ds \quad (21)$$

After taking the first variation with respect to  $H_1$  and equating it to 0,

$$\int_{-j\infty}^{j\infty} \delta H_1^* \left[ -\frac{k_1}{T_1} \Phi_{xx} H_4^* + \frac{K_s^2}{T_1^2} \Phi_{xx} H_1 \sum_n H_{4n} H_{4n}^* + \frac{\lambda G B}{T_1} \Phi_{xx} H_1 \right] ds = 0$$

from which

$$H_1 \left[ \frac{K_s^2}{T_1^2} \Phi_{xx} \sum_n H_{4n} H_{4n}^* + \frac{\lambda G B}{T_1} \Phi_{xx} \right] = \frac{k_1}{T_1} \Phi_{xx} H_4^* \quad (22)$$

Equations (21) and (22) specify the conditions that must be satisfied in order for the total mean square error to be a minimum.

# A1-6 IDEAL NON-REALIZABLE TRANSFER FUNCTIONS

The simultaneous equations which must be satisfied by  $H_1$  and  $H_4$  may be written as

$$H_4 \left[ K_s^2 \sum_n \Phi_{xxn} H_{1n} H_{1n}^* + N_3 T_1 \right] = K_1 T_1 \Phi_{xx} H_1^* \quad (23)$$

and

$$H_1 \left[ K_s^2 \sum_n H_{4n} H_{4n}^* + \lambda G B T_1 \right] = K_1 T_1 H_4^* \quad (24)$$

A general solution to this pair of equations would appear to be quite formidable. If it is assumed, however, that  $H_1$  and  $H_4$  are band-limited so that

$$\begin{aligned} H_1 H_{4n} &= H_1 H_4 & n &= 0 \\ &= 0 & n &\neq 0 \end{aligned}$$

and

$$\begin{aligned} H_4 H_{1n} &= H_1 H_4 & n &= 0 \\ &= 0 & n &\neq 0 \end{aligned}$$

then a solution is readily obtained. This assumption may be justified, a posteriori, by noting that the resulting solutions are, in fact, band-limited.

The solutions obtained by this procedure are

$$H_1 H_1^* = \frac{K_1 T_1}{K_s^2} \sqrt{\frac{N_3}{\lambda G B}} \left[ \frac{\sqrt{\Phi_{xx}} - \frac{1}{K_1} \sqrt{\lambda G B N_3}}{\Phi_{xx}} \right] \quad (25)$$

$$H_4 H_4^* = \frac{K_1 T_1}{K_s^2} \sqrt{\frac{\lambda G B}{N_3}} \left[ \sqrt{\Phi_{xx}} - \frac{1}{K_1} \sqrt{\lambda G B N_3} \right] \quad (26)$$

which exist when  $\sqrt{\Phi_{xx}} > \frac{1}{k_1} \sqrt{16BN_3}$  and are zero otherwise. The value of  $\lambda$  is adjusted by putting (25) into (16) with the desired value for  $S_3$ . This may then be solved for  $\lambda$ .

The solutions given by (25) and (26) are in general not physically realizable because the resulting transfer functions may have RHP poles or complex poles not occurring in conjugate pairs. In addition, the resulting transfer functions may not be rational. Nevertheless, these transfer functions are useful in specifying the irreducible error in the system. This irreducible error is obtained by substituting (25) and (26) into the expression for the mean square error as given by (15). The general result is too complicated to be useful but specific cases can be worked out.

#### A1-7 OPTIMUM REALIZABLE TRANSFER FUNCTIONS

The optimum realizable transfer functions are those which produce minimum error and have all poles in the LHP. In general, these transfer functions would require an infinite number of poles in order to achieve the bandlimited condition and can only be approximated by practical networks. This approximation will not be discussed in this report.

In accordance with the usual procedures for obtaining realizable functions, it is necessary to introduce a shaping filter which yields a constant spectral density at its output. This shaping filter transfer function is then extracted from the ideal transfer function and the remainder is made realizable by retaining only its LHP poles.

Considering the data filter first, the required shaping filter has a transfer function  $H_s(s)$  defined by

$$H_s(s) H_s(-s) = \Phi_{xx}^{-1}(s) \quad (27)$$

or

$$H_s H_s^* = \Phi_{xx}^{-1}$$

The remainder of  $H_1$ , after extracting  $H_s$ , is designated as  $H_{1s}$  and is given by

$$H_{1s} H_{1s}^* = \frac{H_1 H_1^*}{H_s H_s^*} = H_1 H_1^* \Phi_{xx} \quad (28)$$



The physically realizable part of  $H_{1s}$  is  $[H_{1s}]_+$  and is obtained from

$$H_{1s} = [H_{1s}]_+ + [H_{1s}]_- \quad (29)$$

by making a partial fraction expansion of  $H_{1s}$  if it is rational, or by performing the equivalent time-domain separation if it is not. In either case  $[H_{1s}]_+$  contains only LHP poles and  $[H_{1s}]_-$  contains only RHP poles. The resulting overall realizable transfer function,  $H_{1R}$  is now given by

$$H_{1R} = H_s [H_{1s}]_+ \quad (30)$$

Upon using (25) and defining some new terms, the realizable filter becomes

$$H_{1R} = C_1 \frac{[D_x]_+}{\phi_x} \quad (31)$$

where

$$C_1 = \sqrt{\frac{K_1 T_1}{K_s^2}} \sqrt{\frac{N_3}{\lambda G B}}$$

$$D_x D_x^* = \sqrt{\Phi_{xx}} - \frac{1}{K_1} \sqrt{\lambda G B N_3} \geq 0$$

$$\phi_x \phi_x^* = \Phi_{xx}$$

It should be noted that  $H_{1R}$  contains the transfer function which corresponds to the sampling window as well as the data filter. This implies that the data filter  $H_d$  is given by

$$H_d = \frac{H_{1R}}{H_w} \quad (32)$$

The only restriction on the sampling window, therefore, is that  $H_w$  must not have transmission zeros within the passband of  $H_{1R}$ . This condition is almost always satisfied.

Since the input to  $H_4$  is a sequence of impulses, no shaping filter is needed. Hence the realizable filter transfer function is

$$H_{4R} = [H_4]_+ = C_4 [D_x]_+ \quad (33)$$

where

$$C_4 = \sqrt{\frac{K_1 T_1}{K_3^2}} \sqrt{\frac{\lambda G B}{N_3}}$$

$$D_x D_x^* = \sqrt{\Phi_{xx}} - \frac{1}{K_1} \sqrt{\lambda G B N_3} \geq 0$$

#### A1-8 OPTIMUM SAMPLING RATE

It was shown in the previous sections that the optimum data filter and interpolation filter were bandlimited. Hence, any sampling rate greater than that determined by the filter bandwidth will not be effective in reducing signal error. However, increased sampling rates will increase the error due to noise because the video bandwidth must increase (for a fixed number of channels).

It may be concluded from the above that the optimum sampling rate is that determined by the filter bandwidth. The filter bandwidth is that which makes  $D_x$  in (31) and (32) identically zero. Thus, if

$$\Phi_{xx}(2\pi f_0) = \frac{\lambda G B N_3}{K_1^2} \quad (34)$$

then

$$T_1 = \frac{1}{2f_0}$$

#### A1-9 OPTIMUM SAMPLING DELAY AND VIDEO FILTERS

A set of attenuation factors was defined by (10) as

$$K_k = \frac{1}{2\pi j} \int_{-j\infty}^{j\infty} H_2^{(k)}(s) H_3^{(k)}(s) e^{s(\tau + (k-1)t_1)} ds \quad (35)$$

These factors may be interpreted in the time domain by sketching the impulse response corresponding to  $H_2(s) H_3(s)$  under the assumption that these are the same for all channels. The  $K_k$  are then simply samples of this impulse response, as shown in Figure A1-7. It is clear from the mean square

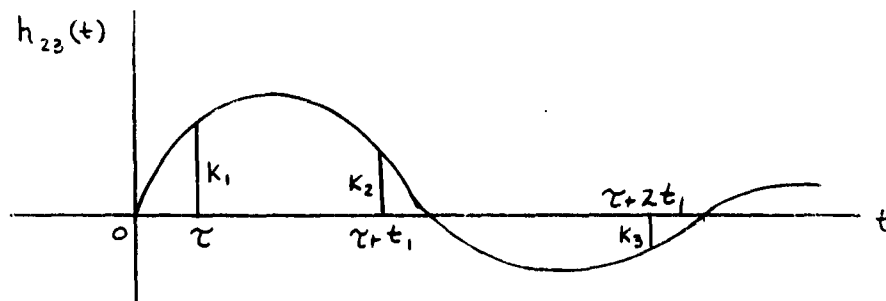


FIG. A1-7 VIDEO ATTENUATION FACTORS

error as given by (15), or simply from the physical interpretation, that  $K_1$  should be as large as possible and all of the others should be as small as possible.

The optimum value of sampling delay,  $\tau$ , should correspond to the location of the maximum of the impulse response. The following zeros of the impulse response should coincide with  $\tau + t_1$ ,  $\tau + 2t_1$ , etc. Hence, if the video filters have been selected so as to minimize crosstalk, the optimum value of  $\tau$  is that which satisfies the equation

$$\left. \frac{dh_{23}(t)}{dt} \right|_{t=\tau} = 0 \quad (36)$$

## APPENDIX 2

### POWER SPECTRUM OF SAMPLER OUTPUT

The sampling operation is considered as equivalent to taking the product of  $[d(t) + N(t)] \cdot s(t) = g(t)$ , where  $s(t)$  is the sampling function shown in Figure 3-2. The Fourier transform of  $s(t)$  is determined below:

$$s(t) = A \sum_{n=-\infty}^{\infty} \left[ u\left(t + \frac{t_1}{2} - nT_s\right) - u\left(t - \frac{t_1}{2} - nT_s\right) \right]$$

$$u(t) = \begin{cases} 1 & t > 0 \\ 0 & t < 0 \end{cases}$$

$$S(f) = \int_{-\infty}^{\infty} s(t) e^{-j\omega t} dt$$

$$= A \sum_{n=-\infty}^{\infty} \int_{-\infty}^{\infty} \left[ u\left(t + \frac{t_1}{2} - nT_s\right) - u\left(t - \frac{t_1}{2} - nT_s\right) \right] e^{-j\omega t} dt$$

$$= A \sum_{n=-\infty}^{\infty} \int_{-\infty}^{\infty} \left[ u\left(x + \frac{t_1}{2}\right) - u\left(x - \frac{t_1}{2}\right) \right] e^{-j\omega(x + nT_s)} dx$$

$$\begin{aligned}
 S(t) &= A \sum_{n=-\infty}^{\infty} e^{-j\omega n T_s} \int_{-\infty}^{\infty} \left[ u(x + \frac{t_1}{2}) - u(x - \frac{t_1}{2}) \right] e^{-j\omega x} dx \\
 &= A \sum_{n=-\infty}^{\infty} e^{-j\omega n T_s} \left[ t_1 \frac{\sin(\omega \frac{t_1}{2})}{\omega \frac{t_1}{2}} \right] \\
 &= A \sum_{n=-\infty}^{\infty} e^{-j\omega n T_s} \left[ t_1 \frac{\sin(\pi f t_1)}{\pi f t_1} \right]
 \end{aligned}$$

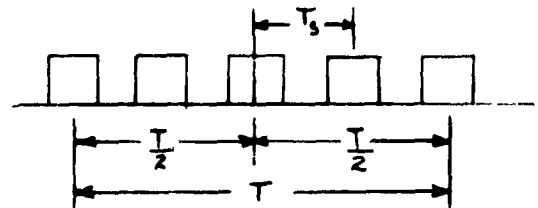
The power spectrum of  $s(t)$  is given by

$$P_s(f) = \lim_{T \rightarrow \infty} \frac{1}{T} \overline{|S(f)|^2}$$

where the bar denotes an ensemble average.

$$P_s(f) = \lim_{T \rightarrow \infty} \frac{1}{T} A^2 \left[ t_1 \frac{\sin(\pi f t_1)}{\pi f t_1} \right]^2 \sum_{k=-\infty}^{\infty} \sum_{n=-\infty}^{\infty} e^{-j\omega T_s (n-k)}$$

$$T = 2NT_s$$



$$P_s(f) = \lim_{N \rightarrow \infty} \frac{A^2}{2NT_s} \left[ t_1 \frac{\sin(\pi f t_1)}{\pi f t_1} \right]^2 \sum_{k=-N}^N \sum_{n=-\infty}^{\infty} e^{-j\omega n T_s} e^{j\omega k T_s}$$

$$\sum_{n=-\infty}^{\infty} e^{-j\omega n T_s} = \frac{1}{T_s} \sum_{n=-\infty}^{\infty} \delta\left(f - \frac{n}{T_s}\right)$$

$$\int_{-\epsilon}^{\epsilon} \delta(x-x_0) dx = 1, \quad -\epsilon \leq x_0 \leq \epsilon$$

$$= 0, \quad \epsilon < |x_0|$$

$$\begin{aligned} \sum_{k=-N}^N \sum_{n=-\infty}^{\infty} e^{-j\omega(n-k)T_s} &= \frac{1}{T_s} \sum_{n=-\infty}^{\infty} \delta\left(f - \frac{n}{T_s}\right) \sum_{k=-N}^N e^{j\omega k T_s} \\ &= \frac{1}{T_s} \sum_{n=-\infty}^{\infty} \delta\left(f - \frac{n}{T_s}\right) \sum_{k=-N}^N e^{j2\pi n k} \\ &= \frac{2N+1}{T_s} \sum_{n=-\infty}^{\infty} \delta\left(f - \frac{n}{T_s}\right) \end{aligned}$$

$$\begin{aligned} P_s(f) &= \lim_{N \rightarrow \infty} \frac{A^2}{2NT_s} \left[ t_1 \frac{\sin(\pi f t_1)}{\pi f t_1} \right]^2 \frac{2N+1}{T_s} \sum_{n=-\infty}^{\infty} \delta\left(f - \frac{n}{T_s}\right) \\ &= A^2 \left(\frac{t_1}{T_s}\right)^2 \sum_{n=-\infty}^{\infty} \left[ \frac{\sin(\pi n \frac{t_1}{T_s})}{\pi n \frac{t_1}{T_s}} \right]^2 \delta\left(f - \frac{n}{T_s}\right) \end{aligned}$$

Note that if  $A = \frac{1}{t_1}$  and  $t_1 \rightarrow 0$ , then  $P_s(f) = \frac{1}{T_s^2} \sum_{n=-\infty}^{\infty} \delta\left(f - \frac{n}{T_s}\right)$

which is the same result obtained if the sampling function is a train of delta functions in the time domain.

The power spectrum of the sampler output signal is determined by convolving the power spectrum of the sampling function with the power spectrum of the sampler input. Let  $h(t) = d(t) + N(t)$

$$\begin{aligned}
 P_g(f) &= \int_{-\infty}^{\infty} P_h(u) P_s(f-u) du \\
 &= A^2 \left( \frac{t_1}{T_s} \right)^2 \sum_{n=-\infty}^{\infty} \left[ \frac{\sin(\pi n \frac{t_1}{T_s})}{\pi n \frac{t_1}{T_s}} \right]^2 \int_{-\infty}^{\infty} P_h(u) \delta(f-u-\frac{n}{T_s}) du \\
 &= A^2 \left( \frac{t_1}{T_s} \right)^2 \sum_{n=-\infty}^{\infty} \left[ \frac{\sin(\pi n \frac{t_1}{T_s})}{\pi n \frac{t_1}{T_s}} \right]^2 P_h(f - \frac{n}{T_s}) \\
 &= A^2 \left( \frac{t_1}{T_s} \right)^2 \sum_{n=-\infty}^{\infty} \left[ \frac{\sin(\pi n \frac{t_1}{T_s})}{\pi n \frac{t_1}{T_s}} \right]^2 \left[ P_d(f - \frac{n}{T_s}) + P_N(f - \frac{n}{T_s}) \right]
 \end{aligned}$$

### APPENDIX 3

#### LIST OF REPORTS AND CONFERENCES ON DATA SPECTRA SURVEY

- 1) "Basic Data Compilation - Short Range Flight Test Operation No. 5", 22 February 1961, Aeronutronic Document 18640-N (Confidential)
- 2) Aliasing Study - Review of Report  
Title: Study and Evaluation of In-Flight Guided Missile Environmental Data  
Date: (1) Interim Report #1, Report #F161g-1 (65248), 13 June 1958  
(2) Final Report, Report #F161-72809, ASTIA AD 306 231, 15 December 1958  
Reports Confidential but title unclassified  
Source: Fairchild Engine & Airplane Corporation  
Applied Science Division  
1334 North Henry Street  
Alexandria, Virginia  
Prepared for: Navy Bureau of Aeronautics  
Contract No. NOar 58-539C  
This report includes an extensive bibliography.
- 3) Wiancko Engr. Rpt. #WC2329-F dated May 1959 "Secondary Isolation System for the High Speed Track Edwards Air Force Base"
- 4) Northrop Aircraft Inc. Report NAI-57-586 "Summary of Launch and Flight Acoustic and Vibration Data N-69D Missiles", dated 12 March 1959
- 5) "Basic Data Compilation Fire Control Static Test I-S-2", 19 April 1961, Aeronutronic D.C. 20025-N (Secret)
- 6) Spectrum Survey Trip Report - JPL - Vibration Analysis Lab.



#### APPENDIX 4

#### BIBLIOGRAPHIES OBTAINED FOR DATA SPECTRA SURVEY

##### Bibliography of Electronics Reports for M.I.T.

Research Laboratory  
February 1, 1958  
Approximately 338 reports referenced

##### A Bibliography of Telemetry

IRE Transactions on Telemetry and Remote Control  
June, 1958  
Approximately 533 books, reports and papers referenced

##### A Report Bibliography on Telemetering and Telemeter Systems

AD 55 316  
Bibliography Secret  
Includes 280 references  
Compiled by H. L. Conn, May 1954

##### A Report Bibliography on Telemetering and Telemeter Systems

AD 30 076  
Bibliography Secret  
Includes approximately 250 references  
Compiled by H. L. Conn, May 1954

ASTIA BIBLIOGRAPHIES

CODE: 6065-812-I/S

1. A Report Bibliography on Phase Detectors  
ARB-6440  
7 secret cards  
14 confidential cards  
54 unclassified cards
2. Bibliography on "Errors" Communication Systems  
ARB-6447  
39 secret cards  
34 confidential cards  
75 unclassified cards
3. A Report Bibliography on Data Processing Systems  
ARB-6445  
219 secret cards  
112 confidential cards  
604 unclassified cards
4. Report Bibliography on Data Transmission Systems  
ARB-6446  
113 secret cards  
234 confidential cards  
455 unclassified cards
5. A Report Bibliography on Phase Measurement  
ARB-6443  
2 secret cards  
6 confidential cards  
Approx. 65 unclassified cards
6. A Report Bibliography on Phase Modulation  
ARB-6444  
13 secret cards  
6 confidential cards  
36 unclassified cards
7. Report Bibliography on "Low Pass Filters"  
ARB-6441  
6 secret cards  
7 confidential cards  
Approx. 60 unclassified cards

8. A Report Bibliography on Telemetering Data  
ARB-6442  
16 secret cards  
21 confidential cards  
90 unclassified cards
9. Atlantic Missile Range  
U. S. Air Force Missile Test Center  
Test Activity Report  
September, 1960  
(Title unclassified but Report Secret)  
AD 319 619
10. A Report Bibliography on Radio and Communication System Interference  
ARB-6681  
ARB-6682  
ARB-6680  
105 Secret cards  
70 confidential cards  
520 unclassified cards

## REFERENCES

### ALIASING BIBLIOGRAPHY

1. Telemetry System Study (U), Final Report, Three Volumes, Aeronutronic Publication No. U-743, 18 December 1959

Volume I of III: Analysis and Design  
Volume II of III: Experimental Evaluation Program  
Volume III of III: Telemetry Systems Test Equipments

Classification: Unclassified

2. Telemetry System Study (U), Final Report, Volume I of II, Aeronutronic Systems, Inc. Publication No. C-162, March 10, 1958, Classification: Confidential
3. Bartlett, M. S., "Periodogram Analysis and Continuous Spectra", Biometrika, Volume 36, June 1950.
4. Bartlett, M. S., Nedhi, J., "On the Efficiency of Procedures for Smoothing Periodograms from Time Series with Continuous Spectra", Biometrika, Volume 42, 1955.
5. Berkowitz, R. S., "Methods of Sampling Band-Limited Function", Proceedings of the I.R.E., February 1956.
6. Brogan, J., "Filters for Sampled Signals", Proceedings of the Symposium on Information Networks, April 12, 13, 14, 1954, Microwave Research Institute Symposia Series, Volume III, Polytechnic Press of the Polytechnic Institute of Brooklyn, Brooklyn, N. Y.

7. Chang, S.S.L., "Optimum Transmission of Continuous Signal Over a Sampled Data Link", Technical Report 400-1, June 1960, New York University, College of Engineering, Department of Electrical Engineering, AD 239 440.
8. Costas, J. P., "Periodic Sampling of Stationary Time Series", May 1950, ATI-83682.
9. Davenport, W. B., Johnson, R. A., Middleton, D., "Statistical Errors in Measurements on Random Time Functions", Journal of Applied Physics, April 1952.
10. Franklin, G., "Linear Filtering of Sampled Data", I.R.E. Convention Record, 1956.
11. Kleene, S. C., "Analysis of Lengthening of Modulated Repetitive Pulses", Proceedings of the I.R.E., October, 1947.
12. Knudtson, N., "Experimental Study of Statistical Characteristics of Filtered Random Noise", July 1949, ATI-73169.
13. Mallinckrodt, A. J., "Data Smoothing Techniques Sampled Data", Phase II Report, Report 1026-P2, 21 March 1955, The Ralph M. Parsons Company, Development and Manufacturing Division, Pasadena 2, Calif.
14. Mazelsky, B., "Extension of Power Spectral Measurements of Generalized Harmonic Analysis to Determine Non-Gaussian Probability Functions of Random Input Disturbances and Output Responses of Linear Systems", Journal of the Aeronautical Sciences, March 1954.
15. Page, C. H., "Instantaneous Power Spectra", Journal of Applied Physics, January 1952.
16. Shapiro, H. S., Silverman, R. A., "Alias-Free Sampling of Random Noise", Research Report No. EM-134, June 1959, New York University, Institute of Mathematical Sciences, Division of Electromagnetic Research, ASTIA Document No. AD 216 368.
17. Spetner, L.M., "Errors in Power Spectra Due to Finite Sample", Journal of Applied Physics, Volume 25, Number 5, May, 1954.
18. Spilker, J. J., "Optimization and Evaluation of Sampled Data Filters", Report LMSD-48335, 18 November 1958, Lockheed Aircraft Corporation, Missile Systems Division, Sunnyvale, California.

19. Stewart, R. M., "Statistical Design and Evaluation of Filters for the Restoration of Sampled Data", Proceedings of the I.R.E., February, 1956.
20. Stutt, C. A., "Experimental Study of Optimum Filters", May 15, 1951, ATI-104170.
21. Swerling, P., "Optimum Linear Estimation for Random Processes as the Limit of Estimates Based on Sampled Data", Report P-1206, The Rand Corporation.
22. Tukey, J. W., "The Sampling Theory of Power Spectrum Estimates", Symposium on Applications of Autocorrelation Analysis to Physical Problems", 13-14 June, 1949, ATI-86556.

Aeronautical Systems Division, Dir/Avionics, Electro-magnetic Warfare & Comm Lab, Wright-Patterson AFB Ohio.

Rpt Nr ASD-TR-61-553. STUDY AND EXPERIMENTAL INVESTIGATION ON SAMPLING RATE AND ALIASING IN TIME-DIVISION TELEMETRY SYSTEMS. Final report, June 62, 16lp. incl illus., 22 refs.

Unclassified Report

A study to determine the effect of 1) data power spectrum and 2) system design parameters on aliasing and data interpolation error has been conducted. Results are applicable to time-division multiplexed telemetry systems. In particular, the results apply to the commonly used PAM-FM, PDM-FM and PCM-FM telemetry systems. Data was obtained on the basis of combined analysis and experiment with emphasis on the derivation

( over )

of experimentally proven design parameters. The program consisted of three phases: 1) A survey was conducted to determine typical telemetry data spectra 2) Analysis was performed to predict accuracy performance of practical data and interpolation filters using selected examples. Included is a more general analysis to determine optimum filter transfer functions, both realizable and non-realizable, 3) Experimental tests using data spectral models were performed to derive proven interpolation accuracy performance on the basis of practical filters and design parameters. The experimental tests utilized a PAM-FM system to derive an accurate measurement of attainable performance and to indicate when other equipment factors begin to impose a limit on data recovery accuracy.

1. Telemetry aliasing study
2. Telemetering data
3. Time division
4. Sampling rate
- I. AFSC Project 4107, Task 410718

II. Contract AF34(619)-8033

III. Aeronutronic, A Division of Ford Motor Company, Newport Beach, Calif.

IV. J.W. Capps, et al.

V. U-1387

VI. Avalfr OTS

VII. In ASTIA collection

Aeronautical Systems Division, Dir/Avionics, Electro-magnetic Warfare & Comm Lab, Wright-Patterson AFB Ohio.

Rpt Nr ASD-TR-61-553. STUDY AND EXPERIMENTAL INVESTIGATION ON SAMPLING RATE AND ALIASING IN TIME-DIVISION TELEMETRY SYSTEMS. Final report, June 62, 16lp. incl illus., 22 refs.

Unclassified Report

A study to determine the effect of 1) data power spectrum and 2) system design parameters on aliasing and data interpolation error has been conducted. Results are applicable to time-division multiplexed telemetry systems. In particular, the results apply to the commonly used PAM-FM, PDM-FM and PCM-FM telemetry systems. Data was obtained on the basis of combined analysis and experiment with emphasis on the derivation

( over )

of experimentally proven design parameters. The program consisted of three phases: 1) A survey was conducted to determine typical telemetry data spectra 2) Analysis was performed to predict accuracy performance of practical data and interpolation filters using selected examples. Included is a more general analysis to determine optimum filter transfer functions, both realizable and non-realizable, 3) Experimental tests using data spectral models were performed to derive proven interpolation accuracy performance on the basis of practical filters and design parameters. The experimental tests utilized a PAM-FM system to derive an accurate measurement of attainable performance and to indicate when other equipment factors begin to impose a limit on data recovery accuracy.